

Preparation and Properties of Long Afterglow CaAl_2O_4 Phosphors Activated by Rare Earth Metal Ions

Faculty of Natural and Agricultural Sciences

Department of Physics



University of the Free State

Republic of South Africa



Ali Halake Wako

November 2011

Preparation and Properties of Long Afterglow CaAl_2O_4 Phosphors Activated by Rare Earth Metal Ions

By



Mr. Ali Halake Wako

[B.Ed (Sc) Hons. Egerton Univ., B. Sc Hons. UFS]

A Thesis Presented in Fulfillment of the Requirements for the Degree of

Magister Scientiae / Master of Science (M.Sc)

In the

Faculty of Natural and Agricultural Sciences,

Department of Physics

At the



University of the Free State

Republic of South Africa



Promoter: Prof. F.B Dejene



Co- Promoter: Prof H.C Swart

November 2011

Dedication

This thesis is dedicated to my Wife Habiba, Sons Adan, Abdullahi and Ibrahim and Daughters Hadijah, Amina and Aisha.

Acknowledgements

- First and foremost I would like to give my most special heartfelt and sincere gratitude to **Almighty ALLAH** for His continuous and everlasting guidance and for making everything possible for me even in tough times, because with Him **Nothing is Impossible and Without Him Nothing is Possible**.
- I would also like to express gratitude to my Promoter, **Prof. F.B. Dejene** and my co-Promoter, **Prof. H.C. Swart** both of the UFS who kindly accepted me as a student in their research group. Their constructive criticisms, valuable comments and suggestions were quite helpful for the completion of my thesis.
- I also wish to convey my sincere thanks to **Dr. A.K. Mesfin** of the CSIR for his generous assistance in my research work.
- I am thankful to all my research colleagues **Dr. D.B. Bem, Mr. L.F. Koao, Mr. S. Motloun, Mr. A.G. Ali, Mr. M. Mbongo, Ms M.A. Lephoto, Ms K.E. Foka, Ms M.A. Tshabalala** and **Ms L. Meiki** of the UFS QwaQwa campus physics department for their contentions help and comments during the completion of this research.
- It is my pleasure to remember research colleagues at the UFS Bloemfontein campus; **Mr. A.A. Seed, Ms M.M. Biggs, Ms P. Mbule and Mr. S. Cronje** for their supports and the help rendered in acquiring PL, SEM, EDX-spectroscopy and XRD measurements / data respectively and also **G. Tshabalala, A. Yusuf, L.L. Noto and J. Madito** for their assistance with drawing various graphs, diagrams and editing of text respectively.
- I am also very grateful to the members of the UFS-QwaQwa campus physics department teaching fraternity for their constant advice on various academic matters relevant to my thesis.
- I am grateful for the financial support from the South African National Research Foundation (NRF) and the University of the Free State.
- Finally, I would like to express my sincere indebtedness to my family for their prayers.

Abstract

This work comprises of several aspects of calcium-aluminate phosphor activated with rare earth metal ions i.e. ($\text{CaAl}_2\text{O}_4:\text{Eu}^{2+}$, Nd^{3+} , and Dy^{3+}). In particular the luminescent and structural properties of the long afterglow $\text{CaAl}_2\text{O}_4:\text{Eu}^{2+},\text{Nd}^{3+},\text{Dy}^{3+}$ phosphors prepared by urea-nitrate solution-combustion method were investigated. The solution-combustion method is more efficient because phosphors with high efficiency were obtained at low temperature ($500\text{ }^\circ\text{C}$) in a very short period of time (5 min). The effects of varying concentration of host matrix composition (Ca:Al), flux i.e. boric acid (H_3BO_3), activator (Eu^{2+}) and co-activator ($\text{Nd}^{3+}/\text{Dy}^{3+}$) mass ratios and urea ($(\text{NH}_2)_2\text{CO}$) on the structural, luminescent, and thermoluminescent(TL) properties of the $\text{CaAl}_2\text{O}_4:\text{Eu}^{2+}$, Nd^{3+} , Dy^{3+} phosphors were studied. It was observed that Ca:Al mass ratios greatly affect the crystalline structure of the material. The results of the X-ray diffraction (XRD) analysis reveal that the formation of several crystalline phases depends on the ratios of the host material. The XRD peaks show the presence of other phases such as $\text{Ca}_3\text{Al}_2\text{O}_6$ and CaAl_4O_7 but the predominant phase formed was that of CaAl_2O_4 . However it was found that the crystalline structure is generally not affected by the variation of the co-dopants concentration. Photoluminescence (PL) studies revealed a general rise in intensity with an increase in the mass ratio of Ca:Al. The highest PL intensity was observed with 0.7% Ca. The luminescent intensities vary from each other when co-doped with various proportions of Nd^{3+} and Dy^{3+} . The addition of H_3BO_3 favored the formation of pure monoclinic CaAl_2O_4 phase while the variation of the amount of $(\text{NH}_2)_2\text{CO}$ showed mixed phases although still predominantly monoclinic. Both boric acid and urea to some extent influence the luminescence intensity of the obtained phosphor but unlike the case of $\text{CO}(\text{NH}_2)_2$, the emission peak for H_3BO_3 , does not shift evidently because the energy level difference of $4f-5d$ does not change obviously. The broad blue emissions consisting mainly of symmetrical bands having maxima between 440–445 nm originate from the energy transitions between the ground state ($4f^7$) and the excited state ($4f^65d^1$) of Eu^{2+} ions while the narrow emissions in the red region 600-630 nm arise from the f-f transitions of the remnant unreduced Eu^{3+} ions. High concentrations of H_3BO_3 generally reduce both intensity and lifetime of the phosphor powders. The optimized content of H_3BO_3 is 5.8 mol % for the obtained phosphor with excellent properties. XRD analysis of the influence of Eu^{2+} and Nd^{3+} doping concentrations on the morphological, structural and PL properties of the $\text{CaAl}_2\text{O}_4:\text{Eu}^{2+};\text{Nd}^{3+}$ phosphor, depict a dominant monoclinic phase that indicates no change in the crystalline structure of the phosphor even with high concentration of Eu^{2+} or Nd^{3+} . The Energy Dispersive x-ray Spectroscopy (EDS) and Fourier Transform Infra-Red Spectroscopy (FTIR) spectra showed the expected chemical components of the phosphor. The excitation

spectra show one broadband from 200 nm to 300 nm centered around 240 nm corresponding to the crystal field splitting of the Eu^{2+} d-orbital. The prepared phosphor compositions exhibit PL emission in the blue region with a maximum around 440 nm. This is a strong indication that there was dominantly one luminescence centre, Eu^{2+} which represents emission from transitions between $4f^7$ ($8S^{7/2}$) ground state and the $4f^6-5d^1$ excited state configuration. Two other, minor peaks, at 580 and 614 nm indicate the presence of remnants of Eu^{3+} ions as a result of incomplete reduction during sample preparation. High concentrations of Eu^{2+} and Nd^{3+} generally reduce both intensity and lifetime of the phosphor powders. The optimized content of Eu^{2+} is 0.36 mol % and for Nd^{3+} is 0.09 mol % for the obtained phosphors with good properties. The decay characteristics exhibit a significant rise in initial intensity with increasing Eu^{2+} doping concentration while the decay time increased with Nd^{3+} co-doping. Analysis of the TL glow curves is one of the most significant ways to measure the number of traps and also the activation energy of the trap levels in luminescent materials. In the present study TL properties of the $\text{CaAl}_2\text{O}_4:\text{Eu}^{2+}, \text{Nd}^{3+}, \text{Dy}^{3+}$ phosphors were investigated above room temperature by use of Nucleonix 1009I TL reader. The trap depths were estimated with the aid of the peak shape method. The glow curve of $\text{CaAl}_2\text{O}_4:\text{Eu}^{2+}$ with a first peak at 50 °C was found to correspond to several traps. The ratio of $\text{Nd}^{3+}:\text{Dy}^{3+}$ ions were observed to influence the position, concentration and type of traps formed. The observed afterglow can be ascribed to the generation of suitable traps due to the presence of the Nd^{3+} trap levels. Trivalent rare earth ions ($\text{Nd}^{3+}/\text{Dy}^{3+}$) are thought to play the role of hole traps in calcium aluminate phosphors ($\text{CaAl}_2\text{O}_4:\text{Eu}^{2+}$). In these phosphors, Eu^{2+} ions act as luminescent centre emitting in the blue ($\lambda_{\text{max}} = 440$ nm) region. Despite a large number of research on the phenomenon the mechanism of the persistent luminescence of $\text{CaAl}_2\text{O}_4:\text{Eu}^{2+}, \text{Nd}^{3+}, \text{Dy}^{3+}$ has not been well presented. A proper understanding of the exact luminescence mechanisms and the identification of trap levels or locations in long phosphorescent materials is required for their use in areas such as detection of radiation, sensors for cracks in buildings, fracture of materials and temperature among others.

Key words

CaAl₂O₄: Eu²⁺, Dy³⁺, Nd³⁺, Solution – Combustion Method, Morphology, Excitation, Band gap, Luminescence, Rare Earth Ions, traps levels, decay time, long afterglow.

Acronyms

- **CL**- Cathodoluminescence,
- **CRTs**- Cathode Ray Tubes
- **EDS**- Energy Dispersive x-ray Spectroscopy
- **FTIR**-Fourier Transform Infra-Red Spectroscopy,
- **LPP**-Long Persistent Phosphors,
- **PL**- Photoluminescence
- **SEM**- Scanning Electron Microscopy
- **TEM**- Transition Electron Microscopy
- **XRD**- X-Ray Diffraction
- **TL**-Thermoluminescence

Table of Contents

Dedication	i
Acknowledgements	ii
Abstract	iii
Key words	v
Acronyms	v
Chapter 1	10
Introduction	10
1.1. Background	10
1.2. Statement of the Problem	14
1.2.1. Environmental Concerns	14
1.2.2. Mechanism of the Persistent Luminescence	14
1.2.3. The Luminescent Centre	15
1.2.4. Phase Transformation	16
1.2.5. Effect of Lattice Defects on Persistent Luminescence	16
1.2.6. Energy Transport and Storage in Luminescent solids	17
1.3. Objectives of the Study	18
1.3.1. Short term objectives	18
1.3.2. Long term objectives	19
1.4. Thesis Layout	19
References	21
Chapter 2	23
General Information on Phosphors	23
2.1. History of Long Persistent Phosphors (LPP)	23
2.2. Phosphor Terminology	24
2.2.1. Luminescence	24
2.2.1.1. Fluorescence	25
2.2.1.2. Phosphorescence	25
2.2.1.3. Electroluminescence	25
2.2.1.4. Cathodoluminescence	26
2.2.1.5. Thermoluminescence	26
2.2.1.6. Chemiluminescence	26

2.2.1.7. Bioluminescence.....	26
2.2.1.8. Electrochemiluminescence	27
2.2.1.9. Photoluminescence (PL).....	27
2.2.1.10. Incandescence	27
2.2.2. Other Forms of Luminescence	27
2.2.2.1. Crystalloluminescence.....	27
2.2.2.2. Mechanoluminescence.....	27
2.2.2.3. Radioluminescence	28
2.2.2.4. Sonoluminescence	28
2.2.3. Absorption-.....	28
2.2.4. Excitation.....	28
2.2.5. Emission-.....	28
2.2.6. Decay-.....	28
2.2.7. Transition-	29
2.2.8. Relaxation-.....	29
2.3. Applications of Phosphors	29
2.3.1. Fluorescent Lamps.....	29
2.3.2. Cathode Ray Tubes (CRTs).....	31
2.3.3. Safety indicators	32
2.3.4. Luminescent paints	33
2.3.5. Textiles	35
References	36
Chapter 3.....	39
Luminescent Mechanism of Long Afterglow $\text{CaAl}_2\text{O}_4:\text{Eu}^{2+}, \text{Nd}^{3+}, \text{Dy}^{3+}$ Phosphor.....	39
Introduction	39
Earlier Models	40
References	44
Chapter 4.....	45
Investigation Techniques of Long Afterglow Phosphors	45
4.1. Synthesis Methods for Long Afterglow $\text{CaAl}_2\text{O}_4:\text{Eu}^{2+}, \text{Nd}^{3+}, \text{Dy}^{3+}$ Phosphors.....	45
4.1.1 Solution-Combustion Method	45
4.2. Characterization Methods for Long Persistent $\text{CaAl}_2\text{O}_4:\text{Eu}^{2+}, \text{Nd}^{3+}, \text{Dy}^{3+}$ Phosphors.....	46
4.2.1. Scanning Electron Microscopy (SEM).....	46
4.2.2. Energy Dispersive x-ray Spectroscopy (EDS)	49

4.2.3. X-ray Diffraction (XRD)	51
4.2.4. Photoluminescence Spectroscopy.....	59
4.2.5. Fourier Transform Infra-Red (FT-IR) Spectroscopy	62
4.2.6. Thermoluminescence Spectroscopy (TL).....	65
References	68
Chapter 5.....	70
Synthesis and Characterization of Structural and Luminescent properties of long afterglow CaAl ₂ O ₄ : Eu ²⁺ ,Nd ³⁺ ,Dy ³⁺ phosphors by solution – combustion technique.	70
5.1. Introduction	70
5.2. Experimental	72
5.2.1. Synthesis.....	72
5.2.2 Characterization.....	73
5.3. Results and Discussion.....	74
5.3.1 The influence of the Ca: Al mass ratio on structure	74
5.3.2. The effects of Ca : Al mass ratio on photoluminescence properties	76
5.3.3. The effects of co-dopants mass ratio (Nd ³⁺ :Dy ³⁺) on the photoluminescence properties	79
Conclusion.....	79
References	80
Chapter 6.....	81
Properties of blue emitting CaAl ₂ O ₄ :Eu ²⁺ ,Nd ³⁺ phosphors by optimizing the amount of flux and fuel.....	81
6.1. Introduction	81
6.2. Experimental	82
6.2.1 Synthesis.....	82
6.2.2 Characterization.....	83
6.3. Results and Discussion.....	83
6.3.1 Influence on structure	83
6.3.2 Influence on photoluminescence properties	91
Conclusion.....	96
References	97
Chapter7.....	99
Effect of Eu ²⁺ and Nd ³⁺ on the properties of blue CaAl ₂ O ₄ :Eu ²⁺ , Nd ³⁺ long afterglow phosphor.....	99
7.1. Introduction	99

7.2. Experimental	100
7.2.1. Synthesis	100
7.2.2. Characterization	101
7.3. Results and Discussion	101
7.3.1. Influence on structure	101
7.3.2 Influence on photoluminescence properties	105
Conclusion	110
References	111
Chapter8	112
Thermoluminescence Study of Long Persistent $\text{CaAl}_2\text{O}_4:\text{Eu}^{2+},\text{Nd}^{3+},\text{Dy}^{3+}$	112
8.1. Introduction	112
8.2. Experimental	113
8.2.1. Synthesis	113
8.2.2. Characterization	114
8.3. Results and Discussion	114
8.3.1. Analysis of the TL glow curves	114
Conclusion	121
References	122
Chapter9	123
Future work	123
List of Figures	124
List of Tables	126
Publications	127
Conferences	127

Chapter 1

Introduction

1.1. Background

A **phosphor** is a solid material that emits light or **luminesces** when exposed to radiation such as ultraviolet light (UV), visible light, thermal radiation (heat) or a beam of electrons or photons [1]. **Luminescence** is a phenomenon of emission of electromagnetic radiation, in visible region, by a physical system in excess of thermal radiation or incandescence [2].

A phosphor (luminescent material) essentially acts as a transducer since it emits light by converting one type of energy into another. A phosphor can be crystalline or non-crystalline [3] and consists of a host lattice and one or more activators ranging in amounts from parts per million to a few mole percent. Both the host and activator are responsible for the luminescent properties of a phosphor. Phosphors are generally powders having average particle sizes ranging from micro-scale (10^{-6}) to nano-scale (10^{-9}) [4]. These phosphors may also be in thin film form.

When the particle size reaches nano scale, new properties are observed like the blue shift of emission intensity i.e. when the diameter of a particle is reduced the band gap (E_g) is blue-shifted due to the effect of quantum confinement [5].

Nanoscale science and technology has emerged as a very active research field in recent years. Its scope encompasses a wide variety of disciplines. Nanoscale science (or Nanoscience) is the study of properties of matter in nano scale i.e. matter in dimensions ranging between approximately 1 and 100 nanometres.

A nanometre (nm) is equal to 1/1,000,000,000th or one-billionth of a meter (10^{-9} m). In the nanoscale, materials exhibit novel properties such as lower melting points, faster chemical reactions and a remarkable lower resistance to electricity.

For phosphors their emission colours also vary depending on the particle sizes. These nano-sized phosphors also display interesting properties such as ultra-fast recombination time, an increase in the band gap due to the decrease in particle size and high quantum efficiency for photoluminescence [6].

Generally, the properties of matter in nanoscale are significantly different from the properties of matter in bulk form. These properties are due to very large surface area -to- volume ratio of the nanoparticles (Figure 1.1).

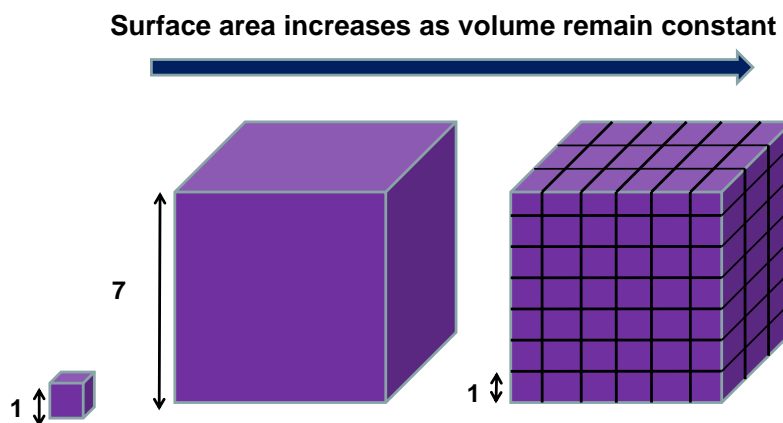


Figure 1.1 Surface area-to-volume ratio.

On the other hand, nanotechnology refers to the process of harnessing and applying principles of nanoscience in the synthesis and manufacture of nanomaterials and devices with sole purpose of improving human environmental and hence lifestyle standards.

The development of nanoscience and nanotechnology so far has been made possible by the success in the production of nanomaterials. The preparation of nanomaterials involves control of size, shape and structure of the materials. During the past few years, nanoparticles of ceramic materials have been produced in large quantities by use of physical and chemical techniques. The significant improvements in the preparation of nanomaterials such as long afterglow phosphors, ceramics and semiconductor has been due to the discovery of new various synthesis techniques such as co-precipitation, sol-gel, combustion method, etc [7].

A long afterglow phosphor is one that continues emitting light even after the irradiating source, UV or visible light has been withdrawn. Hundreds of thousands of phosphors with different characteristic emission colors have been synthesized. Phosphorescent materials have been widely studied by many researchers and found to be significantly useful in device applications like in the production of television screens and computer monitors [8]. For example, the blue-and green-emitting long decay phosphors synthesized by the addition of

Europium (Eu^{2+}) and Dysprosium (Dy^{3+}) rare earth ions as activator and co-activator to the aluminates of strontium [9-11] and calcium [12, 13] respectively.(Figure1.2))

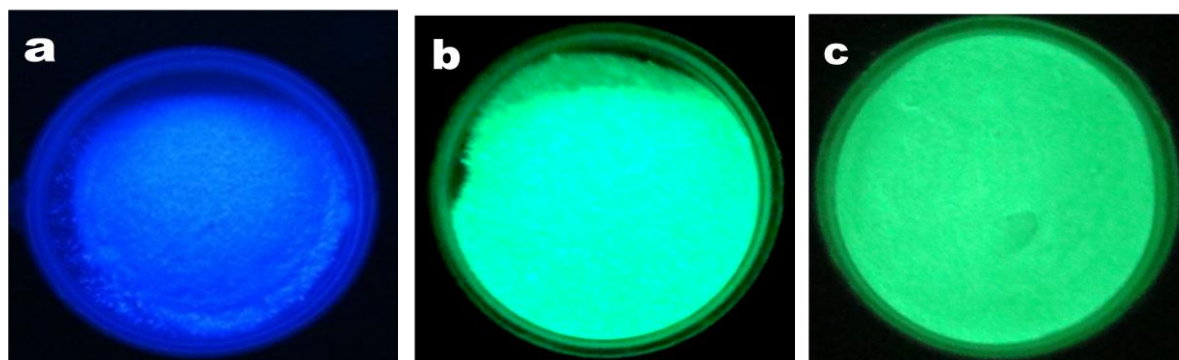


Figure 1.2: Images of (a) $\text{CaAl}_2\text{O}_4:\text{Eu}^{2+},\text{Dy}^{3+}$, (b) $\text{BaAl}_2\text{O}_4:\text{Eu}^{2+},\text{Dy}^{3+}$ and (c) $\text{SrAl}_2\text{O}_4:\text{Eu}^{2+},\text{Dy}^{3+}$ long afterglow phosphors after UV excitation.

Conventional phosphors do not maintain their phosphorescence longer than 30 minutes. For instance $\text{ZnS}:\text{Cu}$, a well known phosphorescent material [14] could not be used for certain applications such as warning signs, escape routes, glow signs, etc for the same reason. The phosphor can be improved by addition of radioactive isotopes but safety and environmental factors and concerns prohibit its use.

Calcium and strontium aluminates doped with Eu^{2+} activator ion possess environmentally safer, chemically stable and intense luminescence (PL) in the visible region [15,16] compared to the conventional sulfide based phosphors, hence they find various applications such as the tri-color low pressure mercury fluorescent lamps, safety indicators, luminescent paints in highways, airport buildings, ceramic products, in textiles, optical data storage, lamp industry, plasma display panel (PDP), radiation dosimeters, X-ray imaging, color display, and dial plate of glow watches among others.

The luminescence of $\text{CaAl}_2\text{O}_4:\text{Eu}^{2+}$ is characterized by a rapid initial decay from the Eu^{2+} activator ions followed by a very long afterglow. The afterglow has been improved by co-doping with some rare earth ions [17]. The luminescence property can be explained to be as a result of the emission from Eu^{2+} [10, 17, 18,]. This intense luminescence originates from transitions between the $4f^7 (8S_{7/2})$ ground state and the $4f^6-5d^1$ excited state configuration, as shown in Figure 1.3.

In this study, Solution-Combustion method was employed because the dissolution process enables the amount of each component to be controlled accurately and uniformly mixed in

liquid phase, while the combustion part is very simple and takes only a few minutes and hence saves energy [16]. Also, the phosphor powders of the Solution-Combustion technique are mostly homogeneous and more pure than the phosphor obtained via other conventional solid-state methods and has been widely applied to produce nano scale materials.

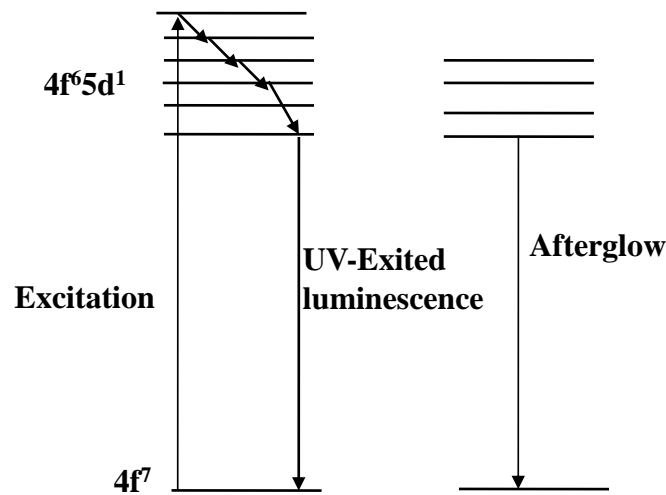


Figure 1.3: Energy level scheme of the Eu^{2+} ions involved in the UV-excited and persistent luminescence processes in $\text{CaAl}_2\text{O}_4:\text{Eu}^{2+}$ [20]

In the present work, a systematic investigation was carried out on $\text{CaAl}_2\text{O}_4:\text{Eu}^{2+}$ co-doped with Nd^{3+} and/or Dy^{3+} . Particularly the effects of variation of concentration of flux (H_2BO_3), host matrix composition [mass ratio of calcium and aluminium (Ca:Al)], dopant (Eu^{2+}), activator (Nd^{3+}) and co-activator (Dy^{3+}) mass ratios and urea ($(\text{NH}_2)_2\text{CO}$) on the structural, luminescent and thermoluminescent properties of the calcium aluminate ($\text{CaAl}_2\text{O}_4:\text{Eu}^{2+}$) phosphor were studied by detailed use of X-ray diffraction (XRD), Scanning Electron Microscopy (SEM), Photoluminescence Spectroscopy (PL), Thermoluminescence (TL), Fourier Transform Infra-Red spectroscopy (FTIR) and Energy Dispersive x-ray Spectroscopy (EDS) techniques respectively.

1.2. Statement of the Problem

1.2.1. Environmental Concerns

The beginning of the 20th century saw the use of ZnS doped with copper (ZnS:Cu) phosphor as a long afterglow material and up to now it is still being used in a variety of applications. But there are some disadvantages in the use of this material; its low luminescent intensity, high sensitivity to moisture, and a short afterglow time [9]. The extreme sensitivity to moisture of ZnS:Cu co-doped with cobalt (ZnS:Cu, Co) makes it chemically unstable. The persistent luminescence of ZnS:Cu, Co is rather strong at the beginning but is limited only to a few hours, too. Hence, ZnS: Cu, Co needs an extra excitation source because the energy storage capacity of the material is not sufficient. Radioactive substances (^3H , ^{147}Pm) have been used to supply this additional excitation but are no longer permitted. Therefore due to environmental reasons stable, efficient and non-radioactive materials to replace ZnS: Cu, Co are urgently needed.

The alkaline earth aluminates doped with Eu^{2+} and rare earth (R^{3+}) ions; $\text{MAl}_2\text{O}_4:\text{Eu}^{2+}$, R^{3+} (M= Ca and Sr) are currently the best substitutes for the ZnS:Cu, Co as commercial persistent luminescence materials [9-15]. Reports have it that the persistent luminescence of $\text{MAl}_2\text{O}_4:\text{Eu}^{2+}$ is significantly improved by co-doping with some trivalent rare earth ions, e.g. Dy^{3+} and Nd^{3+} [16-18]. It is clear that the Eu^{2+} ion acts as a luminescent centre emitting in the blue (440 nm) for $\text{CaAl}_2\text{O}_4:\text{Eu}^{2+}$ and green (520 nm) spectral range for $\text{SrAl}_2\text{O}_4:\text{Eu}^{2+}$ respectively.

1.2.2. Mechanism of the Persistent Luminescence

Although the overall mechanism of the persistent luminescence of $\text{CaAl}_2\text{O}_4:\text{Eu}^{2+}$ is now quite well agreed on [10, 16-18], the details involved are largely unknown.

Long persistent luminescence of $\text{CaAl}_2\text{O}_4:\text{Eu}^{2+}$ is thought to have originated from alkaline earth vacancies [10]. The formation of both electron and hole trapping and subsequent slow thermal excitation of the traps followed by emission from Eu^{2+} ions (Figure 1.4) are being taken to be the root causes of the persistent luminescence [16-18, 20, 21]. According to this model the trapped electrons and holes act as pairs and luminescence can take place as a result of indirect centre to centre transitions. In other similar systems (e.g. photo-stimulated materials [22]) the main charge carriers were observed to be electrons and ions but the effect of holes has gained more importance in the persistent luminescence materials. However, with

the addition of some trivalent RE^{3+} ions the persistent luminescence lifetime and intensity can be improved further [16]

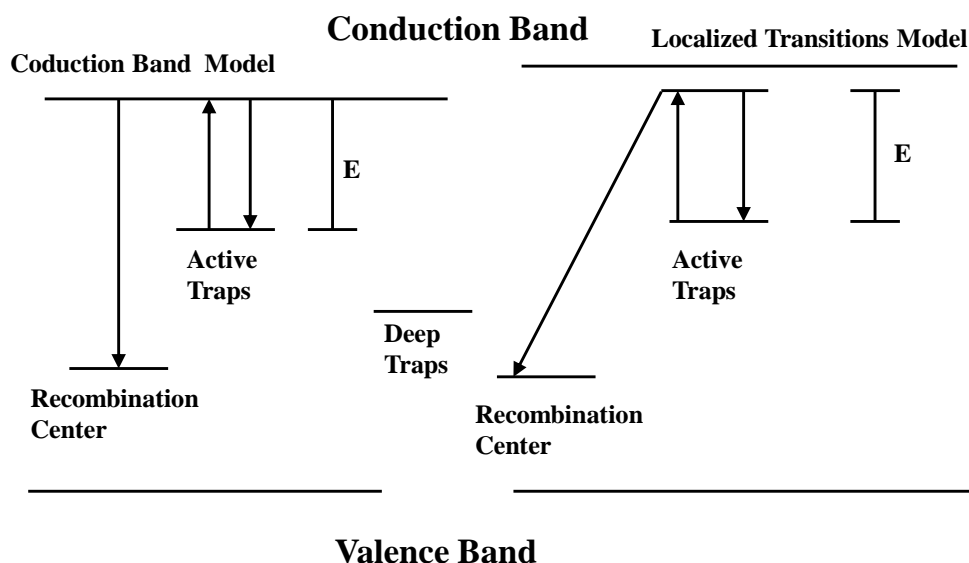


Figure 1.4: Model showing Persistent Luminescence Mechanism.

The knowledge of the underlying mechanism of long persistence is very necessary and would significantly assist in the search for persistent luminescence materials. In the present study, a detailed investigation was carried out on the Eu^{2+} doped alkaline earth aluminates ($CaAl_2O_4:Eu^{2+}$). Especially, the role of co-doping with different trivalent rare earth [RE^{3+}] ions (Dy^{3+} and Nd^{3+}) in the enhancement of the afterglow of $CaAl_2O_4:Eu^{2+}$, RE^{3+} was studied by several spectroscopic methods viz Photoluminescence (PL) and Thermoluminescence (TL).

1.2.3. The Luminescent Centre

Despite the fact that considerable amount of study on the aspects of luminescence could be carried out by taking into account a simple model for the centre it is quite hard to find out what is exactly going on inside the centre.

Several theories or approaches have to be put to trial depending on the complexity of the centre. One such famous approach is the **configurational coordinate model**. This approach assumes that the luminescent centre has some equilibrium position in the crystal lattice and that a change in energy occurs due to some displacement from this position. The interaction of the centre with the crystal lattice in terms of its electronic state and the vibrations of the

lattice can be seen to be as a function of the position of the nuclei and the model can be employed to easily explain such effects as the Stokes shift between absorption and emission. But owing to the fact that electronic transitions of the centre are coupled to the movements of the lattice around the centre the simple model is not generally acceptable.

To differentiate the electronic state from vibrational state of the luminescent centre the **Born-Oppenheimer approximation** is used but it has been shown by Fowler and Dexter (1962) that the potential energy curves in the configurational coordinate diagram are also a function of the electronic state.

In condensed systems the **Einstein relations** are not valid as such and the complex relaxations which occur after an excitation do not simplify the scenario because the electronic states in emission are likely not to be the same with those in absorption. Furthermore, because of the **Jahn-Teller effect**, which tends to remove degeneracy of an excited state by creating asymmetry in the centre, there may be a separation in the excited state. There are also transition probabilities for the absorption and the emission. One of the most important points is that the matrix element for the absorption transition may be different from that for the emission transition. A lot of interest in luminescence now needs to be taken in quantitative studies of phonon-photon interactions (preferably at very low temperatures) [23].

1.2.4. Phase Transformation

In spite of a great deal of research work on $\text{CaAl}_2\text{O}_4:\text{Eu}^{2+}$ phosphors, the phase transformations of Eu doped calcium aluminate compounds and their effects on luminescent properties have been rarely reported until now.

1.2.5. Effect of Lattice Defects on Persistent Luminescence

Generally, when the mean particle size of phosphors is smaller than 1-2 μm , there is a drop in their luminescence efficiency. This is due to the fact that surface defects become more important with decreasing particle size and an increase in the surface area. This can often lead to the reduction of the emission intensity [24]. The presence of any kind of lattice defect in the host lattice in most cases has been found to greatly reduce the efficiency of luminescence. It also brings about the long afterglow observed in some potentially efficient luminescent materials. These defects are usually considered to be disadvantageous as far as the properties of a phosphor are concerned when the practical applications are considered [25]. Consequently, the luminescence applications based on phosphors with lattice defects are rare.

1.2.6. Energy Transport and Storage in Luminescent solids

The dominant role played in luminescence mechanisms by the transport of energy was pointed out by Broser in an invited paper [26]. In condensed systems the interatomic distance is considerably smaller than in gases and the probability of interaction between a luminescent centre and distant atoms are much greater. Energy transfer may take place by free charge carriers, excitons, quantum mechanical resonance, photons or phonons, and may be studied by direct measurements of such properties as velocity, lifetime and carrier range, or by indirect measurements. Two important parameters are lifetime and diffusion coefficient. Great advances have been made in the study of energy transport by direct mechanisms in phosphors during the last ten years. New experiments have been devised (particularly for excitons) to measure transport parameters and older experiments have been perfected. Nevertheless in the field of energy transport in phosphors there are ample problems remaining to be solved in the next decade.

Storage of energy in phosphors is still being studied extensively by thermal ejection measurements on trapped charge carriers [27-30]. Interpretation of glow curves in terms of traps or metastable states is obviously more difficult in organic compounds than inorganic compounds. Even in inorganic compounds it is not likely that the method gives the true or complete distribution of trapping states in a phosphor.

The conventional method of filling the traps at low temperature is by illuminating the specimen, but if the traps are filled by space-charge injection of charge using a high field across the specimen it is possible to remove any ambiguity as to the sign of the charge carrier responsible for the peak [28]. If a blocking electrode is used as the cathode during the heating-up process it is also possible to distinguish between surface and volume states. The use of high fields causes the carrier transit time to be reduced, the probability of re-trapping to be reduced, and the kinetics to be more like those of the monomolecular theoretical model. For the investigation of trap spectra with a continuous energy distribution the fractionated glow technique is proving to be of value [30].

1.3. Objectives of the Study

1.3.1. Short term objectives

The short term objectives of the present study are:

1. To synthesize the $\text{CaAl}_2\text{O}_4:\text{Eu}^{2+}, \text{Nd}^{3+}, \text{Dy}^{3+}$ phosphor particles by solution-combustion method.
2. To characterize the calcium aluminate phosphor *viz.* $\text{CaAl}_2\text{O}_4:\text{Eu}^{2+}, \text{Dy}^{3+}, \text{Nd}^{3+}$
3. Determining the morphology of the samples with Scanning Electron Microscopy (SEM).
4. To determine the chemical composition of the samples by Energy Dispersive X-Ray spectroscopy (EDS).
5. Determining the crystal structure and particle size with X-Ray Diffraction (XRD).
6. Measuring the absorption and emission intensity of the samples and determining the band gap and particle sizes from the spectral data.
7. To find out the effects of various parameters like use of flux, urea, variation of host lattice chemical composition and additives (emission centers, co-dopants) on the structural, morphological, TL and PL intensity of the samples for the better phosphorescence properties.
8. To explore the scope of phosphor materials, especially, long persistent phosphor.
9. To explore the existing mechanisms of long persistent phosphorescence and find out the improved one to satisfy all the characteristics observed for a long persistent phosphor.

1.3.2. Long term objectives

The long term objectives of the study are:

1. To develop more phosphor materials with long persistence for dark vision and other applications.
2. To establish a standard fabrication process for similar RE metal ions doped aluminate phosphors.
3. Finally, to promote phosphor materials as a source of alternative energy for societal and environmental sustainability.

1.4. Thesis Layout

The *1st Chapter* begins with a general introductory overview of phosphor materials outlining what phosphorescent materials are, their properties, development, a brief description of the different applications of phosphors, synthesis and characterisation methods and the mechanism of phosphorescence. It also presents the short term and long term objectives of this undertaking. The shortcomings encountered and areas that need to be streamlined or emphasised in research works involving phosphor materials are schemed out under the subtopic ‘problem statement’.

Chapter 2 follows by outlining the background information on phosphors; the history of long persistent phosphors (LPP), theory of luminescence and some common terminology applied to phosphors. The different applications of phosphors are also briefly discussed in this chapter.

Chapter 3 reports detailed information about the luminescent or phosphorescence mechanism of long persistent $\text{CaAl}_2\text{O}_4:\text{Eu}^{2+}$ phosphor as well as the electronic transition of rare earth (RE) ions (Eu^{2+} , Eu^{3+}). Also how the luminescent properties are influenced by crystal field changes and the distortion in the host matrix of the $\text{CaAl}_2\text{O}_4:\text{Eu}^{2+},\text{Nd}^{3+},\text{Dy}^{3+}$ phosphor prepared by the solution-combustion method is provided.

Chapter 4 gives a brief description of the experimental equipment, environmental and/or atmospheric requirements, techniques used to design, synthesize and characterize alkaline earth aluminate phosphors. The solution - combustion method used to synthesize the phosphors is discussed in detail. A summary of the different characterization techniques are also given. This includes a description of the operation of each of the techniques such as SEM, EDX-S, XRD, FTIR and TL.

In *Chapter 5*, the $\text{CaAl}_2\text{O}_4:\text{Eu}^{2+}$, Nd^{3+} , Dy^{3+} phosphor was synthesized by solution combustion method. The microstructure variation and its effect on the photoluminescence (PL) and thermoluminescence (TL) properties were studied.

In *chapter 6*, the effects of variation of flux (H_3BO_3) and the amount of fuel, urea ($\text{CO}(\text{NH}_2)_2$) on the morphological, structure and photoluminescence (PL) properties of $\text{CaAl}_2\text{O}_4:\text{Eu}^{2+}$, Nd^{3+} systems were investigated.

The influence of Eu^{2+} and Nd^{3+} doping concentrations on the morphological, structural and photoluminescence (PL) properties of the $\text{CaAl}_2\text{O}_4:\text{Eu}^{2+};\text{Nd}^{3+}$ phosphor were investigated by various techniques in *chapter 7*.

In *chapter 8*, thermoluminescence properties of the $\text{CaAl}_2\text{O}_4:\text{Eu}^{2+}$, Nd^{3+} , Dy^{3+} phosphors was investigated above room temperature. Analysis of the thermoluminescence (TL) glow curves were used to measure the number of traps and also the activation energy of the trap levels in the luminescent material.

The detailed suggestions for possible future works are summarized in *chapter 9*.

References

- [1] M.M. Biggs, M.Sc Thesis, University of the Free State, South Africa 2008, 13.
- [2] D. R. Vij, N. Singh, Nova Publishers, New York, 1997 169.
- [3] S. E. kambaram, K.C. Patil, M. Maaza, Purdue University, USA, 2005.
- [4] J. C. Whitaker, The Electronics Hand Book, CRC Press, USA, 1996 469.
- [5] K.K. Nanda, F.E. Kruis, H. Fissan, M. Acet, J. Appl. Phys, 2002, **91(4)** 2315.
- [6] M.S. Dhlamini, PhD Thesis, University of the Free State, South Africa 2008, 4.
- [7] Y. Gogotsi, Nanomaterials Handbook, Routledge Publishers, USA, 2006, 5.
- [8] Z. Liu, Y. Liu, J. Zhang, J. Rong, L. Huang, D. Yuan, Optics Communications 2005, **251** 388.
- [9] Y. Murayama, N. Takeuchi, Y. Aoki and T. Matsuzawa, U.S. Patent 5, 1995, **424** 006.
- [10] T. Matsuzawa, Y. Aoki, N. Takeuchi, Y. Murayama, J. Electrochem. Soc. 1996, **143** 2670.
- [11] T. Katsumata, T. Nabae, K. Sasajima, S. Komuro and T. Morikawa, J. Electrochem. Soc. 1997, **144** L243.
- [12] T. Katsumata, T. Nabae, K. Sasajima and T. Matsuzawa, J. Cryst. Growth 1998, **183** 361.
- [13] T. Katsumata, T. Nabae, K. Sasajima, S. Komuro and T. Morikawa, J. Am. Ceram. Soc. 1998, **81** 413.
- [14] R. Sakai, T. Katsumata, S. Komuro and T. Morikawa, J. Lumin. 1999, **85** 149-154.
- [15] I. Tsutai, T. Kamimura, K. Kato, F. Kaneko, K. Shinbo, M. Ohta and T. Kawakami. Electron. Eng. Jpn 2000, **132** 7.
- [16] E. Nakazawa and T. Mochida, J. Lumin. 1997, **72-74** 236.
- [17] H. Yamamoto, J. Lumin. 1997, **72-74** 287.
- [18] W. Jia, H. Yuan, L. Lu, H. Liu, W. M. Yen, J. Lumin. 1998, **76-77** 424.
- [19] J. Holsa, H. Jungner, M. Lastusaari and J. Niittykoski, J. Alloys Compds. 2001, **326** 323.
- [20] K. Kato, I. Tsutai, T. Kamimura, F. Kaneko, K. Shinbo, M. Ohta, T. Kawakami, J. Lumin. 1999, **82** 213.
- [21] W. Jia, H. Yuan, L. Lu, H. Liu, S. Holmstrom, W.M. Yen, J. Lumin. 1999, **465** 83.
- [22] H. Ruan, F. Gan, J. Xu, Y. Chang, Mater. Sci. Eng. B 2000, **76** 73.

- [23] G. F. J. Garlick, Department of Physics, University of Hull.
- [24] T. Hirai, Y. Asada and I. Komasaawa, *J. Colloid Interface Sci.* 2004 **276** 339.
- [25] G. Blasse, B.C. Grabmaier, *Luminescent Materials*, Springer, Berlin, 1994, 65.
- [26] I. Broser, Institut für Elektronenmikroskopie am Fritz-Haber-Institut der Max-Planck-Gesellschaft, Berlin, Germany.
- [27] J. Bullo, A. Derouledé, F. Kieffer and M. Magat, Faculté des Sciences, Orsay (Seine-et-Oise), France.
- [28] M. C. Driver, Associated Electrical Industries Limited, Rugby, Warwicks.
- [29] B. Thomas, Welsh, College of Advanced Technology, Cardiff.
- [30] H. Gobrecht, D. Hofmann and H. Nelkowski, Physikalisches Institut der Technischen Universität, Berlin, Germany.

Chapter 2

General Information on Phosphors

2.1. History of Long Persistent Phosphors (LPP)

Lightning, the dim light of glow worms, the aurora borealis and of fungi have always been known to mankind. However the first investigations of luminescence began in the early 17th century with a synthetic material when in the year (1603) Vincenzo Cascariolo, an alchemist and cobbler in Bologna, Italy, heated a mixture of barium sulphate and coal; ($\text{BaSO}_4 + 2\text{C} \rightarrow \text{BaS} + 2\text{CO}_2$) in the form of barite, (heavy spar) which he discovered at the foot of a volcanic mountain, Monte Paderno. The powder obtained after cooling exhibited a bluish glow at night, and Cascariolo observed that this glow could be restored by exposure of the powder to sunlight. The name *lapis Solaris*, or “sunstone,” was given to the material because alchemists at first hoped it would transform base metals into gold, the symbol for gold being the Sun. The discovery of the afterglow aroused the interest of many scholars of that period, who gave the material other names, including phosphorus, meaning “light bearer,” which thereafter was applied to any material that glowed in the dark. The stone which is currently known as “Bolognian Stone” opened the trend for scientific research on a class of materials known as phosphors [1]. More discoveries were made when in the year 1768 CaS was obtained by Canton and later in 1866 when the first green emitting ZnS crystals were prepared by Sidot. It was however found out later in 1886 by Verneuil that un-doped CaS did not emit any light until small amounts of Bi was added to it. This discovery unearthed the deeper understanding of the nature of luminescence in materials when eventually it was observed that Cr^+ ion was required for the production of red light from BaS and Cu^+ for emission of a green light from ZnS. Since the beginning of the last century ZnS: Cu^+ phosphors have been well known for long persistent times as long as 40 minutes [2] and are used in a variety of applications. The effects of co-doping ZnS: Cu^+ with Co^{2+} were also observed to double the persistent time of the phosphor [3]. The next generation of long persistent phosphors were known as Lenard’s phosphors [4]. They comprised of the alkali earth sulphides, such as CaS, and SrS. These phosphors exhibited long persistency over hours when doped with such ions as Bi^{3+} , Eu^{2+} ,

Ce^{3+} etc. Since these phosphors can be excited by the visible light they provide a variety of applications. But due to their chemical instability and release of H_2S gas when it comes into contact with moisture the applications of these sulphide based phosphors were limited [5].

In 1990s, $\text{SrAl}_2\text{O}_4:\text{Eu}^{2+},\text{Dy}^{3+}$, with a strong emission centred at 520 nm (green) was reported as a new type of long persistent phosphor with persistent time longer than 16 h [6-7]. This was followed by a new similar long persistent phosphor $\text{CaAl}_2\text{O}_4:\text{Ce}^{3+},\text{Nd}^{3+}$ emitting at 420 nm (dark-blue) [8]. Later, $\text{Sr}_4\text{Al}_{14}\text{O}_{25}:\text{Eu}^{2+},\text{Dy}^{3+}$ phosphor showing extremely prolonged phosphorescence that lasts over 20 h in blue-green (495 nm) region was developed [9-10].

Because of their chemical stability, ability to persist overnight, wide range of excitation, high quantum yield etc these phosphors opened prospects for various applications [11-12]. Recent researches on long persistent phosphors have dwelt on two major aspects; the mechanism of trapping-de-trapping phenomena [13-15] and the development of new long persistent phosphor materials that cover the whole range of the visible spectrum. For instance studies on alkaline earth aluminates doped with Ce^{3+} or Eu^{2+} have led to the conclusion that trapping-de-trapping mechanisms may be due to the electrons delocalization processes [16-17]. Over hundred different kinds of long persistent phosphors developed during the past two decades, are doped with rare earth metal ions, for example, Eu^{2+} , Eu^{3+} , Ce^{3+} , Tb^{3+} , Sm^{3+} , Pr^{3+} , Dy^{3+} , Er^{3+} , Tm^{3+} etc as an activator ion .

2.2. Phosphor Terminology

2.2.1. Luminescence

Luminescence, which includes both fluorescence and phosphorescence, is defined as a phenomenon in which the electronic states of substance is excited by some kind of external energy and the excitation energy is given off as light of various wavelengths [1]. Luminescence is the general case in which a higher energy photon is absorbed and a lower energy photon is emitted (such a process is called a Stokes process). In this case, the excess energy is absorbed by the solid and appears as lattice vibrational (heat) energy [18]. It refers to the luminous emission which is not thermal in origin and is thus a form of cold body radiation. This distinguishes luminescence from incandescence, which is light generated by a body at high temperatures. In luminescence when the electrons in the ground state (lowest state) of an atom absorb extra energy in form of radiation they are raised to an excited state (highest state). However, since the electron in this excited state is not stable it jumps back

(de-excited) to the ground state giving off energy in form of light. With few exceptions, the excitation energy is always greater than the energy (wavelength, colour) of the emitted light. In nature luminescence phenomenon occur in form of glow worms, fire-flies and in certain bacteria and aquatic animals.

Luminescence can be divided into two broad categories viz: By **duration** (fluorescence or phosphorescence) or by the **mechanism that creates the light** i.e. the type of excitation sources (chemical reactions, electrical energy, subatomic motions, or stress on a crystal):

a) By duration;

2.2.1.1. Fluorescence

The term Fluorescence denotes the imperceptible short afterglow of the materials after excitation. This is to distinguish the emission from the phosphorescence which is used to denote a long afterglow [18-19]. Fluorescence is the emission of light with a characteristic time of less than 10^{-8} seconds. Fluorescent things stop emitting light very soon (in about 10 ns) after the exciting energy is cut off. Fluorescence is generally not affected by temperature.

2.2.1.2. Phosphorescence

Phosphorescence is when the recombination of the photo-generated electrons and holes is significantly delayed in a luminescent material [19]. Phosphorescence continues for a longer time than fluorescence. Glow-in-the-dark stickers and watch hands that glow are examples of phosphorescence. A less obvious but more exact definition of the difference is that the amount of time phosphorescence continues after the material has been excited may change with temperature, but in fluorescence, this decay time does not change. Also, phosphorescence tends to occur at longer wavelengths than fluorescence.

b) By the mechanism that creates the light or the type of excitation source;

2.2.1.3. Electroluminescence

Refers to the process by which light is generated from a solid semi-conducting material or a gas due to application of electric field in the form of high electric voltage (AC-Voltage). Some crystalline substances also exhibit electroluminescence (EL). When an electric current is passed through them, the electrons in the material are accelerated which in turn excite the

activator ions that occupy energy levels in the chemical bond of the crystal structure by impact excitation. Electron-hole pairs get excited due to the applied field and as they recombine, they emit photons [19, 20]. These excited electrons emit visible light as they decay back to the ground state.

2.2.1.4. Cathodoluminescence

Is the emission of light by invisible energetic electrons (cathode rays) produced by electrical discharges in vacuum tubes when they strike the glass walls of the tubes [21]. The modern name for cathode rays is electrons. Cathodoluminescence is widely applied, for instance the electron microscope uses beams of electrons to produce high resolution images of small images.

2.2.1.5. Thermoluminescence

Also known as Thermally Stimulated Luminescence (TSL), it is a phenomenon in which light is emitted by a solid which has been exposed to some radiation while being subjected to increasing heat. The heat only acts as a stimulant whereas the ionizing radiation plays the role of an exciting agent. All phosphorescent materials have a minimum temperature; but many have a minimum triggering temperature below normal temperatures and are not normally thought of as thermoluminescent materials [20].

2.2.1.6. Chemiluminescence

Occurs as a result of the energy of a chemical reaction i.e. reduction-oxidation (REDOX) reaction whereby the chemical energy formed by the exothermic reaction is transformed into visible light. Sometimes the energy is directly transferred to the electrons in the chemical bonds raising them to the excited states. The electrons then emit light as they decay back to lower or ground states. Because of the slow chemical reactions light can be emitted for a longer time. Chemiluminescence is used, for instance, in the detection and concentration measurements of some atmosphere contaminants, such as NO₂ and NO [22]. A light stick emits a form of light by chemiluminescence [23].

2.2.1.7. Bioluminescence

As a particular class of chemiluminescence, bioluminescence is defined as the emission of light by a living organism due to some form of chemical reactions within their bodies in which chemical energy is transformed into light energy. These reactions which mostly involve the substance adenosine triphosphate (ATP) occur either inside or outside the cell.

Bioluminescence is the predominant source of light in the deep ocean [22]. Bacteria, jellies, algae, and other organisms, such as fish and squids, are able to produce light by chemicals that they have stored in their bodies. Fireflies, glow worms, some insects, insect larvae, annelids, arachnids and even species of fungi belong to forms of land bioluminescence [23].

2.2.1.8. Electrochemiluminescence

ECL or (EL) is the phenomenon in which electrical energy is converted to luminous energy by an electrochemical reaction without thermal energy generation. EL finds wide application in the so-called high field electroluminescent thin film materials. These materials are different in principle from standard light emitting diode (LED) and diode lasers where electrons and holes recombine to create light. In these high field EL materials, typically rare earth and transition metal ions are doped in wide band gap materials. This phosphor layer is sandwiched between two insulators to limit the current and driven with an alternating current at high fields.

2.2.1.9. Photoluminescence (PL)

Is excitation caused by electromagnetic radiations. In solids, PL takes place when the electronic states are excited by a photon and the excitation energy is absorbed and emitted in the form of light [19].

2.2.1.10. Incandescence

Incandescence is light from heat energy. A conducting body is heated and the spectrum of the radiation generated corresponds to the temperature of the heated body (black body radiation) [24]. Incandescent light is produced by lattice vibrations, called phonons, which emit part of their energy in the form of electromagnetic radiation [20].

2.2.2. Other Forms of Luminescence

Depending on the type of excitation sources, other forms of luminescence include:

2.2.2.1. Crystalloluminescence which occurs during crystallization,

2.2.2.2. Mechanoluminescence which occurs as a result of some mechanical action on a solid. Examples are,

- *Triboluminescence* – Triboluminescence by the mechanical energy [18-19], when bonds in a material are broken when that material is scratched, crushed or rubbed

- *Fractoluminescence* – luminescence generated when bonds in certain crystals are broken by fracturing.
- *Piezoluminescence* – luminescence produced by the action of pressure on certain solids.

2.2.2.3. Radioluminescence - luminescence produced in a material by the bombardment of ionising radiation.

2.2.2.4. Sonoluminescence - refers to luminescence from imploding bubbles in a liquid when excited by sound is called.

In this dissertation, we are particularly concerned with photoluminescence (PL) and thermoluminescence (TL) hence the other types of luminescence will not be discussed onward.

2.2.3. Absorption- is the process by which a substance takes up energy in form of electromagnetic radiation (UV or visible light) and stores it within itself. In luminescent materials, the absorption of energy takes place by either the host lattice or by intentionally doped impurities [24].

2.2.4. Excitation- also called "photo-excitation", it is the process in which light is directed onto a sample where it is absorbed and imparts excess energy into the material. This excess energy may cause electrons in the material to be raised from ground state to excited states.

2.2.5. Emission- electrons in the excited states are usually unstable. When these electrons return to their equilibrium states, the excess energy is released, a process referred to as emission. The process may involve the emission of light (a radiative process) or it may not (a non-radiative process). The energy of the emitted light, or photoluminescence, is related to the difference in energy levels between the two electron states involved in the transition, that is, between the excited state and the ground state. The energy of the emitted radiation is always less than that of the absorbed radiation.

2.2.6. Decay- is the gradual decrease in the intensity of emitted energy over time after the excitation source has been stopped. The decrease is usually exponential, but most long-persistence phosphors exhibit what is called hyperbolic decay. The energy of an electronically

excited state may be lost in a variety of ways. A **radiative decay** is a process in which a molecule discards its excitation energy as a photon. A more common fate is **non-radiative decay**, in which the excess energy is transferred into the vibration, rotation, and translation of the surrounding molecules. This thermal degradation converts the excitation energy into thermal motion of the environment (i.e., to heat) [25].

2.2.7. Transition- refers to the movement or transfer of electrons from one energy level to another due to either absorption or release of energy. Excitation and emission occurs due to electronic transitions at the center.

2.2.8. Relaxation- After excitation the nuclei adjust their positions to the new excited situation, so that the inter-atomic distances equal the equilibrium distances belonging to the excited state. This process is called relaxation. During relaxation there is usually no emission. The system can return to the ground state spontaneously under emission of radiation from the lowest level of the excited state. The emission occurs at a lower energy than the absorption due to the relaxation process. The energy difference between the maximum of the lowest excitation band and that of the emission band is called **Stokes shift** [25].

2.3. Applications of Phosphors

2.3.1. Fluorescent Lamps

Basically, fluorescent Lamps consist of a tube in which a phosphor layer is applied on the inside wall and electrodes sealed at both ends (Figure 2.1). The two electrodes have the same construction and serve alternately as the cathode and anode. This is possible because they work with AC power supply. Small amounts of mercury and rare gas, such as argon, are added after the electrodes have been sealed to the tube and the air inside the tube has been evacuated. The pressure of the rare gas is usually 0.2 to 0.7 kPa (1.5 to 5.2 Torr).

The optimum mercury vapor pressure for common fluorescent lamps is 0.5 to 1.4 Pa (3.7 to 10.5 mTorr), which corresponds to the vapor pressure of Hg at about 40°C. Hence, fluorescent lamps are designed so that the temperature of the coldest point of the tube wall during normal operation is about 40°C.

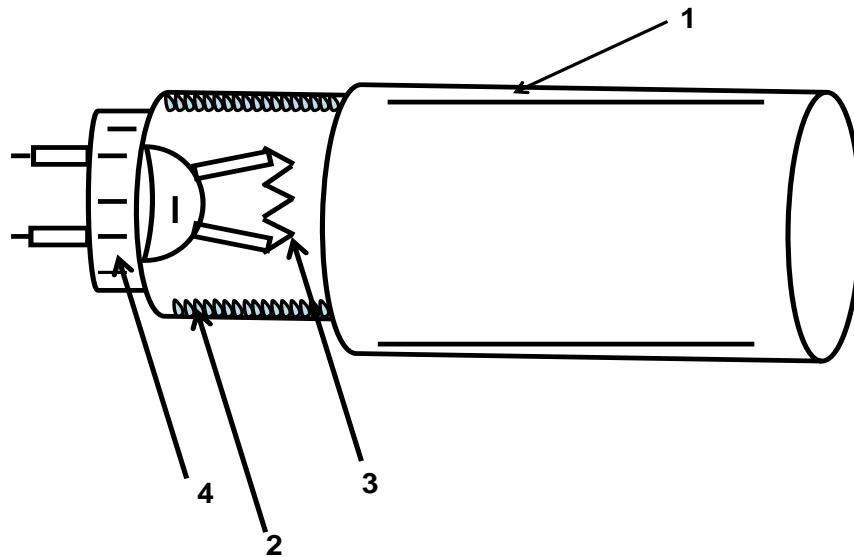


Figure 2.1: Cross section of a low-pressure luminescent lamp; 1-glass tube; 2-luminescent powder; 3-Cathode; 4-lamp cap[1].

When the fluorescent lamp is in use under the rated power specifications, a uniform electric field of about 1 Vcm^{-1} is formed at the positive end of the discharge between the two electrodes, and electrons and ions in this plasma are accelerated in the direction of the anode.

But the kinetic energy of the electrons increases gradually more than that of the ions since the ions has much larger mass than the electrons. Hence the electric energy supplied to the fluorescent lamp is mostly converted to the kinetic energy of the electrons. During this acceleration, the electrons collide with other particles to create the plasma and other forms of energy [19].

In the discharge the mercury atoms are excited. When they return to the ground state they emit (mainly) ultraviolet radiation. A fluorescent lamp is a very efficient generator of ultraviolet energy. About 85% of the emitted radiation is at 254nm and 12% at 185nm. The remaining 3% is found in the longer wavelength ultraviolet and visible region (365,405,436, and 546nm). The lamp phosphor converts the 254nm and the 185nm into visible light [1].

2.3.2. Cathode Ray Tubes (CRTs)

The cathode-ray tube (CRT) was invented by Professor Karl Ferdinand Braun in 1897 and hence it is now popularly known as the Braun tube in Japan and some other countries. It is the most widely used display device which finds applications in color television sets, giant screens and computers among others. Figure 2.2 shows the structure of a typical CRT. It consists of a glass vacuum envelope which has a neck tube, a funnel, and a face plate with a phosphor screen applied on the back. The neck tube encloses the electron gun that generates the electron beam and the deflection plates while the deflection yoke is positioned outside the neck tube [19].

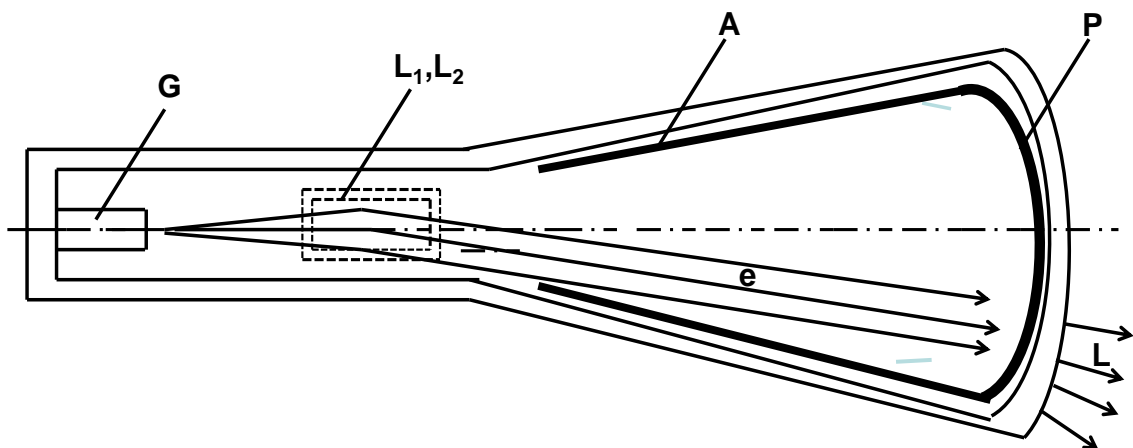


Figure 2.2: Schematic diagram of a standard cathode ray tube (CRT); Electrons (e) leaving the electron gun (G) are deflected by systems L_1, L_2 and excite the luminescent material (P). A is the anode and L the emitted radiation [1].

When the filament is heated which in turn heats the cathode, hot fast moving electrons called cathode rays are generated which are then formed into a beam by tuning the voltage applied to the grids in the gun and the anode.

When the beam of electrons fall on the phosphors they become electrically charged since they are generally insulators. A negatively charged phosphor screen has lower potential with

respect to that of the cathode and this interferes with the beam trajectory resulting in distortion of the image on the screen. Also collision between ions produced in the cathode and the screen may cause the phosphor to be “burned,” thus reducing the light intensity emitted from the phosphor. In order to avoid these problems and to improve light output from the phosphor, a coat of thin aluminium film is applied on the phosphor by vacuum evaporation method (metal-backed phosphor screen).

A conventional colour CRT delivers three electron beams and has the corresponding three primary-colour phosphors [26]. In order to enhance the contrast of the picture image on the screen, an ambient-light absorbing graphite layer is placed between the phosphors [27]. Blue and red pigments are coated on the blue and red phosphor particles to obtain a similar enhancement of the contrast ratio and to improve the colour fidelity [28]. Another way to achieve the same effect is to place red, green, and blue inorganic filters between the front panel and the corresponding colour phosphors [29–30].

Calcium halophosphate $(3(\text{Ca,Sr,Ba})_3(\text{PO}_4)_2 \cdot (\text{Ca,Sr,Ba})\text{X}_2: \text{Sb}^{3+}, \text{Mn}^{2+})$ is the dominant phosphor in the lamp industry [31]. In this phosphor, it was possible to control the intensity ratio of the blue and orange components, and to produce white lights with a wide range of colour temperatures. Moreover, it was chemically stable and had good lumen maintenance properties. Furthermore, this phosphor was cheap and produced light with high efficiency [19].

2.3.3. Safety indicators

Long afterglows phosphors can be used in safety applications, e.g., in exit signs which still operate in case of a current blackout (Figure 2.3). Other long afterglow materials are, e.g., ZnS:Cu and SrS:Bi





Figure 2.3 (a) Luminescent signs [43] and (b) a neon sign [44]

2.3.4. Luminescent paints

Fluorescent paints are made by mixing a fluorescent pigment with a varnish, such as the normally dry type, the baked type, and the hardened type. Paints made in this way have distinct brightness that is at least three times as the normal colour under sunlight and further show high colour purity (Figure 2.4).

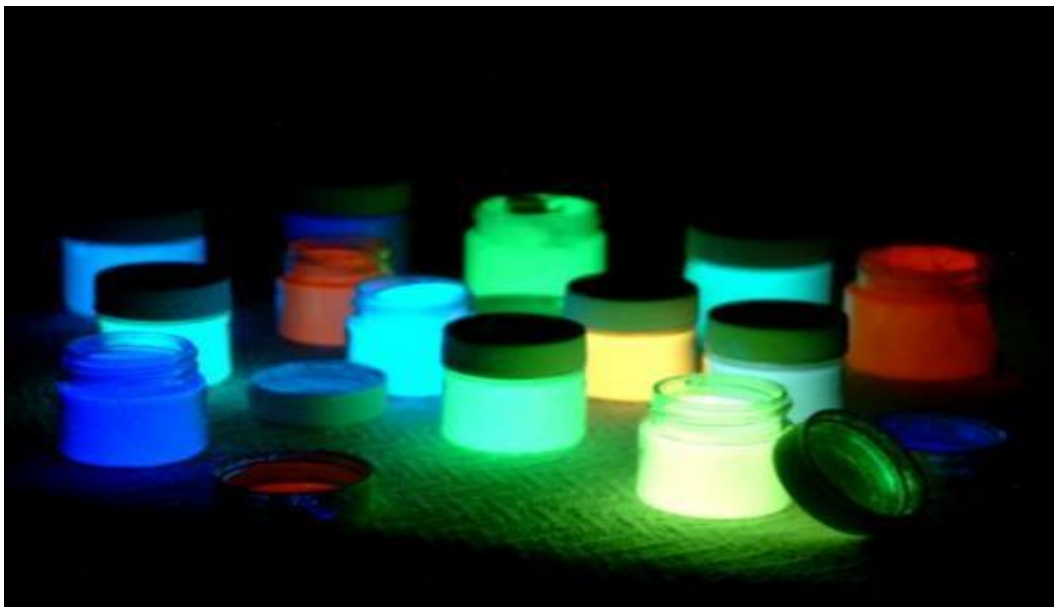


Figure 2.4: Luminescent Paints [43]

Deep colour paints are attractive to the human eye while light colours have soft and clear tone that creates a refreshing sensation. Due to their high visibility under different conditions fluorescent paints have a broad range of applications such as in notice boards, signs, window stickers, posters, etc in the fields of advertisement and decoration and also as warning and instruction signs in the fields of safety and disaster prevention.

Fluorescent paints effective for disaster prevention are specified in JIS (Japanese Industrial Standards) Z9106, “Fluorescent Safety Colours—General Rules for Application.” Fluorescent paints are weak in covering power, so when they are used on objects that are not white, a white base coat must first be applied. These paints also have low resistance to weathering, so when used outdoors they must be coated with a transparent paint that contains an ultraviolet light-absorbing material to prevent discoloration [19].



Figure 2.5: Luminescent (a) t-shirt and (b) shoes [46, 47].

2.3.5. Textiles

Fluorescent dyes are also used for textile printing. This is done by adding a binder to the fluorescent color base consisting of a fluorescent pigment. The mixture is then used to make prints on the fabric (Figure 2.5). A reactive dye is usually used together with the fluorescent color base.

When used in dyeing cotton reactive dyes bring about distinct and stable colours. Yellows, greens, and blues produced in this way are very attractive, but oranges, reds, and pinks are not attractive like those obtained through cation-dyed colours on acrylic textiles. To make up for this weakness fluorescent colour bases are used.

References

- [1] G. Blasse, B.C. Grabmailer, Springer-Verlag, 1994.
- [2] W. de Groot, *Physica* 1939 **6** 275.
- [3] F.A. Kroger, Elsevier, Amsterdam, 1948.
- [4] W. Lehmann, *J. Lumin.* 1972 **5** 87.
- [5] G.F.J. Garlick, D.E. Mason, *J. Electrochem. Soc.* 1949 **96** 90.
- [6] Y. Murayama, N. Takeuchi, Y. Aoki, T. Matsuzawa, US Patent No. 5, 1995 **424** 006.
- [7] T. Matsuzawa, Y. Aoki, N. Takeuchi, Y. Murayama, *J. Electrochem. Soc.* 1996 **143** 2670.
- [8] H. Yamamoto, T. Matsuzawa, *J. Lumin.* 1997 **72** 287.
- [9] J.T.C van Kemendo, G.P.F. Hoeka, *Electrochem. Soc. Spring Meeting Abstract*, San Francisco, 1983, Abstract No. 607.
- [10] B.M.J Smets, *Mater. Chem. Phys.* 1987 **16** 283.
- [11] E. Nakazawa, T. Mochida, *J. Lumin.* 1997 **236** 72.
- [12] T.Katsumata, T. Nabae, K. Sasajima, S. komuro, T. Morikawa, *J. Electrochem. Soc.* 1997 **144** L243.
- [13] C.W. Thiels, H. Cruguel, Y. Sun, *J. Lumin.* 2001 **1** 94.
- [14] E. Nakazawa, Y. Murazaki, S. Saito, *J. Appl. Phys.* 2006 **100** 113.
- [15] F. Clabau, X. Rocquefelte, S. Jobic, P. Denieard, M.H. Whangbo, A. Garcia, T. Mercier, *Solid State Sci.* 2007 **9** 608.
- [16] D. Jia, W.M. Yen, *J. Electrochem. Soc.* 2003 **150** H61.
- [17] F. Clabau, X. Rocquefelte, T. Le Mercier, P. Deniard, S. Jobic, M.H. Whangbo, *Chem. Mater.* 2006 **18** 3212.
- [18] R. C. Ropp, Elsevier, 2004.
- [19] W.M. Yen, S. Shionoya, H. Yamamoto, *Phosphor Hand Book*, CRC press, 1995.
- [20] Luminescence, [online]. Available from <http://www.uvminerals.org/luminese.htm>

[Accessed 11 August 2011].

- [21] Cathodoluminescence [online]. Available from <http://www.cmeba.univ-rennes1.fr/niveau2/PagePrincipeMEB.htm> [Accessed 11 August 2011].
- [22] J. Garc'ia Sol'e, L.E. Baus'a and D. Jaque, Universidad Aut'onoma de Madrid, Madrid, Spain 2005 17.
- [23] Chemoluminescence, [online]. Available from <http://en.wikipedia.org/wiki/Chemoluminescence> [Accessed 12 Sept 2011].
- [24] C. R Ronda, Willy-VCH, Germany, 2008 XIII.
- [25] G. Michael, R. Renata, P. G'érard, 2005 20.
- [26] H.G. Jenkins and J.N. Bowtell, Trans. Illum. Eng. Soc. (London), 1948 **13** 61.
- [27] H.C. Froelich, Trans. Electrochem. Soc. 1948 **93** 101.
- [28] B. Fujita and T.Itou, Toshiba Rev. 1950 **4** 147 (in Japanese).
- [29] H.G.Jenkins, H.G. McKeag and P.W. Ranby J. Electrochem. Soc., 1949 **96** 1.
- [30] Y.Aoki, Japanese Patent Publication (Kokoku) 1954 29-967.
- [31] R. Kane and H. Sell, The Fairmont Press, Georgia (2001) p93.
- [32] S. Itoh, H.Toki, F. Kataoka, K.Tamura and Y.Sato, Extended Abstracts of The Third International Conference on the Science and Technology of Display Phosphors, 1997 275.
- [33] FED, [online]. Available from http://www.televisions.com/News/Sony_spinoff_gives_up_development_of_FED.php [Accessed 16 June 2011].
- [34] Weber, L. F. Conf. Proc. SID 00 Digest 2000 402.
- [35] B. Gellert, and U. Kogelschatz Appl. Phys. B, 1991 **52** 14.
- [36] L. F. Weber, (ed. L. E. Tannas), Van Nostrand Reinhold Company, New York 1985 332.
- [37] Flat panel display, [online]. Available from http://en.wikipedia.org/wiki/Flat_panel_display [Accessed 12 July 2010].
- [38] G. Destriau, J. Chem. Phys., 1936 **33** 587.
- [39] D. Kahng, Appl. Phys. Lett., 1968 **13** 210.
- [40] E.W. Chase, R.T. Hoppelwhite, D.C. Krupka and D. Kalong, J. Appl. Phys.1969 **40** 2512.

- [41] T. Inoguchi, M.Takeda, Y. Kakihara, Y.Nakata and M.Yoshida in Digest, 1974 SID (Society for Information Display) Int. Symp., 1974, 84.
- [42] M. R. Krames, et al. Appl. Phys. Lett., 1999 **75** 2365.
- [43] Signs & Tape, [online]. Available from <http://www.glonation.com/signs-and-tape.html> [Accessed 17 July 2010].
- [44] Neon open sign, [online]. Available from <http://www.neonlick.de/index.htm> [Accessed 10 June 2010].
- [45] Glow in The Dark Ink and Paint, [online]. Available from <http://www.made-inchina.com/showroom/santana44/product-detailHoemBgCPXzhp/China-Glow-in-The-Dark- Ink-and-Paint.html>. [Accessed 17 June 2010].
- [46] Glow in the dark tees, [online]. Available from <http://nsb.org/index.php/2007/03/21/nikeglow-in-the-dark-tees/>. [Accessed 17 June 2010].
- [47] Nike 'Illumination' Pack, [online]. Available from <http://english.mashkulture.net/2007/03/01/nike-illumination-pack/> . [Accessed 17 June 2010].

Chapter 3

Luminescent Mechanism of Long Afterglow $\text{CaAl}_2\text{O}_4:\text{Eu}^{2+}, \text{Nd}^{3+}, \text{Dy}^{3+}$ Phosphor

Introduction

Long afterglow phosphors are luminescent materials that have emission that persist for long even after the removal of the exciting source. The long afterglow phosphors to be discussed in this study are different from the radiation stimulated phosphors which rely on nuclear decay radiation as an excitation source [1]. The mechanism of long afterglow of $\text{CaAl}_2\text{O}_4:\text{Eu}^{2+}, \text{Nd}^{3+}, \text{Dy}^{3+}$ phosphor rather relies on the trapped electrons produced by an excitation source. $\text{CaAl}_2\text{O}_4:\text{Eu}^{2+}, \text{Nd}^{3+}, \text{Dy}^{3+}$ phosphors are solid inorganic materials consisting of a host lattice (CaAl_2O_4), usually intentionally doped with impurities (Eu^{2+} as dopant, Nd^{3+} and/or Dy^{3+} as co-dopants).



Figure 3.1: White body colour of phosphors

The concentration of these impurities are generally kept low due to the fact that the efficiency of the luminescence process usually decreases at higher concentrations due to effect of concentration quenching. Most phosphors have white body colour, (see Figure 3.1) which is an essential feature that prevents absorption of visible light by the phosphors [2].

Earlier Models

Many researchers differently explained with experimental evidences the mechanism of long persistent phosphorescence of the inorganic phosphors doped with rare earth metal ions.

Earlier model by Matsuzawa *et al* (Figure 3.2) [3] proposed that when $\text{SrAl}_2\text{O}_4:\text{Eu}^{2+},\text{Dy}^{3+}$ phosphor is irradiated with UV, the Eu^{2+} cations are excited from the ground state ($4f^7$) to an excited state ($4f^65d^1$): $\text{Eu}^{2+} (4f^7) + h\nu \rightarrow \text{Eu}^{2+*} (4f^65d^1)$ thereby leaving behind a hole in the f orbital in the vicinity of the valence band (VB).

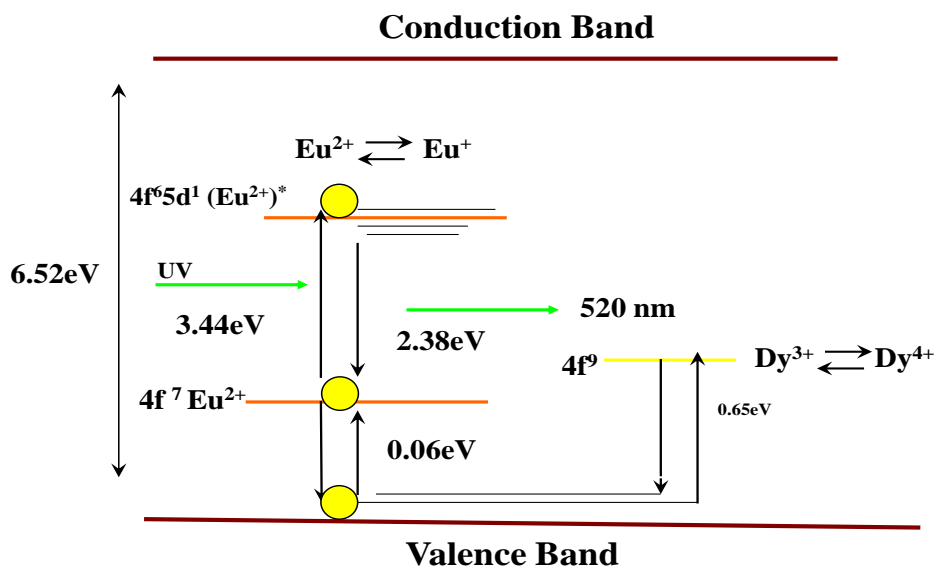


Figure 3.2: Phosphorescence mechanism proposed by Matsuzawa *et al.* [3] (Eu^{2+*} - excited state of Eu^{2+})

Consequently an electron from the CB is captured causing Eu^{2+} be reduced to $\text{Eu}^+:\text{Eu}^{2+}:\text{Eu}^{2+*} + e^- \rightarrow \text{Eu}^+$. A Dy^{3+} cation located in suitable depth captures the hole created in the VB to form a Dy^{4+} cation: $\text{Dy}^{3+} + h^+ \rightarrow \text{Dy}^{4+}$. It is purported that the de-excitation of Eu^{2+} to the ground state is due to the thermo-activation of an electron from the VB to the first unoccupied

levels of Dy^{4+} followed by the migration of trapped hole to a photo-generated Eu^+ cation [4]. This model was supported by photoconductivity measurements that confirmed the hole as the main photo carrier [5, 6]. This approach was aimed in part to support the hole type photoconductivity of $\text{SrAl}_2\text{O}_4:\text{Eu}^{2+}$ phosphor under the UV illumination discovered by Abbruscato [6] and was for long period of time used to explain the phosphorescence mechanism of numerous materials.

However, it has recently been shown by researchers that the model operates on highly improbable assumptions. First, the reduction $\text{Eu}^{2+} + e^- \rightarrow \text{Eu}^+$ is highly unlikely (and needs high energy ≥ 4 eV), and so is the oxidation $\text{Dy}^{3+} + h^+ \rightarrow \text{Dy}^{4+}$, due to the chemical instabilities of Eu^+ and Dy^{4+} ions [4].

Secondly, Dorenbos recently pointed out that the proposed $\text{VB} \rightarrow \text{Eu}^{2+*} (4f^{6+}5d^1)$ transition leading to the final $4f^75d^1$ electronic configuration of Eu^+ is based on an incorrect concept of a hole state [7]. Calculations of electronic band structure for $\text{SrAl}_2\text{O}_4:\text{Eu}^{2+}$ showed that the Eu d -block lies just below the bottom of CB and $4f$ -block of Eu at approximately 3eV above the top of VB [8]. These observations are not in agreement with the mechanism of Matsuzawa *et al.*

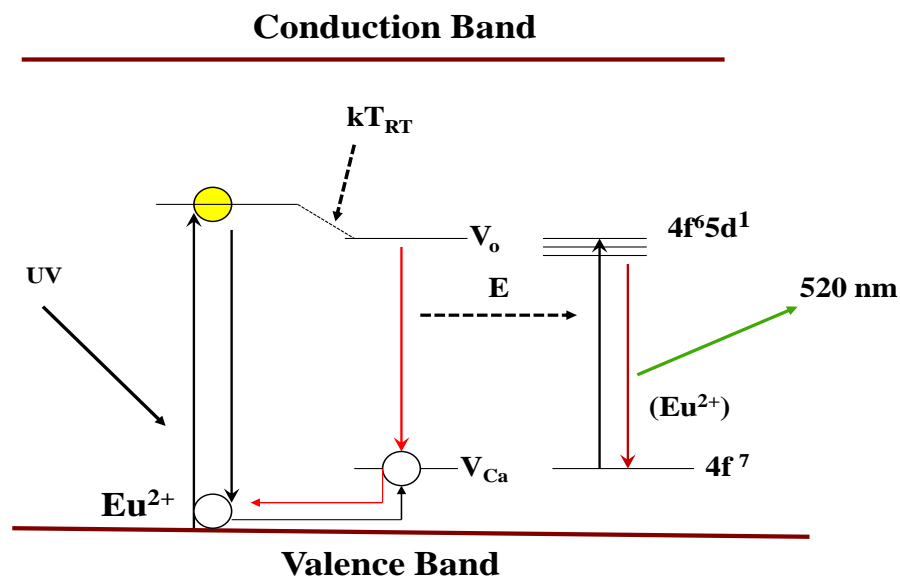


Figure 3.3: Phosphorescence mechanism proposed by Aitasalo *et al* [10].

These drawbacks opened a new set of studies that saw the modification of the Matsuzawa model of long persistent phosphorescence by Beauger [9] and then by Aitasalo *et al.* [10]. They proposed that the UV excitation promotes an electron from the VB to a discrete level of unknown origin, while the hole created near the VB is trapped by an alkaline earth cation vacancy level V_{Ca} . Then, the thermal energy (kT_{RT}) enables the electron to be transferred from the discrete level of unknown origin to the oxygen vacancy (V_o) located near to it, from which recombination takes place towards the V_{Ca} level. The energy dissipated in the process is then transferred to a Eu^{2+} ion, which gets excited and then de-excited instantaneously leading to emission of visible light. The Dy^{3+} co-dopant is considered to play the role of increasing the number of cation vacancies and the depth of the existing vacancies [4]. This model is shown in Figure 3.3.

In $SrAl_2O_4:Eu^{2+},Dy^{3+}$ phosphor the concentration of Eu^{2+} cation has been shown by EPR measurements to decrease under UV irradiation and increases once the irradiation is stopped [11]. This observation is not in line with the process of energy transfer proposed by Beauger and by Aitasalo *et al* [4].

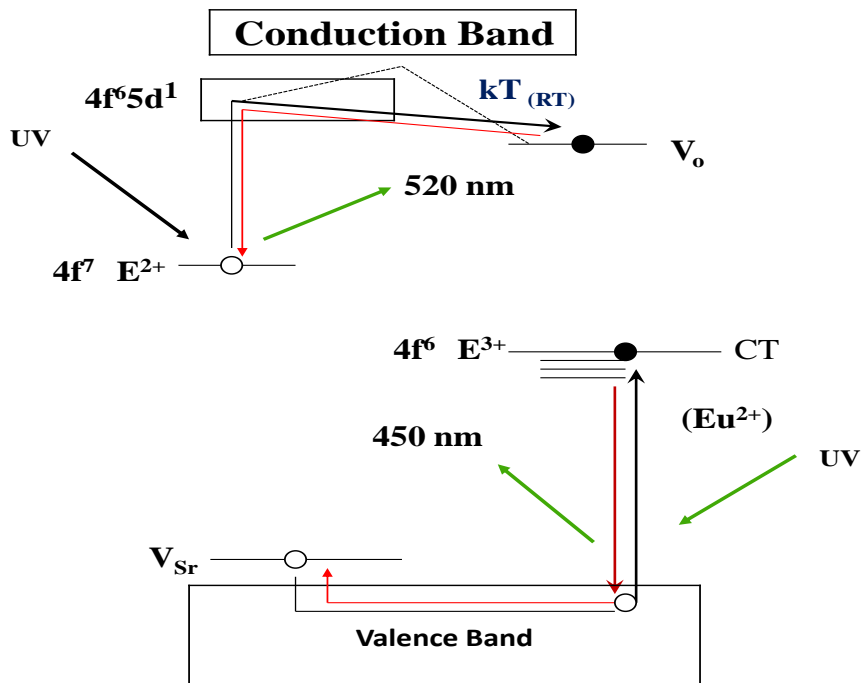


Figure 3.4: Phosphorescence mechanism proposed by F. Clabau *et al* [5, 8].

In order to account for these shortcomings, F. Clabau *et al.* proposed a new phosphorescence mechanism [5, 8] which is schematically represented in Figure 3.4. It puts into considerations the facts that;

(a) the *d*-block levels of Eu^{2+} cations partially overlap with the bottom of the conduction band (CB) as suggested from electronic band structure calculations performed for a hypothetical composition $\text{Sr}_{0.75}\text{Eu}_{0.25}\text{Al}_2\text{O}_4$ [4],

(b) the f^7 ground state of Eu^{2+} lies in the middle of the forbidden band gap as suggested by X ray Photoelectron Spectroscopy (XPS) experiments[12],

(c) the Eu^{2+} cations can be oxidized under irradiation because both Eu^{2+} and Eu^{3+} species are stable species in oxides thus the concentration of Eu^{2+} cations could be changed under UV irradiation [4].

The mechanism proposed by F. Clabau *et al* can also be adopted to describe the process of long afterglow in $\text{CaAl}_2\text{O}_4: \text{Eu}, \text{Nd}^{3+}, \text{Dy}^{3+}$ phosphors studied in this work as follows; Optical excitation energy is stored in the lattice by trapping of photo excited charge carriers. After optical excitation of Eu^{2+} , Eu^{2+} is oxidized to Eu^{3+} and $\text{Nd}^{3+}/ \text{Dy}^{3+}$ is reduced to $\text{Nd}^{2+}/ \text{Dy}^{2+}$. Thermal excitation of $\text{Nd}^{2+}/ \text{Dy}^{2+}$ to $\text{Nd}^{3+}/ \text{Dy}^{3+}$, followed by capture of the electron by Eu^{3+} and subsequent Eu^{2+} emission, results in time-delayed Eu^{2+} emission. The thermal excitation process of $\text{Nd}^{3+}/ \text{Dy}^{3+}$ determines the time delay. This particular material still generates visible emission after several hours in the dark [2].

References

- [1] S. Shionoya, W.M. Yen, Phosphors Handbook, CRC Press, USA, 1998, 95.
- [2] C. R Ronda, Willy-VCH, Germany, 2008, 3.
- [3] T. Matsuzawa, Y. Aoki, N. Takeuchi, N. Maruyama, Y. J. Electrochem. Soc. 1996, **143** 2670.
- [4] H. N. Luitel, PhD Thesis, Saga University, 2010, 94-95.
- [5] F. Clabau, X. Rocquefelte, S. Jobic, P. Denieard, M.H. Whangbo, A. Garcia, T. Mercier, Solid State Sci. 2007 **9** 608.
- [6] V. Abbruscato, J.Electrochem.Soc. 1971 **118** 930.
- [7] P. Dorenbos, J. Electrochem. Soc. 2005 **152** H107.
- [8] F. Clabau, X. Rocquefelte, S. Jobic, P. Deniard, M.H. Whangbo, A. Garcia, T.L. Mercier, Chem. Mater. 2005 **17** 3904.
- [9] C. Beauger, Thesis, Universite de Nice, France, 1999.
- [10] T. Aitasalo, P. Deren, J. Hölsa, H. Jungner, J. Krupa, M. Lastusaari, J. Legendziewicz, J. Niittykoski, W. Streck, J. Solid State Chem. 2003 **171** 114.
- [11] Rhodia Electronics and Catalysis, Private Communication, 2001.
- [12] F. Clabau, thesis, University of Nantes, France, 2005.

Chapter 4

Investigation Techniques of Long Afterglow Phosphors

4.1. Synthesis Methods for Long Afterglow $\text{CaAl}_2\text{O}_4:\text{Eu}^{2+}, \text{Nd}^{3+}, \text{Dy}^{3+}$ Phosphors

4.1.1 Solution-Combustion Method

The solution – combustion method is an important chemical route for the synthesis and processing of advanced ceramics (structural and functional), catalysts, composites, alloys, inter-metallics and nanomaterials [1]. The method has generated more interest in the field of nanomaterials such as luminescent materials (phosphors) and other ceramic materials, because fine particle sizes, multi-component, crystalline and homogenous materials can be achieved at relatively low temperature and less time [2].

In this technique (3-8) a saturated aqueous solution of the desired metal salts and a suitable organic fuel is made to boil, until the mixture ignites and a self-sustaining and rather fast combustion reaction occurs, resulting in a dry, usually crystalline, fine oxide powder. To form a mixed oxide, a mixture containing the desired metal ions, in the form of, for instance, water soluble nitrate salts, a fuel such as urea, glycine or ethylene glycol can be used. usually redox reactions such as this are exothermic in nature and often lead to explosion if not controlled, but in this technique the combustion of metal nitrates-urea mixtures usually occurs as a self-propagating and non-explosive exothermic reaction. The large amounts of gases formed can result in the appearance of a flame, which can reach temperatures in excess of 1000 °C.

In this method, the energy released from the exothermic reaction between the nitrates and the fuel, which is usually ignited at a temperature much lower than the actual phase transformation temperature, can rapidly heat the system to a high temperature and sustain it long enough, even in the absence of an external heat source, for the synthesis to occur [9].

The luminescent materials (phosphors) prepared by this method have low density, fluffy texture and ultra fine particles. As more gases are released, either agglomerates are not formed or disintegrated into fine particles [10].

In recent years, with the development of the synthesis technologies on materials, several chemical methods have been applied to prepare luminescence powders [11], of which combustion synthesis is the most important one. There are many merits of the combustion synthesis. First, the process is conducted in the liquid state, so that each component can be accurately controlled and uniformly mixed. Second, the process, which has been extensively applied to preparation of various nano-scale materials, takes only a few minutes [12]. Third, it involves inexpensive processing equipment. Fourth, the final product is obtained in only one step using the chemical energy of the reactants and finally the final products are of high purity due to liberation of volatile impurities [13].

4.2. Characterization Methods for Long Persistent $\text{CaAl}_2\text{O}_4:\text{Eu}^{2+}, \text{Nd}^{3+}, \text{Dy}^{3+}$ Phosphors

In this research work, the $\text{CaAl}_2\text{O}_4:\text{Eu}^{2+}, \text{Nd}^{3+}, \text{Dy}^{3+}$ phosphor powders were characterized using Scanning Electron Microscopy (SEM), Energy Dispersive x-ray Spectroscopy (EDS), X-ray Diffraction (XRD), Photoluminescence spectroscopy (PL), Fourier Transform Infra-Red (FT-IR) spectroscopy and Thermoluminescence spectroscopy (TL). The theory of these characterization techniques are covered in this chapter. It also gives the experimental set-up and layout of the methods used for characterization.

4.2.1. Scanning Electron Microscopy (SEM)

Scanning electron microscopy (SEM) is used to study the topographical and morphological structures of specimens at very high magnifications which can go to more than 30 000 X. During SEM analysis, a beam of energetically well-defined and highly focused electrons is scanned across a sample. The SEM consists of an electron optical column mounted on a vacuum chamber with electron gun placed on top of the column [13], as illustrated in Figure 4.1. The microscope electron gun consists of tungsten or lanthanum hexaboride (LaB_6) filament source or a field emission electron gun which is used to generate electrons, when the applied current causes resistance heating which generates the electrons [14]. It is pumped using turbo and ion pumps to maintain the highest possible vacuum [15].

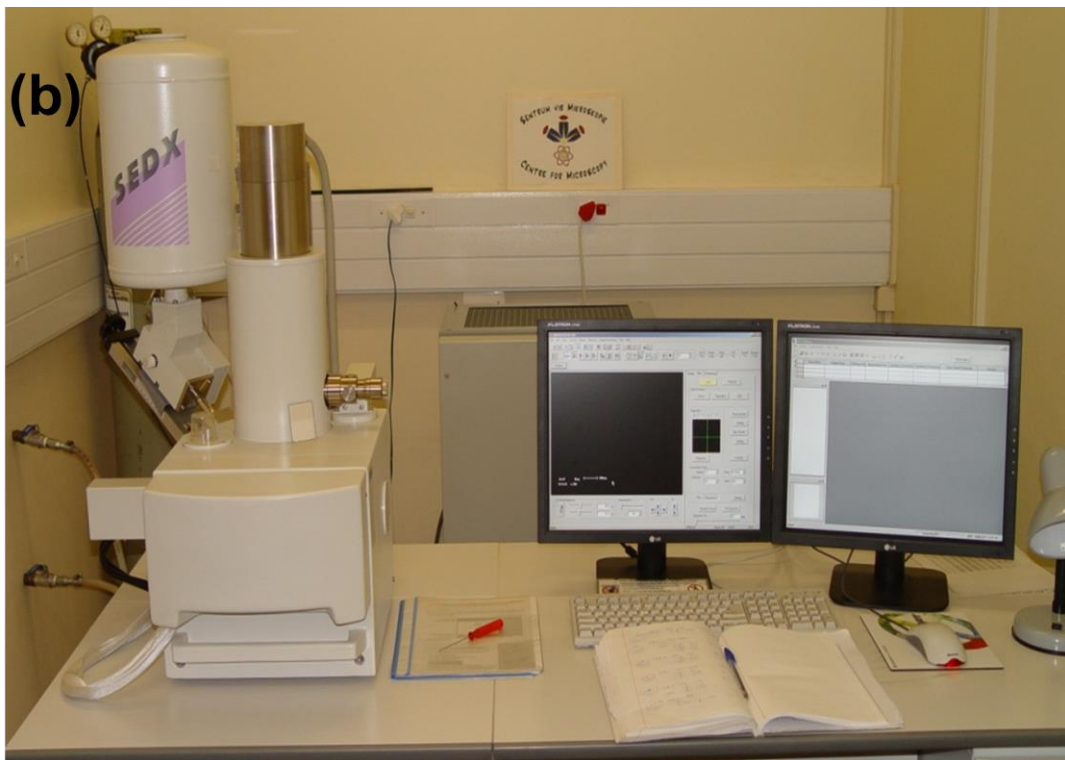
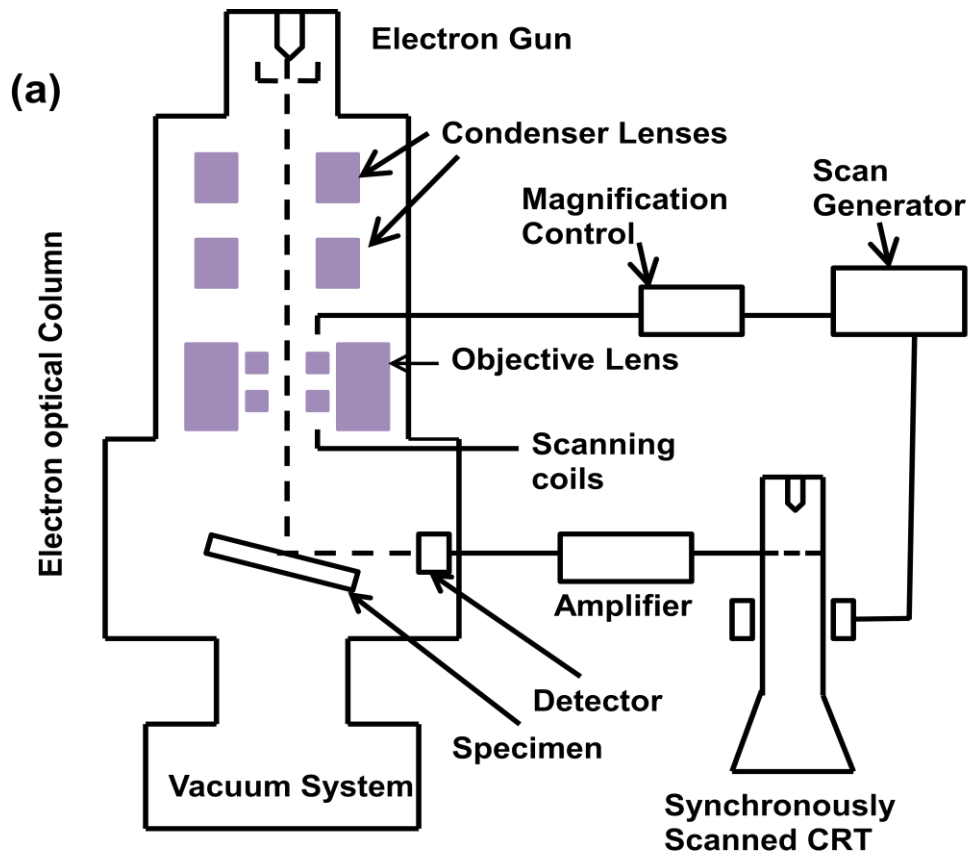


Figure 4.1(a) Schematic Diagram of a SEM [14]. (b) SEM system at the Centre for Microscopy at UFS

The technique can provide information about topography, morphology and crystallography of only conducting and semiconducting materials [16].

If the system is equipped with energy dispersive x-ray spectrometer (EDS), it can also provide information about chemical composition of the material [17].

The basic principle of the system is that, when a high energy electron beam impinges on the sample surface it generates a splash of electrons with kinetic energies much lower than the primary incident electrons called secondary electrons [15]. Depending on the nature of the sample, these can include secondary electrons (electrons from the sample itself), backscattered electrons (beam electrons from the filament that bounce off nuclei of atoms in the sample) and X-rays [13] as shown in Figure 4.2.

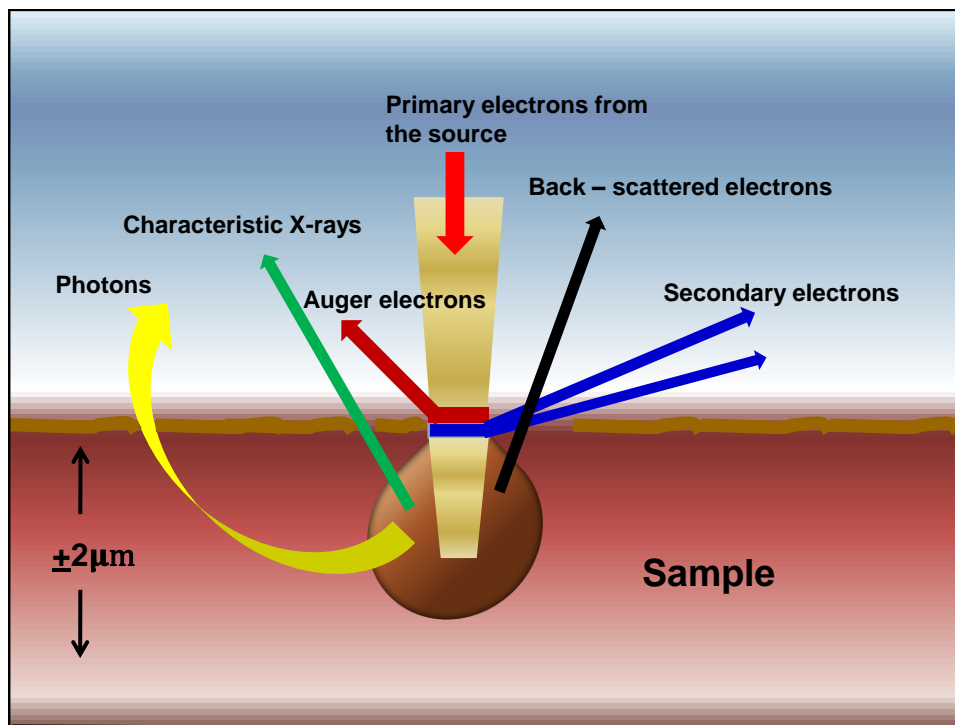


Figure 4.2: Electrons produced in SEM [19].

An image of the sample surface is constructed by measuring the secondary electron intensity as a function of the primary beam position. The SEM has many advantages over traditional microscopes. It has a large depth of field, which allows more of a specimen to be in focus at one time. The SEM also has much higher resolution, so closely spaced specimens can be magnified at much higher levels. Because the SEM uses electromagnetic lenses, the researcher has much more control in the degree of magnification. All of these advantages, as well as the actual strikingly clear images, make the scanning electron microscope one of the most useful instruments in research today [18].

4.2.2. Energy Dispersive x-ray Spectroscopy (EDS)

The surface chemical or elemental composition of the synthesized powders grown in this research study was determined by EDS spectroscopy. (EDS or EDX) is a chemical microanalysis technique used in conjunction with scanning electron microscopy (SEM). The EDS technique detects X-rays emitted from the sample during bombardment by an electron beam to characterize the elemental composition of the analyzed volume. Features or phases as small as 1 μm or less can be analyzed [20].

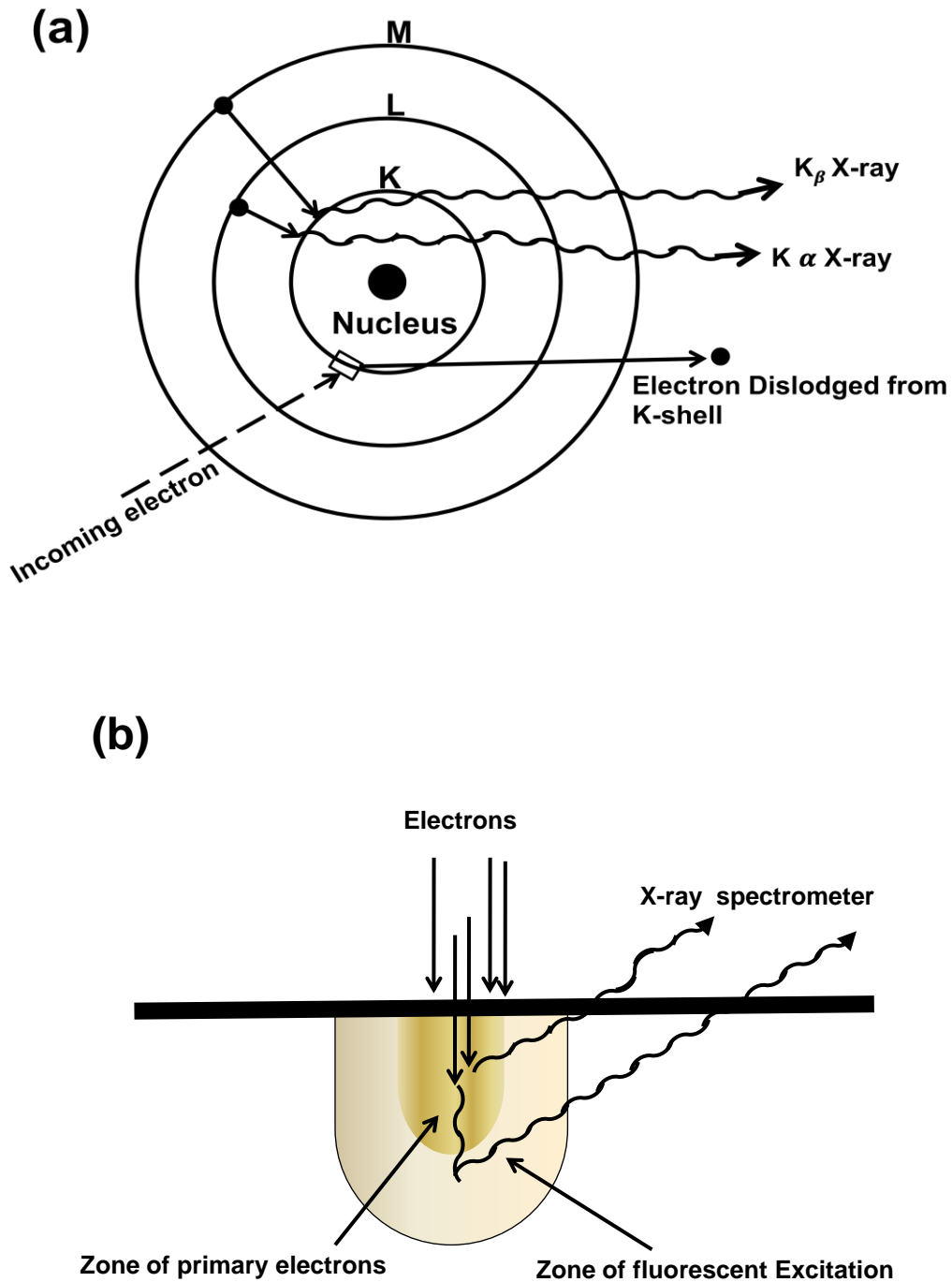


Figure 4.3: (a) and (b) Characteristic x-ray radiation [22].

Information about the chemical composition of the sample is obtained by measuring the intensity distribution and energy of the signal generated by a focussed electron beam impinging on the sample. The source of the electron is the electron gun of a scanning electron microscope. The incident beam of electrons interacts with core electrons of the sample's atoms transferring sufficient energy to it, thereby ejecting it from the target atom. This results in the creation of a hole within the atom's electronic structure. An electron from an outer, higher energy shell then occupies the hole releasing excess energy in the form of an X-ray photon. As a result of electronic transitions which occur between the outer and inner core levels a characteristic X-ray is emitted when the ionized atom 'relaxes' to a lower energy state by the transition of an outer-shell electron to the vacancy in the core shell which provide a quantitative and qualitative elemental composition of the sample [21]. Due to a well defined nature of the various atomic energy levels, it is clear that the energies and associated wavelengths of the set of x-rays will have characteristic values for each of the atomic species present in a sample [21] as shown in Figure 4.3.

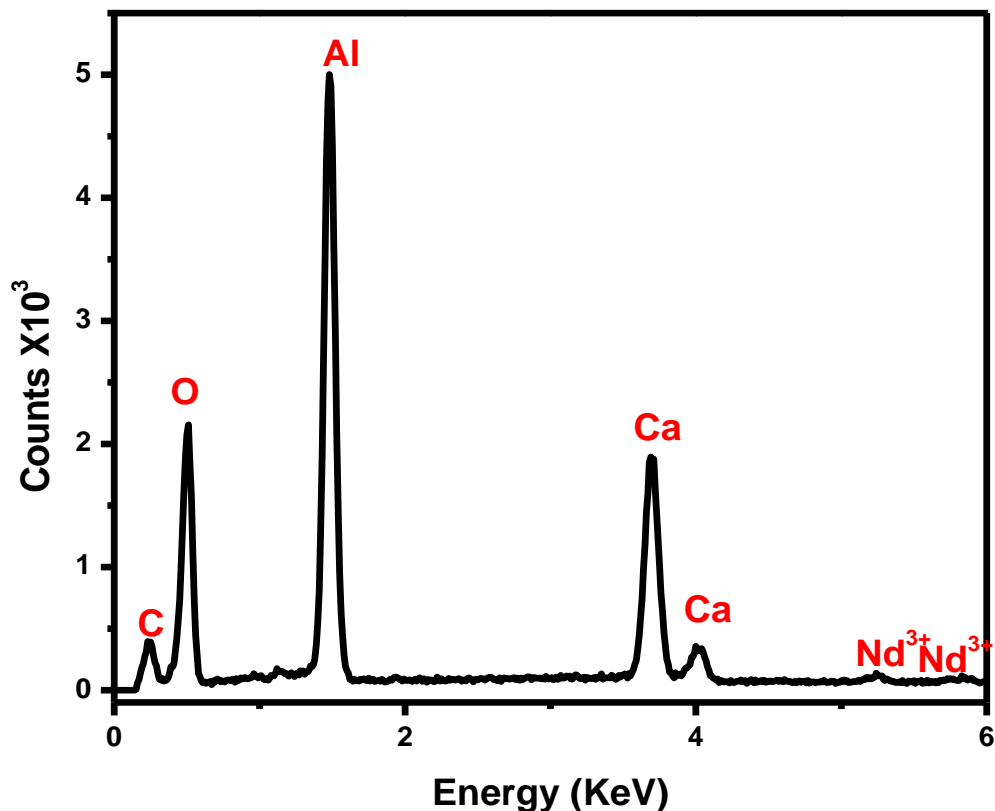


Figure 4.4: Example of an EDS spectrum of $\text{CaAl}_2\text{O}_4:\text{Eu}^{2+}, \text{Nd}^{3+}$.

A characteristic X-ray is usually emitted when the ionized atom ‘relaxes’ to a lower energy state by the transition of an outer-shell electron to the vacancy in the core shell. The X-ray is called characteristic because its energy equals the energy difference between the two levels involved in the transition and this difference is characteristic of the material.

From the output of an EDS analysis we obtain an EDS spectrum, see Figure 4.4. The EDS spectrum shows the frequency in counts of X-rays received for each energy level. The spectrum normally plots the peaks corresponding to the energy levels for which the most X-rays have been received. Each of these peaks corresponds to a specific atom, and therefore characteristic of a specific element. The intensity of a peak in the spectrum correlates with the concentration of the element in the sample [23].

4.2.3. X-ray Diffraction (XRD)

X-ray diffraction (XRD) is an efficient analytical non-destructive technique used to investigate structural properties of crystalline materials. It is also used for phase identification, determination of grain size, composition of solid solution, lattice constants, and degree of crystallinity in a mixture of amorphous and crystalline substances [24]. An amorphous sample consists of atoms arranged in a random way for example glasses. A sample is said to be crystalline if the atoms are arranged in such a way that their lattice positions are exactly periodic.

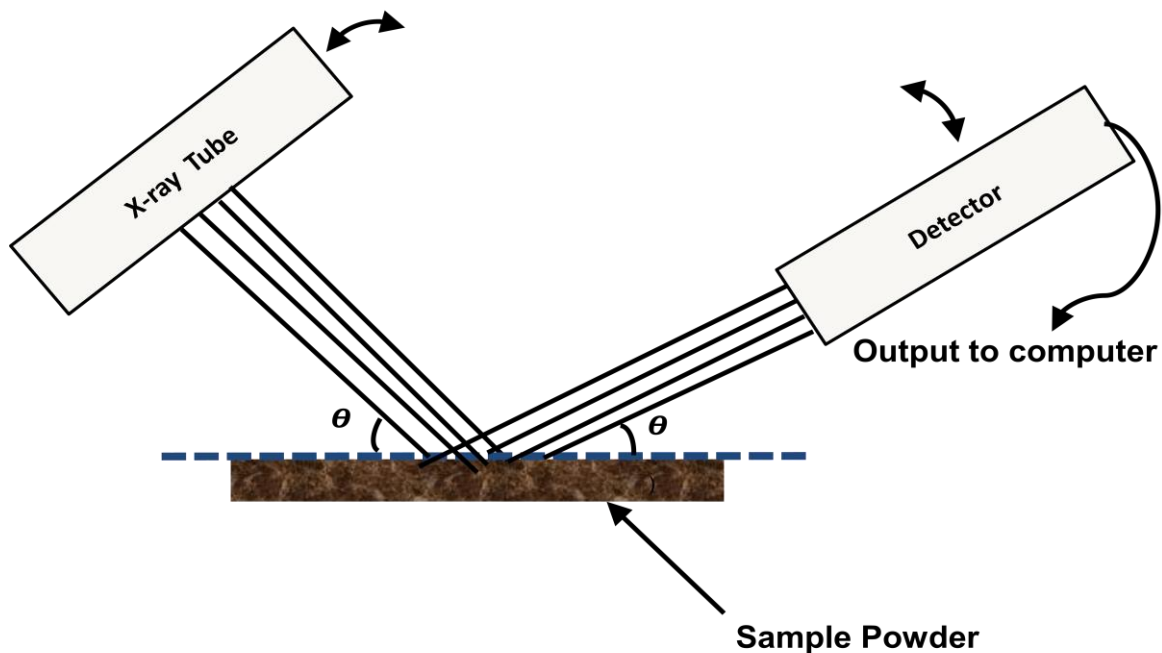


Figure 4.5: An x-ray powder diffractometer [27].

Crystalline materials include ceramics, metals, electronic materials, organics and polymers. The X-ray diffractometer fall into two broad classes viz; single crystals and powder. The powder diffractometer, Figure 4.5 is routinely used for phase identification and quantitative phase analysis [25]. X-ray diffractometer consist of three basic elements: an X-ray tube, a sample holder, and an X-ray detector. X-rays are produced in the X-ray tube. Such a tube is illustrated in Figure 4.6. It consists of an evacuated chamber with a tungsten filament at one end of the tube, called the cathode, and a metal target at the other end, called an anode. Electrical current is run through the tungsten filament, causing it to glow and emit electrons. A large voltage difference (measured in kilovolts) is placed between the cathode and the anode, causing the electrons to move at high velocity from the filament to the anode target.

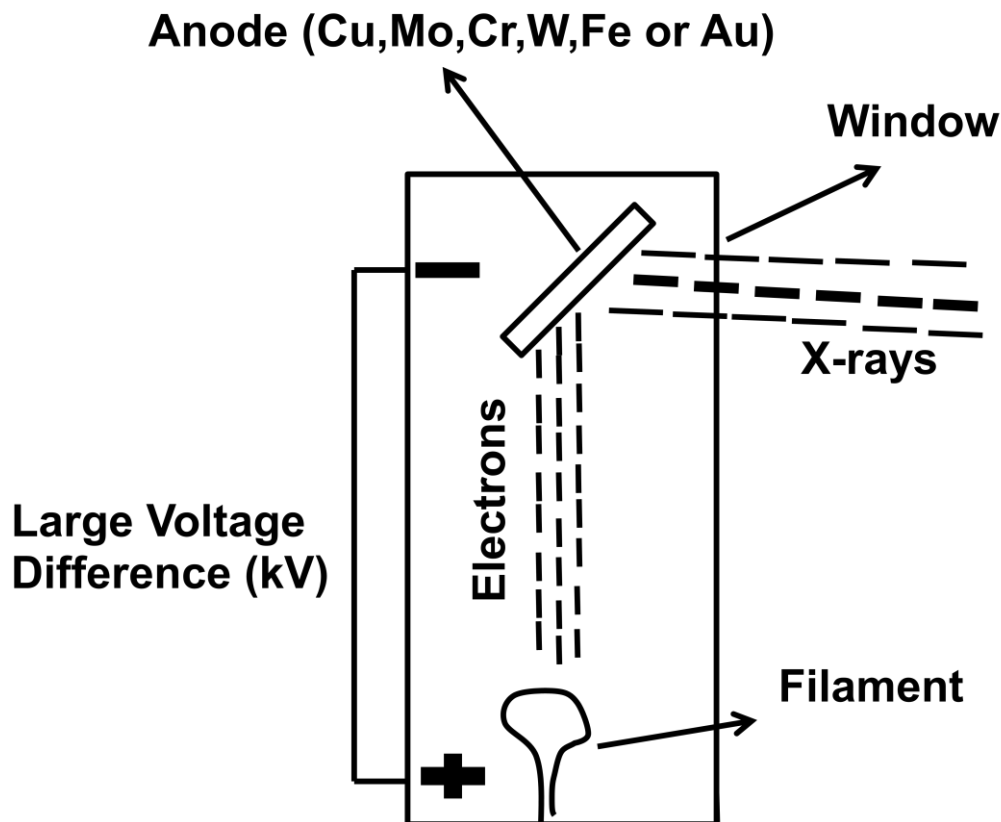


Figure 4.6: Schematic diagram of an X-ray tube [27].

Upon striking the atoms in the target, the electrons dislodge inner shell electrons resulting in outer shell electrons having to jump to a lower energy shell to replace the dislodged electrons. These electronic transitions results in the generation of X-rays. The X-rays then move through a window in the X-ray tube producing characteristic X-ray spectra which can be used to provide information on the internal arrangement of atoms in crystals or the structure of

internal body parts. These X-ray spectra consist of several components and the most common are $K\alpha$ and $K\beta$ as shown in Figure 3.7 (a) [27].

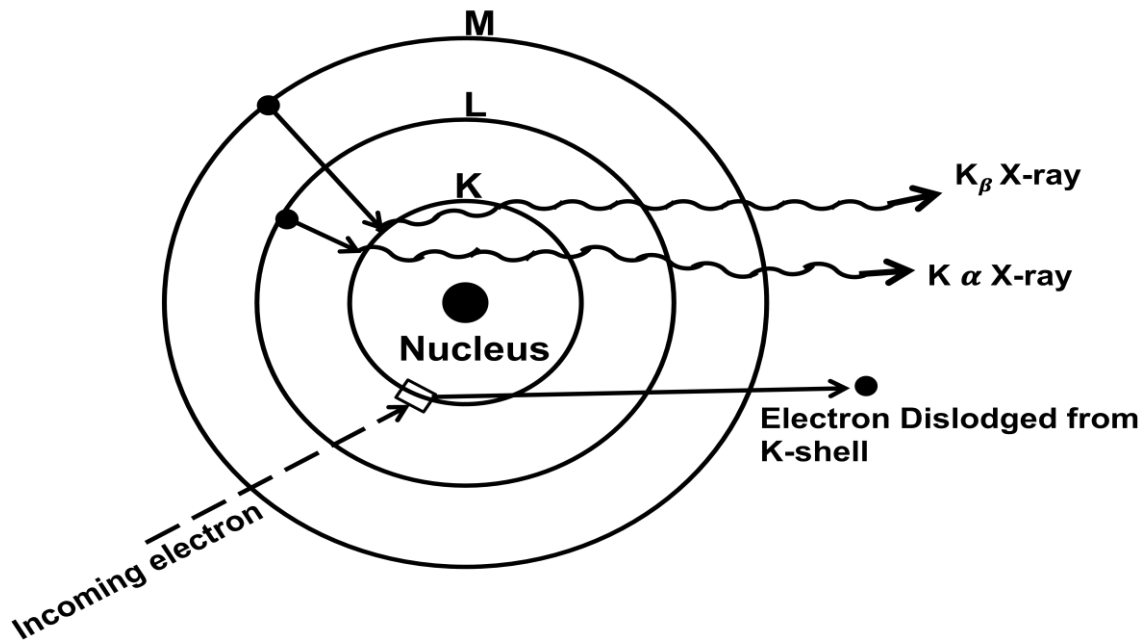


Figure 4.7: Characteristic X-ray Radiation [27]

The target materials that are usually used are Cu, Fe, Mo and Cr. Each of these has specific characteristic wavelengths [26] as shown in table 4.1.

Table 4.1: Characteristic wavelengths of target materials [27].

	Element	$K\alpha$ Wavelength (λ) \AA
	Mo	0.7107
	Cu	1.5418
	Co	1.7902
	Cr	2.2909

4.2.3.1. Continuous and Characteristic X-ray Spectra

When the target material of the X-ray tube is bombarded with electrons accelerated from the cathode filament, two types of X-ray spectra are produced. The first is called the **continuous spectra**. The continuous spectra consist of a range of wavelengths of X-rays with minimum wavelength and intensity (measured in counts per second) dependent on the target material and the voltage across the X-ray tube. The minimum wavelength decreases and the intensity increases as voltage increases as shown in Figure 4.8.

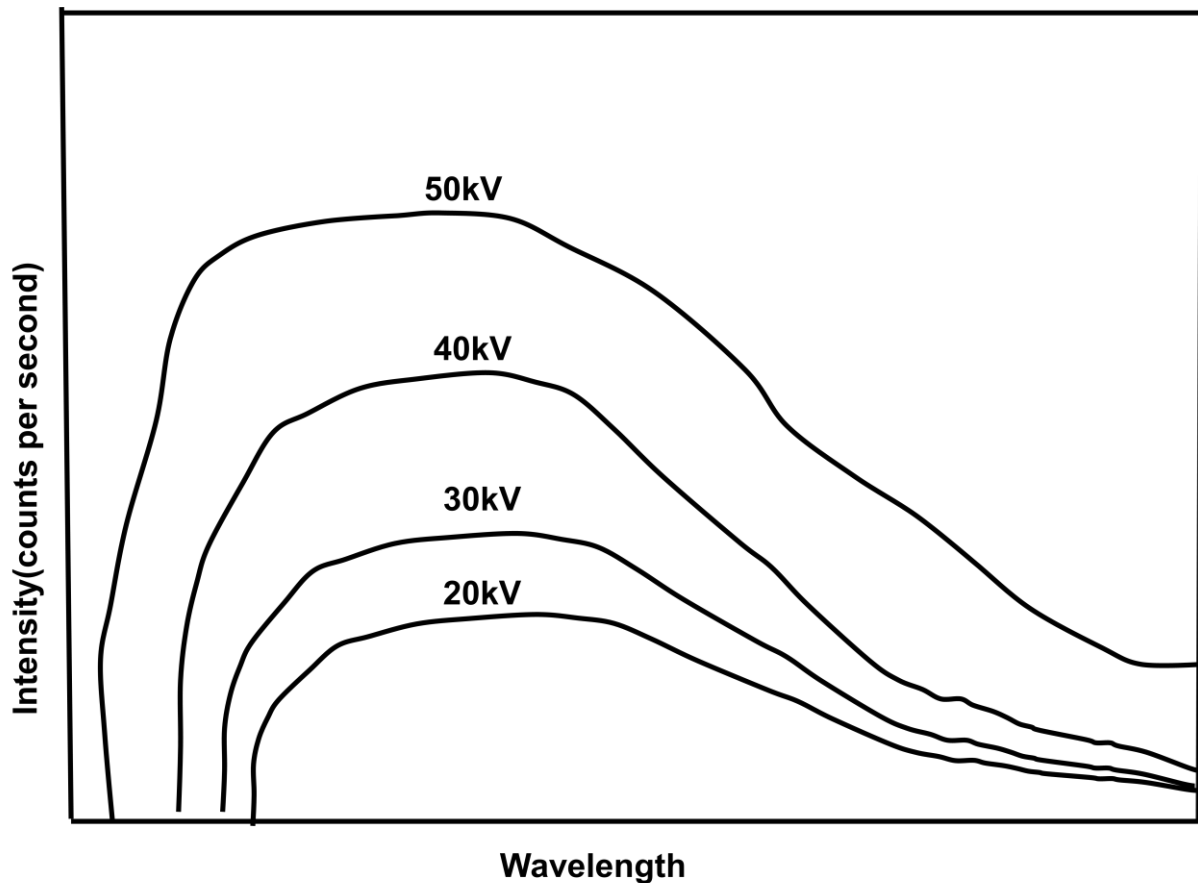


Figure 4.8: The continuous X-ray spectra [27].

The second type of spectra, called the *characteristic spectra*, is produced at high voltage as a result of specific electronic transitions that take place within individual atoms of the target material. This is easiest to see using the simple Bohr model of the atom. In such a model, the nucleus of the atom containing the protons and neutrons is surrounded by shells of electrons. The innermost shell, called the K- shell, is surrounded by the L- and M - shells. When the energy of the electrons accelerated toward the target becomes high enough to dislodge K-shell electrons, electrons from the L - and M - shells move in to take the place of those

dislodged. Each of these electronic transitions produces an X-ray with a wavelength that depends on the exact structure of the atom being bombarded. A transition from the L – shell, to the K- shell produces a $K\alpha$ X-ray, while the transition from an M - shell to the K- shell produces a $K\beta$ X-ray. These characteristic X-rays have a much higher intensity than those produced by the continuous spectra, with $K\alpha$ X-rays having higher intensity than $K\beta$ X-rays see Figure 4.9. The important point here is that the wavelength of these characteristic x-rays is different for each atom in the periodic table (of course only those elements with higher atomic number have L- and M - shell electrons that can undergo transitions to produce X-rays).

A filter is generally used to filter out the lower intensity $K\beta$ X-rays. For commonly used target materials in X-ray tubes, the X-rays have the well-known experimentally determined wavelengths shown in table 4.1.

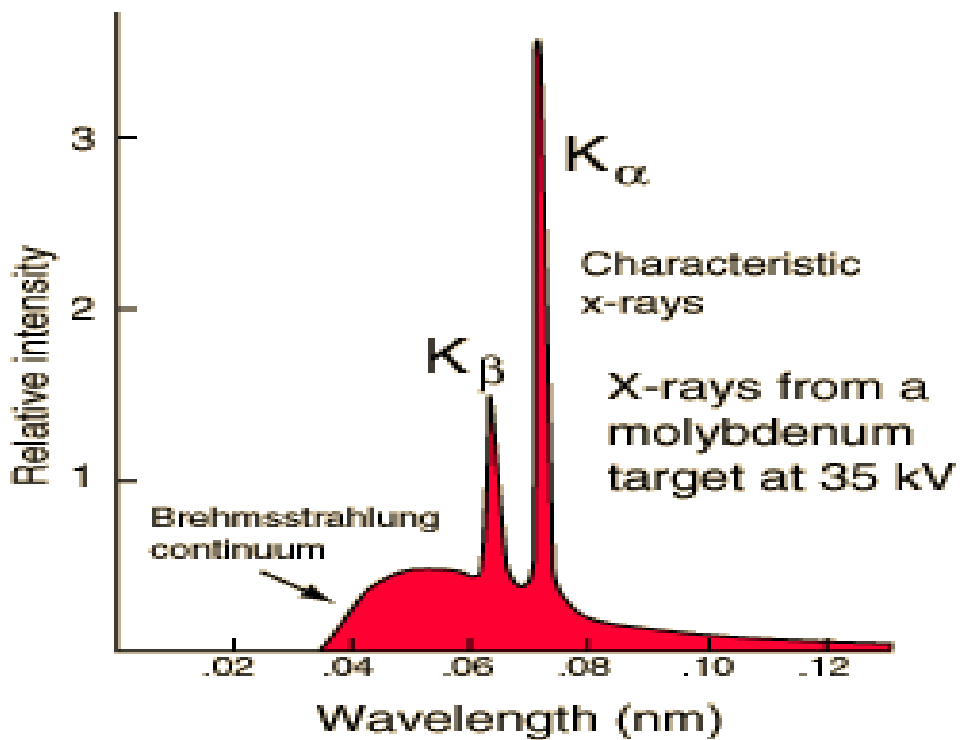
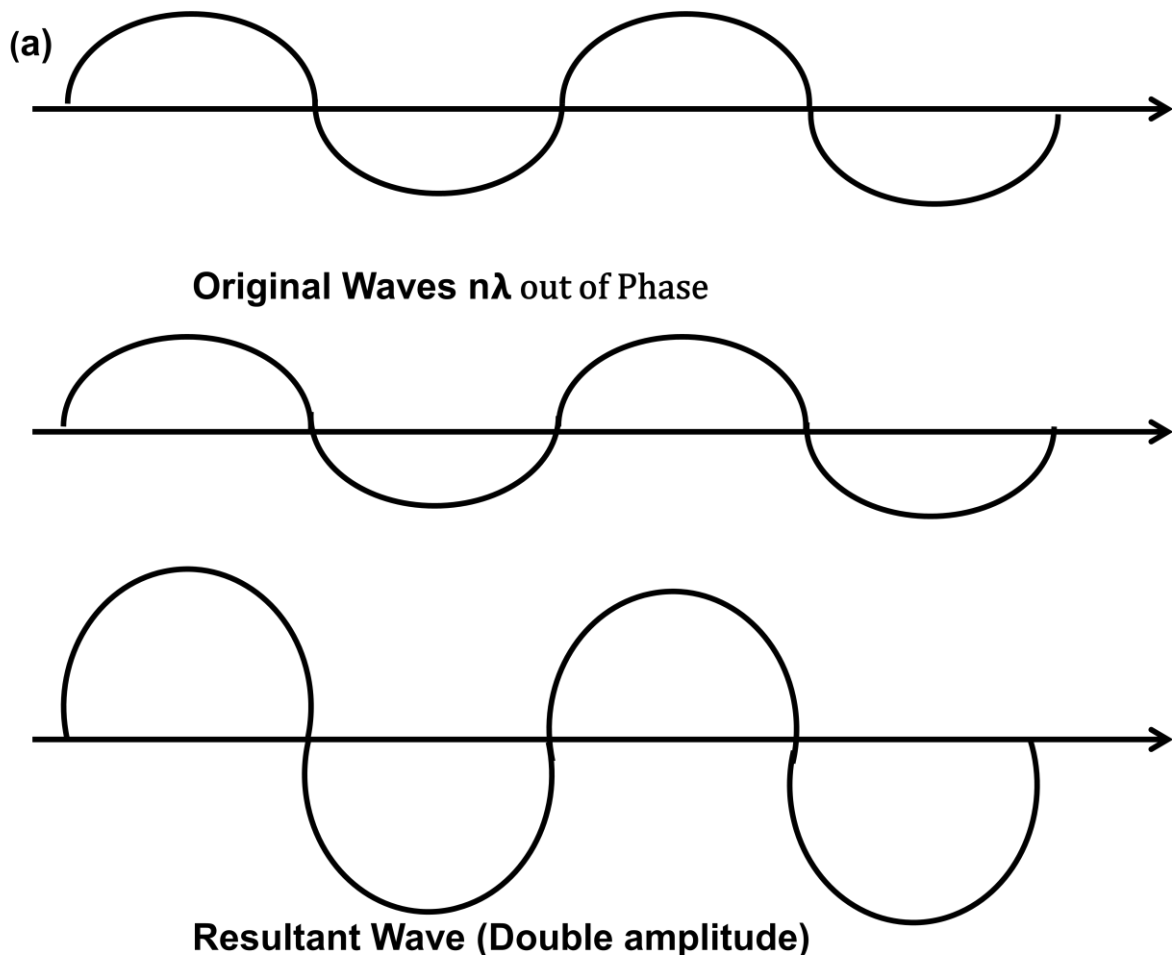


Figure 4.9: Intensity of characteristic $K\alpha$ X-rays and $K\beta$ X-rays [27].

4.2.3.2. Interference

A beam of X-rays consists of a bundle of separate waves which can interact with one another. Such interaction is termed *interference*. Interference of waves can be either *constructive* or *destructive*.

Constructive interference When a monochromatic beam of wavelength λ is projected on to a crystalline material at angle θ diffraction occurs only when the distance travelled by the rays reflected from the successive planes differs by a complete number n of wavelengths.



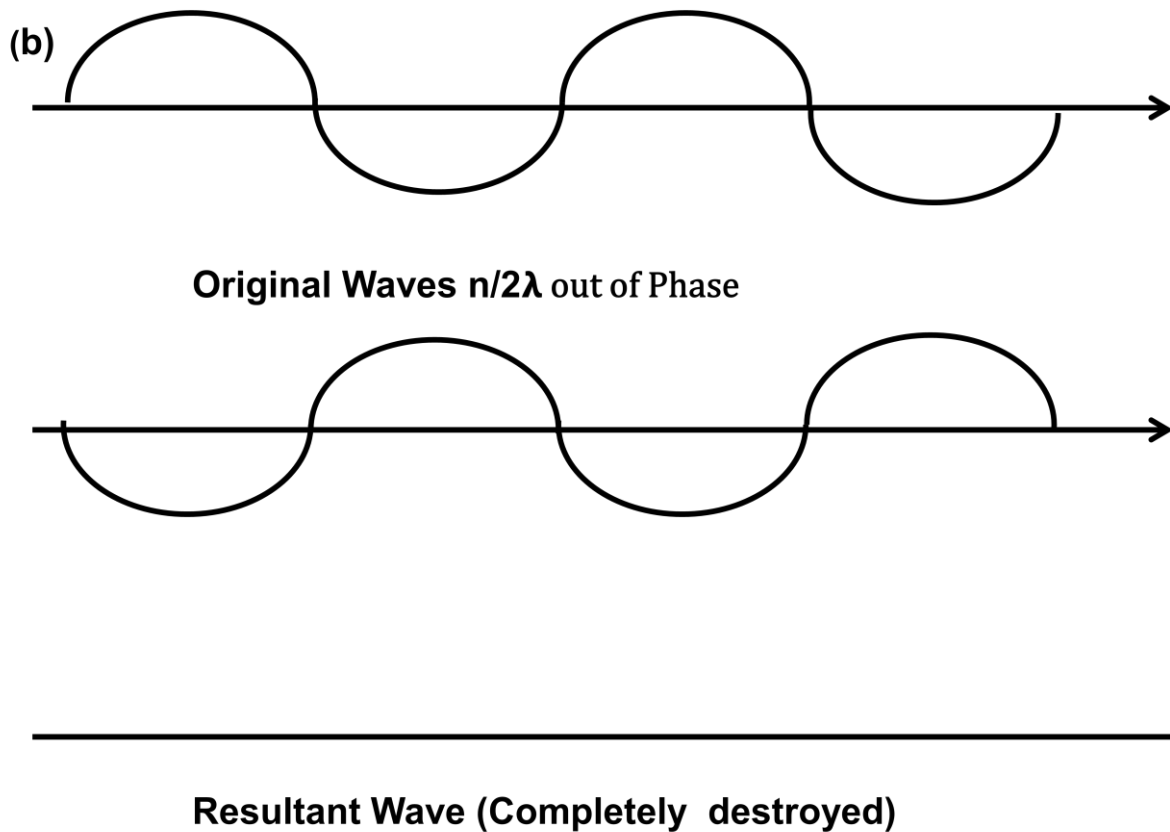


Figure 4.10: (a). Constructive interference (b) destructive interference [27]

All the waves in the bundle are in phase, that is their crests and troughs occur at exactly the same position such that they are an integer number of wavelengths out of phase, $n\lambda$, $n = 1, 2, 3, 4$, etc. The waves will interfere with one another and their amplitudes will reinforce (add together) to produce a resultant wave that has a higher amplitude as shown in Figure 4.10 (a).

Destructive interference Occurs when the waves are out of phase by a non-integer number of wavelengths and the amplitude of the waves will be reduced. In an extreme case, if the waves are out of phase by an odd multiple of $1/2\lambda$ [$(2n+1)/2\lambda$], the resultant wave will have no amplitude and thus be completely destroyed, Figure 4.10 (b).

4.2.3.3. Crystal Lattice

A crystal lattice is a regular three-dimensional distribution (cubic, rhombic, etc.) of atoms in space. These are arranged so that they form a series of parallel planes separated from one another by a distance d (figure 4.11(a) and (b)), which varies according to the nature of the material. For any crystal, planes exist in a number of different orientations - each with its own specific d -spacing.

4.2.3.4. Bragg's Law

The atoms in crystals interact with X-rays in such a way as to produce interference. The interaction can be thought of as if the atoms in a crystal structure reflect the waves. But, because a crystal structure consists of an orderly arrangement of atoms, the reflections occur from the atomic planes. Consider a beam of monochromatic X-rays entering a crystal with one of its planes oriented at an angle of θ to the incoming beam. Figure 4.11 shows two such X-rays, where the spacing between the atomic planes occurs over the distance, d .

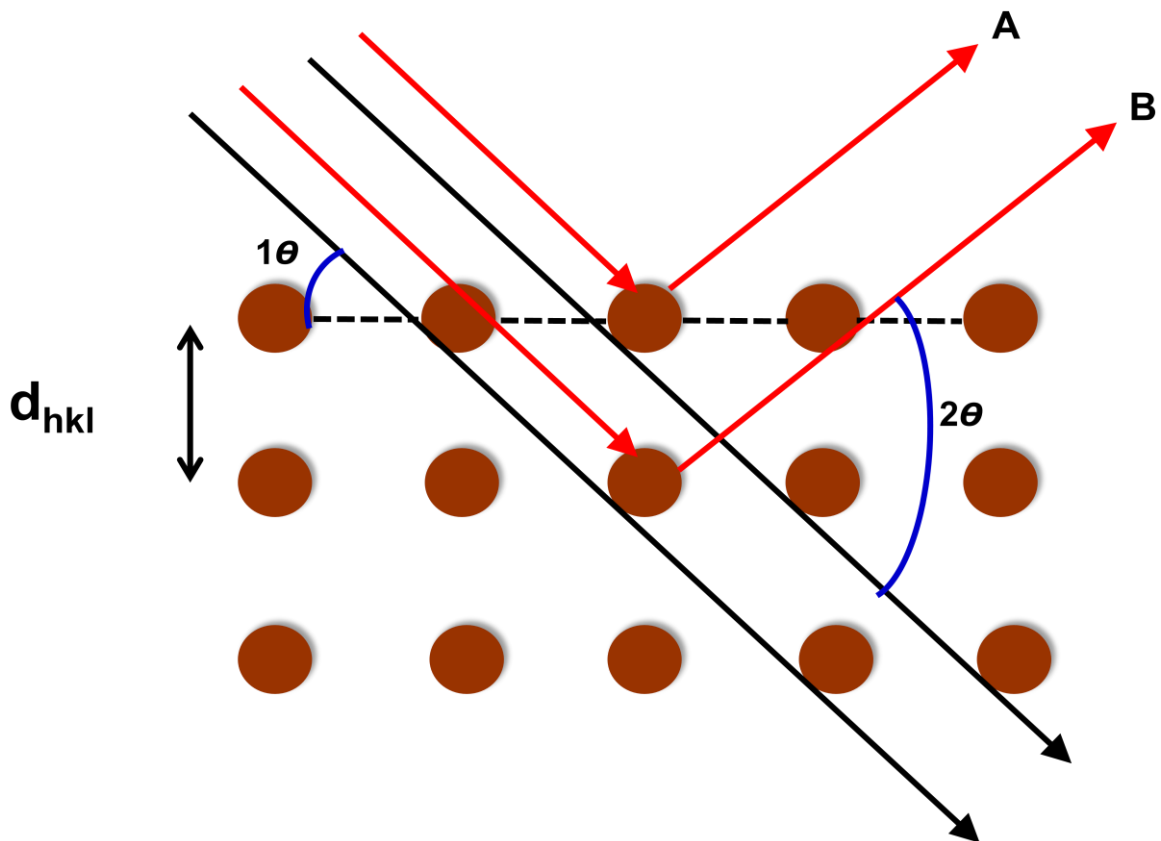


Figure 4.11: Monochromatic X-rays entering a crystal [28].

Ray A reflects off of the upper atomic plane at an angle θ equal to its angle of incidence. Similarly, Ray B reflects off the lower atomic plane at the same angle θ . While Ray B is in the crystal, however, it travels a distance of $2a$ farther than Ray A. If this distance $2a$ is equal to an integral number of wavelengths ($n\lambda$), then Rays A and B will be in phase on their exit from the crystal and constructive interference will occur. If the distance $2a$ is not an integral number of wavelengths, then destructive interference will occur and the waves will not be as

strong as when they entered the crystal. Thus, the condition for constructive interference to occur is

$$n\lambda = 2a.$$

But, from trigonometry, we can figure out what the distance $2a$ is in terms of the spacing, d , between the atomic planes.

$$a = d \sin \theta$$

$$\text{or } 2a = 2 d \sin \theta$$

$$\text{thus, } n\lambda = 2d \sin \theta$$

This is known as **Bragg's Law** for X-ray diffraction.

What it says is that if we know the wavelength λ , of the X-rays going in to the crystal, and we can measure the angle θ of the diffracted X-rays coming out of the crystal, then we know the spacing (referred to as *d-spacing*) between the atomic planes.

$$d = n\lambda / 2 \sin \theta$$

4.2.4. Photoluminescence Spectroscopy

Luminescence refers to the emission of light by a material through any process other than blackbody radiation [30]. **Photoluminescence** is luminescence by which electromagnetic radiation, i.e. photons, are used to excite a material, usually by use of ultraviolet light. Excitation occurs when light is directed onto a sample and it gets absorbed and imparts excess energy into the material. This excess energy can be released by the sample through the emissions of light [29], a process called luminescence. When the luminescence is accompanied by photo-excitation it is called photoluminescence (Figure 4.12).

Photoluminescence Spectroscopy is a contactless, nondestructive method of probing the electronic structure of materials. In PL one measures physical and chemical properties of materials by using photons to induce excited electronic states in the material system and analyzing the optical emission as these states relax. Typically, light is directed onto the sample for excitation, and the emitted luminescence is collected by a lens and passed through an optical spectrometer onto a photon detector. See Figures 4.13(a, b and c).

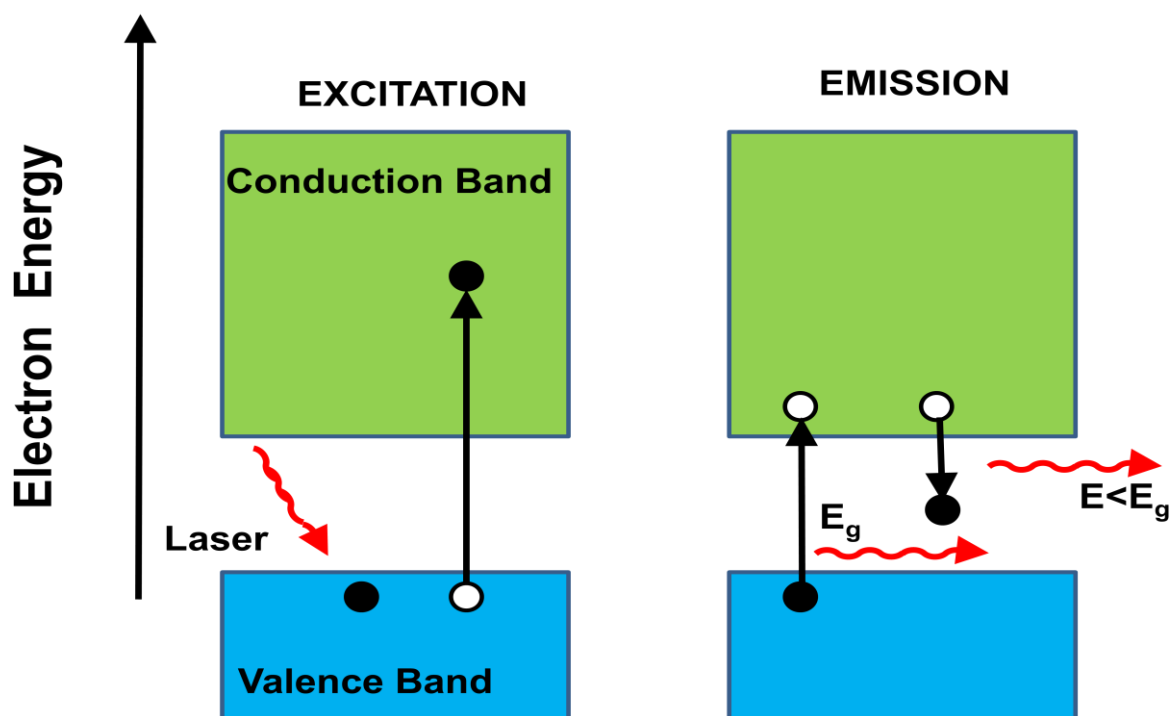


Figure 4.12: Excitation and Emission processes

The spectral distribution and time dependence of the emission are related to electronic transition probabilities within the sample, and can be used to provide qualitative and, sometimes, quantitative information about chemical composition, structure, impurities, kinetic process and energy transfer. Sensitivity is one of the strengths of the PL technique, allowing very small quantities (nanograms) or low concentrations (parts-per-trillion) of material to be analyzed. Precise quantitative concentration determinations are difficult unless conditions can be carefully controlled, and many applications of PL are primarily qualitative.

In PL, a material gains energy by absorbing photon at some wavelength by promoting an electron from a low to a higher energy level. This may be described as making a transition from the ground state to an excited state of an atom or molecule, or from the valence band to the conduction band of a semiconductor crystal or polymer (electron-hole creation). The system then undergoes a non-radiative internal relaxation involving interaction with crystalline or molecular vibrational and rotational modes, and the excited electron moves to a more stable excited level, such as the bottom of the conduction band or the lowest vibrational molecular state. After a characteristic lifetime in the excited state, electron will return to the ground state.

(a)

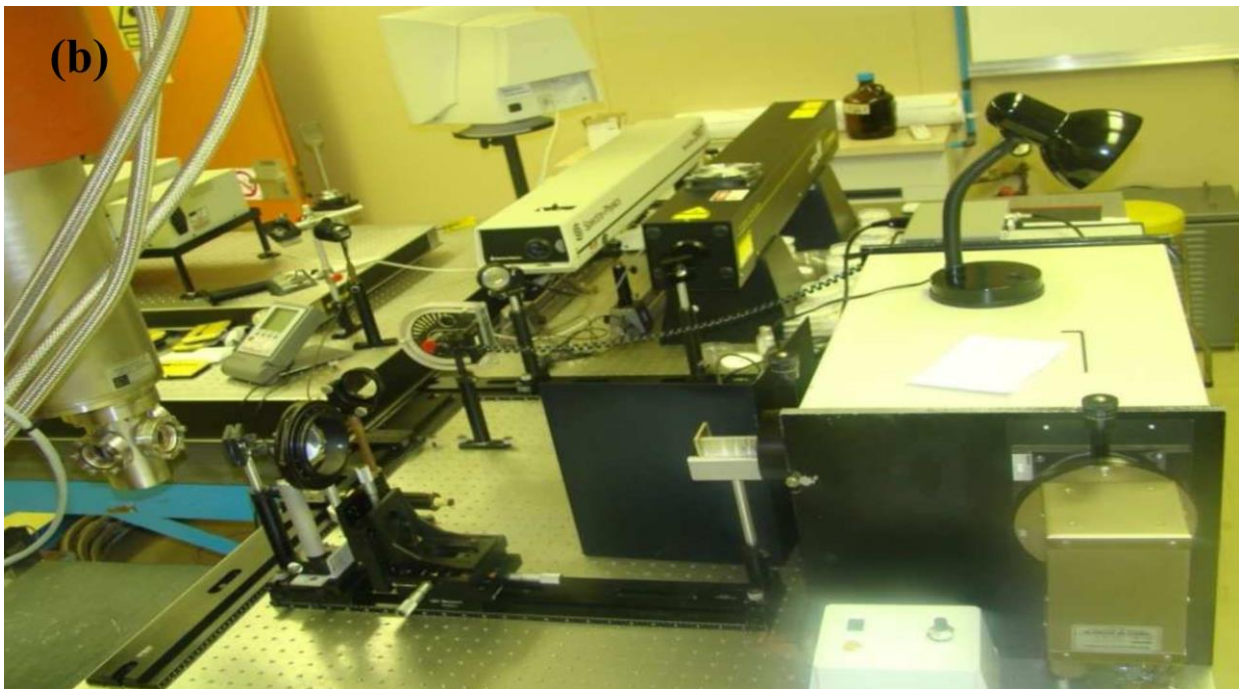
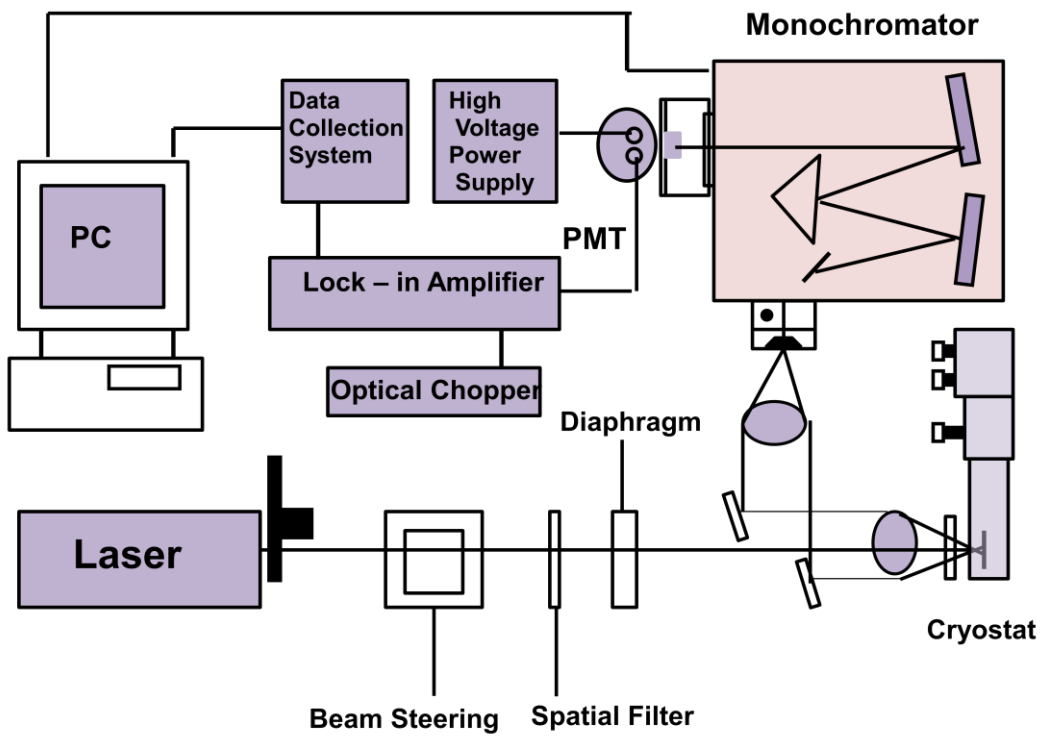




Figure 4.13: (a) Schematic diagram of the PL system (b) PL system used to investigate the luminescent properties of phosphors and (c) Cary Eclipse fluorescence spectrophotometer.

In luminescent materials some or all of the energy released during this final transition is in the form of light, in which case the relaxation is called radiative. The wavelength of the emitted light is longer than that of the incident light. It should be noted that depending on the characteristic life-time of emission, fast PL with life-time of sub microsecond is also called “fluorescence”, whereas slow ones, 4 to 10 s, are referred to as “phosphorescence” [31].

4.2.5. Fourier Transform Infra-Red (FT-IR) Spectroscopy

FT-IR stands for Fourier Transform Infra Red, the preferred method of infrared spectroscopy. In infrared spectroscopy, IR radiation is passed through a sample. Some of the infrared radiation is absorbed by the sample and some of it is passed through (transmitted). The resulting spectrum represents the molecular absorption and transmission, creating a molecular fingerprint of the sample. Like a fingerprint no two unique molecular structures produce the same infrared spectrum. This makes infrared spectroscopy useful for several types of analysis. FT-IR can identify unknown materials, it can determine the quality or consistency of a sample and it can determine the amount of components in a mixture.

The detector measures the amount of energy at each frequency which has passed through the sample. This result in a spectrum which is a plot of intensity versus frequency. An infrared

spectrum represents a fingerprint of a sample with absorption peaks which correspond to the frequencies of vibrations between the bonds of the atoms making up the material. The size of the peaks in the spectrum is a direct indication of the amount of material present. Fourier transform infrared spectroscopy is preferred over dispersive or filter methods of infrared spectral analysis for several reasons:

- It is a non-destructive technique
- It provides a precise measurement method which requires no external calibration
- It can increase speed, collecting a scan every second
- It can increase sensitivity – one second scans can be co-added together to ratio out random noise
- It has greater optical throughput
- It is mechanically simple with only one moving part [32].

4.2.5.1. Fourier Transform Spectrometer

The basic configuration of an FTIR spectrometer is schematically shown in Figure 4.14.

There are three basic spectrometer components in an FT system: radiation source, interferometer, and detector.

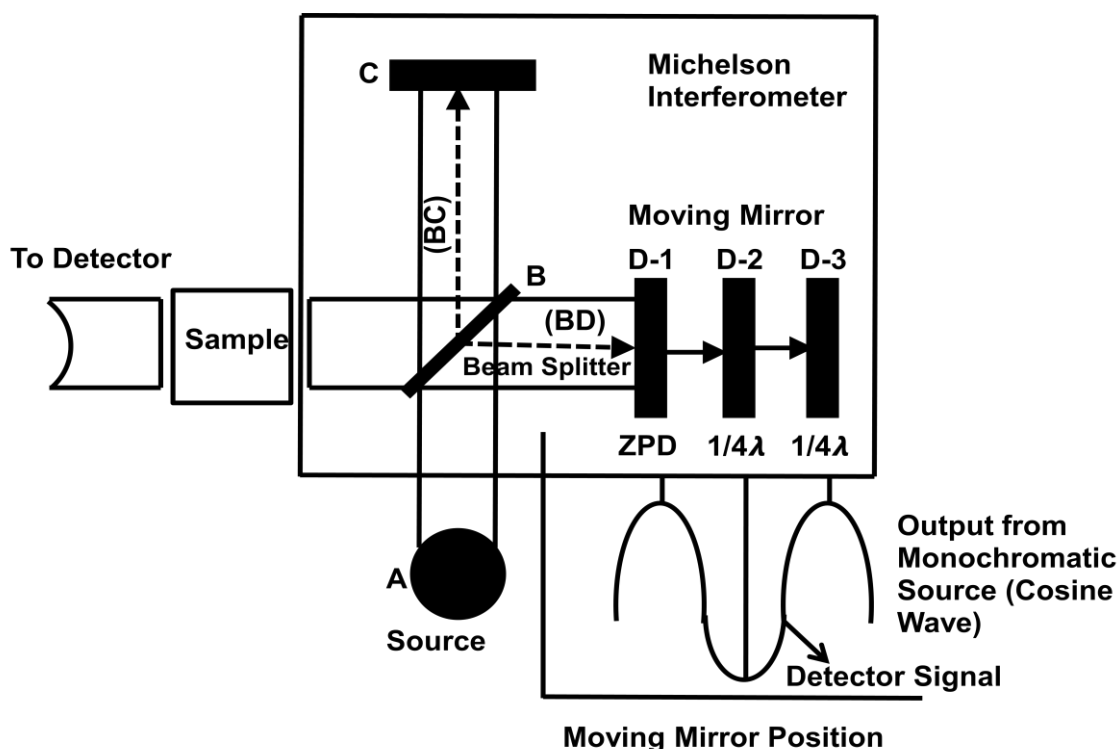


Figure 4.14: Simplified optical layout of a typical FTIR spectrometer. (Reprinted by permission of Nicolet Instrument Corporation.)

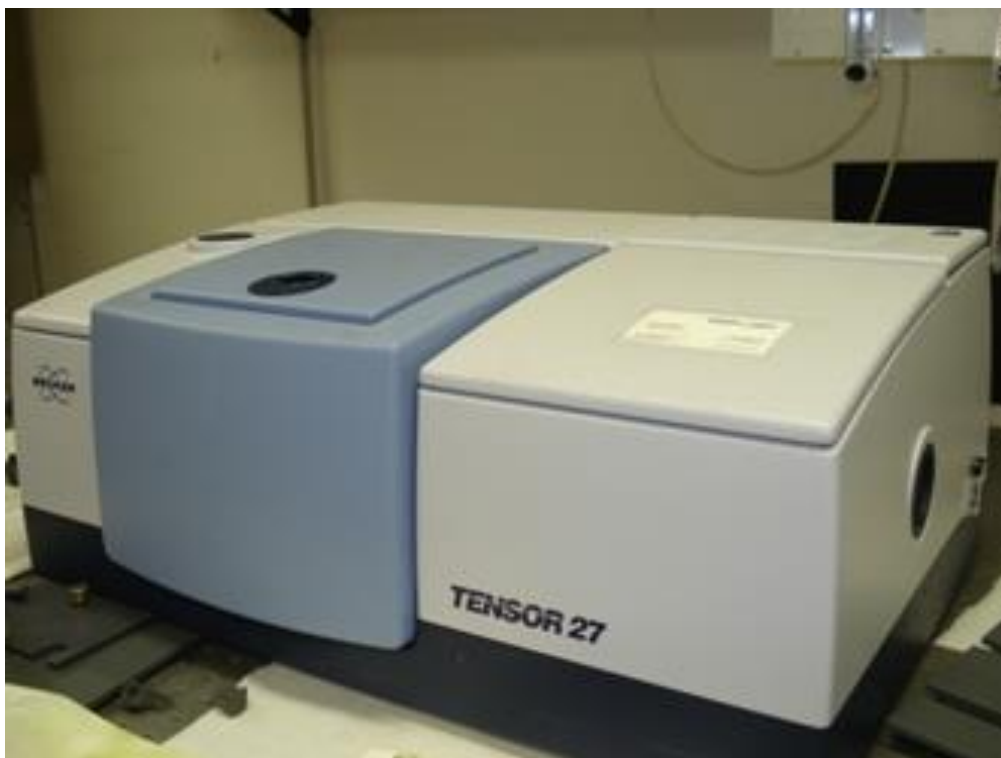


Figure 4.15: FTIR system at UFS Chemistry Department.

The monochromator is replaced by an interferometer which divides radiant beams. It generates an optical path difference between the beams, and then recombines them in order to produce repetitive interference signals measured as a function of optical path difference by a detector. As its name implies, the interferometer produces interference signals, which contain infrared spectral information generated after passing through a sample. The most commonly used interferometer is a Michelson interferometer. It consists of three active components: a moving mirror, a fixed mirror, and a beam splitter (Figure 4.14). The two mirrors are perpendicular to each other. The beam splitter is a semi reflecting device and is often made by depositing a thin film of germanium onto a flat KBr substrate. Radiation from the broadband IR source is collimated and directed into the interferometer, and impinges on the beam splitter. At the beam splitter, half the IR beam is transmitted to the fixed mirror and the remaining half is reflected to the moving mirror. After the divided beams are reflected from the two mirrors, they are recombined at the beam splitter. Due to changes in the relative position of the moving mirror to the fixed mirror, an interference pattern is generated. The resulting beam then passes through the sample and is eventually focused on the detector [33].

Consider an input monochromatic IR beam of wavelength λ , propagating in the empty interferometer (i.e., without a sample). If the two mirrors (moving and fixed) are at the same distance, L , from the beam splitter, the two light beams that recombine at the beam splitter travel the same distance $2L$ (i.e., there is no extra distance between them; $x = 0$) and they interfere constructively, so that a maximum is observed in the detector. If the moving mirror is displaced away from the beam splitter by a distance $\lambda/2$, the beam reflected in the moving mirror will now travel an extra distance of $x = 2(\lambda/2) = \lambda$, and constructive interference will again be observed in the detector. However, for a moving mirror displacement of $\lambda/4$, the beam reflected in the moving mirror will now travel an extra distance of $x = 2(\lambda/4) = \lambda/2$. Then, the two halves recombine in the beam splitter with a retardation of $\lambda/2$ to each other and so they interfere destructively, giving a minimum in the detector. In order to register a spectrum, the moving mirror is displaced along a distance $\gg \lambda$. Thus, for the case of a monochromatic beam of a given wavelength (or a given wave number), we should obtain an interference pattern like the one shown in Figure 1.18(a), with maximum detector signals for a mirror displacement that gives a retardation of $x = n\lambda$ and minimum detector signal for $x = (n + 1/2)\lambda$ ($n = 0, 1, 2, \dots$). This interference pattern is called an interferogram. At this point, it should be noted that the Fourier transform of the interferogram, $I(x)$, is just the spectrum $I(\nu)$ of the monochromatic radiation[34]. The interferogram contains information over the entire IR region to which the detector is responsive. A mathematical operation known as Fourier transformation converts the interferogram (a time domain spectrum displaying intensity versus time within the mirror scan) to the final IR spectrum, which is the familiar frequency domain spectrum showing intensity versus frequency. This also explains how the term **Fourier transform infrared spectrometry** is created [33].

4.2.6. Thermoluminescence Spectroscopy (TL)

When a phosphor with deep traps is excited for a while at rather low temperatures and then heated, it shows an increased after-glow called thermally stimulated luminescence due to the recombination of electrons thermally reactivated from the deep traps. This emission is also called thermoluminescence, and the temperature dependence of the emission intensity is called the glow curve, which is a good means to measure the depth (i.e., the activation energy of traps) [29]. The measurement of a glow curve of a phosphor sample proceeds as follows.

1. The sample is cooled to a low temperature (liquid nitrogen is often used as coolant).
2. The sample is excited by UV light until the traps are filled with electrons or holes.

3. The excitation is terminated, and the temperature of the sample is raised at a constant rate, $dT/dt=\beta$, while the intensity is recorded.
4. The temperature dependence of fluorescence is then measured under a constant UV excitation, which is used to calibrate the effect of temperature quenching on the thermoluminescence intensity.

4.2.6.1. The TL Spectrometer

The TSL glow curves in this study were obtained by Thermoluminescence Reader Type TL1009I (Fig. 4.15) with PMT type 9924 designed and offered by M/s Nucleonix Systems Pvt. Ltd., India interfaced to a PC where the TL signals were analyzed. It is a versatile controller based unit, facilitating the user to subject the TL sample under study to the desired heating profile, to record the digitized TL glow curve. This unit stores both integral value and digitized glow curve into EEPROM memory.



Figure 4.16: Thermoluminescence Reader Type TL1009I designed and offered by Nucleonix Systems Pvt. Ltd., India [35].

This unit records the data in 200 channels, temperature, TL intensity & Run time values.

Entire electronics including PMT, HV bias, Temperature controller circuit, Heater transformer heater strip, sample drawer assembly, data acquisition electronics is all integrated into a single enclosure.

The user interface to the unit is through a powerful software GUI, coded in VB which runs on Windows platform. This system essentially works as a PC controlled TLD reader with command buttons and dropdown menus defined for various functions.

Built-in serial port in the unit facilitates the user to connect it to a PC for GUI and to achieve full functionality [35].

References

- [1] K.C. Patil, S.T. Aruna, and T. Mimani, *Solid State and Materials Science* 2002 **6** 507 512.
- [2] J.J. Kim, J.H. Kang, D.C. Lee and D.Y. Jeon, *American Vacuum Society* 2003.
- [3] S.S. Manoharan and K.C. Patil, *J. Am. Ceram. Soc.* 1992 **75**141, 1012.
- [4] M.A. Sekar and K.C. Patil, *J. Mater. Chem.* 1992 **2**[7] 739.
- [5] R.G. Chandran and K.C. Patil, *Mater. Res. Bull.* 1992 **27** 147.
- [6] P. Ravindranathan, S. Komameni and R. Roy, *J. Mater. Sci. Lett.* 1993 **12** 369.
- [7] N.A. Dhas and K.C. Patil, *Ceram. Inter.* 1994 **20** 57.
- [8] Y. Zhang and G.C. Stangle, *J. Mater. Res.* 1994 **9** [8] 1997.
- [9] D.A. Furnor, M.R. More and A.M. Segadhes' *Materials Research Bulletin*, 1996 31[10] DD 1243-1255.
- [10] N. Suriyamurthy and B.S. Panigrahi, *J. Lumin. (In Press)* SCIENCE-53.
- [11] Hirata GA, Raamos F, Garcia R, Bosze EJ, Kittrick JM, et al. *J. Phys. Stat. Sol.(a)* 2001 188 179.
- [12] Zifeng Qiu, Yuanyuan Zhou, Mengkai Lu", Aiyu Zhang and Qian Ma, *Acta Materialia* 2007 **55** 2615.
- [13] B.M Mothudi, PhD Thesis, University of the Free State, South Africa 2008 35-36.
- [14] R. W. Kelsall, I. W Hamley, M. Geoghegan, *Nanoscale Science and Technology*, Wiley, 2005.
- [15] M.S. Dhlamini, PhD Thesis, University of the Free State, South Africa 2008 4-5.
- [16] University of Nebrasaka-Lncon: Available from <http://www.unl.edu/CMRAcfem/semoptic.htm>.
- [17] Binghamton University: Available from <http://nue.clt.binghamton.edu/semtem.html>.
- [18] J. Schweitzer, Available from <http://www.purdue.edu/REM/rs/sem.htm> 2008 ,
Electrons in Scanning electron microscopy, [online]. [Accessed 17 June 2010].
- [19] <http://www.vcbio.science.ru.nl/en/fesem/info/principe/> [Accessed 12 May 2011].

- [20] Description of EDS Technique <http://mee-inc.com/index.html> [Accessed 03/10/2011].
- [21] B. G. Yacobi, D. B. Holt, and L.L. Kazmerski Microanalysis of Solids, New York, Plenum Press, 1994.
- [22] Energy Dispersive X-ray Spectroscopy (EDS/EDX), [online]. Available from <http://www.thermo.com/com/cda/technology/detail/1,,12700,00.html> [Accessed 13 May 2011].
- [23] Energy Dispersive Spectroscopy [online]. Available from http://ion.eas.asu.edu/descript_ed.s.htm [Accessed 17 May 2011].
- [24] G. Cao, 6th edition, London, 2004.
- [25] F. A. Settle, Handbook of Instrumental Techniques for Analytical Chemistry, Prentice Hall PTR, USA, 339.
- [26] http://serc.carleton.edu/research_education/geochemsheets/techniques/XRD.html accessed [15 Sept2011].
- [27] Prof. Stephen A. Nelson ,Tulane University 2010 46.
- [28] X-Ray Diffraction, [online]. Available from, <http://www.doitpoms.ac.uk/tlplib/index.php> [Accessed 10 Sept 2011].
- [29] S. Shionoya, W.M. Yen, Phosphors Handbook, CRC Press,USA, 1998, 95.
- [30] C. Colvard, C.R. Brundle, C.A. Evans Jr., and S. Wilson, Buttenvorth-Heinemann, Stoneham, MA, *Encyclopaedia of Materials Characterization* 1992, 373.
- [31] G. Cao, University of Washington, USA, 346.
- [32] Thermo Electron Scientific Instruments LLC., Madison, [online]. Available from <http://www.thermonicolet.com> [online]. [Accessed 05/10/2011].
- [33] C.P. Sherman Hsu, Infrared Spectroscopy, Ch. 15 244-245.
- [34] J. Garc'ia Sol'e, L.E. Baus'a and D. Jaque. An Introduction to the Optical Spectroscopy of Inorganic Solids 2005, 33.
- [35] <http://www.nucleonix.com/cancer/ch22.html> [online]. [Accessed 21/10/2011].

Chapter 5

Synthesis and Characterization of Structural and Luminescent properties of long afterglow CaAl_2O_4 : Eu^{2+} , Nd^{3+} , Dy^{3+} phosphors by solution – combustion technique.

5.1. Introduction

Aluminates doped with rare earth ions have advantages of being highly stable, bright and versatile in industrial processes that are appropriate for lighting and display devices [1, 2]. Unlike other phosphors so far reported in the literature [3-5], in this study rare earth metal ions, Europium (Eu^{2+}), Dysprosium (Dy^{3+}) and Neodymium (Nd^{3+}) and the host CaAl_2O_4 are added together to improve the luminescent properties of the phosphor. The solution-combustion synthesis method also has the merits of low temperature, low cost and time saving. Earlier studies explained the mechanism of persistent luminescence as being caused by the interplay of the rare earth ions with the host band structure and the lattice defects (Figure 5.1(a)).

The ability of the rare earth species to trap electrons/holes can be predicted from the positions of the 4f and 5d levels of the Eu^{2+} ion and the other R^{3+} ions in the host lattice structure [6], but the energy storage and luminescent mechanisms cannot be explained from the level locations alone [1]. The radiative transitions are highly affected by the crystal field components because the 5d orbital is exposed to the surrounding ion. Thus the structure of the host crystals strongly influences the wavelength of a maximum emission peak. This explains why for instance, Eu^{2+} -doped Ca and Sr aluminates show blue and green emissions, respectively [7].

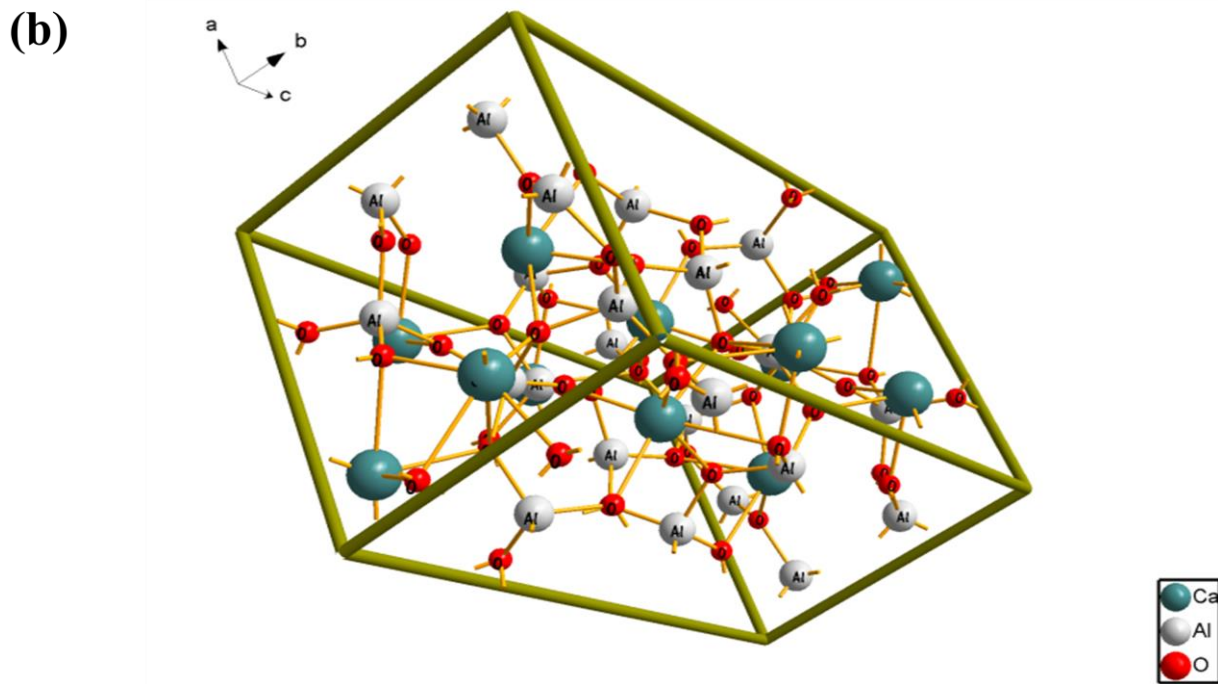
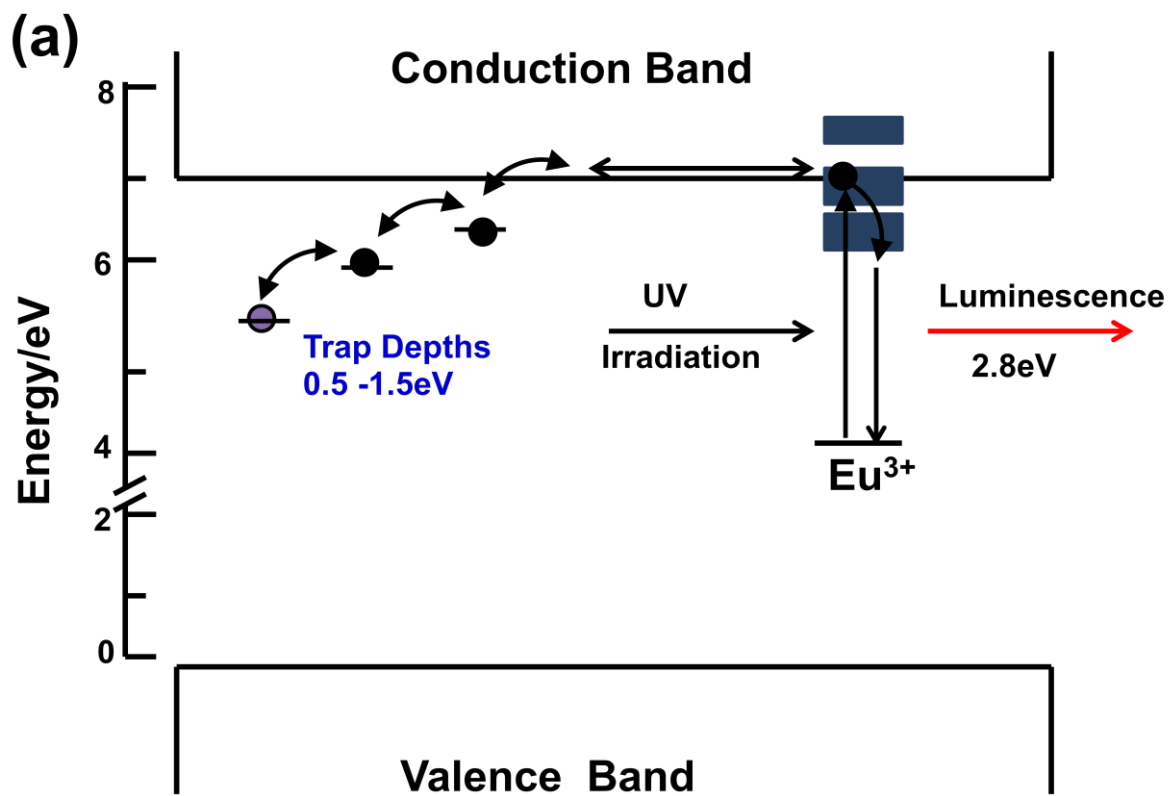


Figure 5.1: (a). Persistent luminescence mechanism for $\text{CaAl}_2\text{O}_4:\text{Eu}^{2+}, \text{R}^{3+}$ materials. (b) Parking diagram of monoclinic CaAl_2O_4 .

CaAl_2O_4 has a tridymite type monoclinic structure (space group: P21/n (No. 14), Z: 12) [8], where $[\text{AlO}_4]$ tetrahedral construct a three-dimensional framework. Each aluminium ion is bonded to two oxygen ions [9]. The structure consists of channels built up of rings formed by six corner-sharing AlO_4 tetrahedra and Ca^{2+} cations situated within the channels (Figure 5.1(b)).

There are three different Ca^{2+} sites in the CaAl_2O_4 lattice: one (Ca_3) is nine-coordinated and two of them (Ca_1 and Ca_2) are six-coordinated [10]. Doped Eu^{2+} ions prefer nine-coordinated Ca^{2+} sites (rCa: 1.18 Å) to two six-coordinated ones (rCa: 1.0 Å), because larger spaces are necessary for the substitution of Eu^{2+} ions (rEu: 1.30 Å) due to the difference in ionic size. The average Ca–O distances 2.42 Å and 2.43 Å for the six-coordinated Ca^{2+} ions are clearly shorter compared to that of the nine-coordinated ones (2.78 Å) [11].

By doping with Eu^{2+} ions, CaAl_2O_4 powders exhibit a strong blue emission around 440 nm when excited with 320 nm [12]. $\text{CaO–Al}_2\text{O}_3$ systems easily degenerate into multi-phased compounds with slight deviation from the exact stoichiometric composition and firing temperature which makes it difficult to obtain CaAl_2O_4 single phase. So the synthesis conditions, such as host elements, dopant concentration and temperature are very important to the formation of single phase. However, in spite of many previous studies, a thorough investigation has so far not been carried out.

This study focuses on the blue emitting persistent luminescence, $\text{CaAl}_2\text{O}_4:\text{Eu}^{2+},\text{Nd}^{3+},\text{Dy}^{3+}$ phosphor of which $\text{CaAl}_2\text{O}_4:\text{Eu}^{2+},\text{Nd}^{3+}$ is already in commercial use.

5.2. Experimental

5.2.1. Synthesis

$\text{CaAl}_2\text{O}_4:\text{Eu}^{2+},\text{Nd}^{3+},\text{Dy}^{3+}$ phosphors were synthesized using the solution - combustion method. The starting raw materials used in the experiment include various proportions of analytical pure grade $\text{Ca}(\text{NO}_3)_2 \cdot 4\text{H}_2\text{O}$, $\text{Al}(\text{NO}_3)_3 \cdot 9\text{H}_2\text{O}$, $\text{Eu}(\text{NO}_3)_3 \cdot 5\text{H}_2\text{O}$, $\text{Nd}(\text{NO}_3)_3$, $\text{Dy}(\text{NO}_3)_3$, urea ($\text{CH}_4\text{N}_2\text{O}$) and boric acid (H_3BO_3). The raw materials were weighed according to the chemical composition of $\text{CaAl}_2\text{O}_4:\text{Eu}^{2+},\text{Nd}^{3+},\text{Dy}^{3+}$, dissolved in 10 ml of de-ionized water and thoroughly mixed using a magnetic stirrer for 15 minutes without heating to obtain a uniform solution.

In the first group, eight samples were prepared without flux. To study the influence of variation of the host matrix, Ca and Al molar ratio on the structural and luminescent properties of the $\text{CaAl}_2\text{O}_4:\text{Eu}^{2+}$ phosphor, the Al concentration was kept constant at 1.5 mass

% for all the prepared solutions. This was combined with varying concentrations; 0.1, 0.4, 0.5, 0.6, 0.7, 0.8, 1.0, and 1.5 mass % of Ca were taken.

The second set consist of five samples used to study the influence of variation of co-dopants, Nd^{3+} and Dy^{3+} molar ratio on the structural and luminescent properties of the $\text{CaAl}_2\text{O}_4:\text{Eu}^{2+}$ phosphor. The samples were mixed in the mass ratios 0:1, 0.25:0.75, 0.5: 0.5, 0.75:0.25 and 1:0 of $\text{Nd}^{3+}:\text{Dy}^{3+}$.

The solutions were then poured into China crucibles and placed one at a time in a muffle furnace pre-heated at 500°C . Combustion time was 5–6 min per sample. White voluminous foam was obtained by combusting the mixture at temperatures of $400\text{--}500^\circ\text{C}$. Initially, the solution boiled and underwent dehydration, followed by decomposition releasing large amounts of gases (oxides of carbon, nitrogen and ammonia). Then, spontaneous ignition and smoldering occurred which gradually led to an explosion with enormous swelling. When taken out of the muffle furnace and cooled down, voluminous foam was obtained, which was a mixture of the incomplete combustion compound CaAl_4O_7 and the complete combustion compound CaAl_2O_4 . The voluminous foam was milled to obtain the fine, white powders. The powders were stored in transparent sample glass bottles for characterization.

5.2.2 Characterization

The synthesized products were characterized by X-ray diffraction (XRD) using a Bruker D8 X-ray diffractometer operating at 40 kV and 4 mA using $\text{Cu K}\alpha = 0.15406$ nm for elemental analysis. The morphologies were investigated using a Shimadzu model ZU SSX-550 Super scan Scanning Electron Microscope (SEM) and an Energy Dispersive X-ray Spectrometer (EDS). The decay curves, excitation and emission spectra were measured at room temperature using a Cary Eclipse fluorescence spectrophotometer model: LS- 55 with a built-in 150W xenon flash lamp operating at excitation of 325 nm.

5.3. Results and Discussion

5.3.1 The influence of the Ca: Al mass ratio on structure

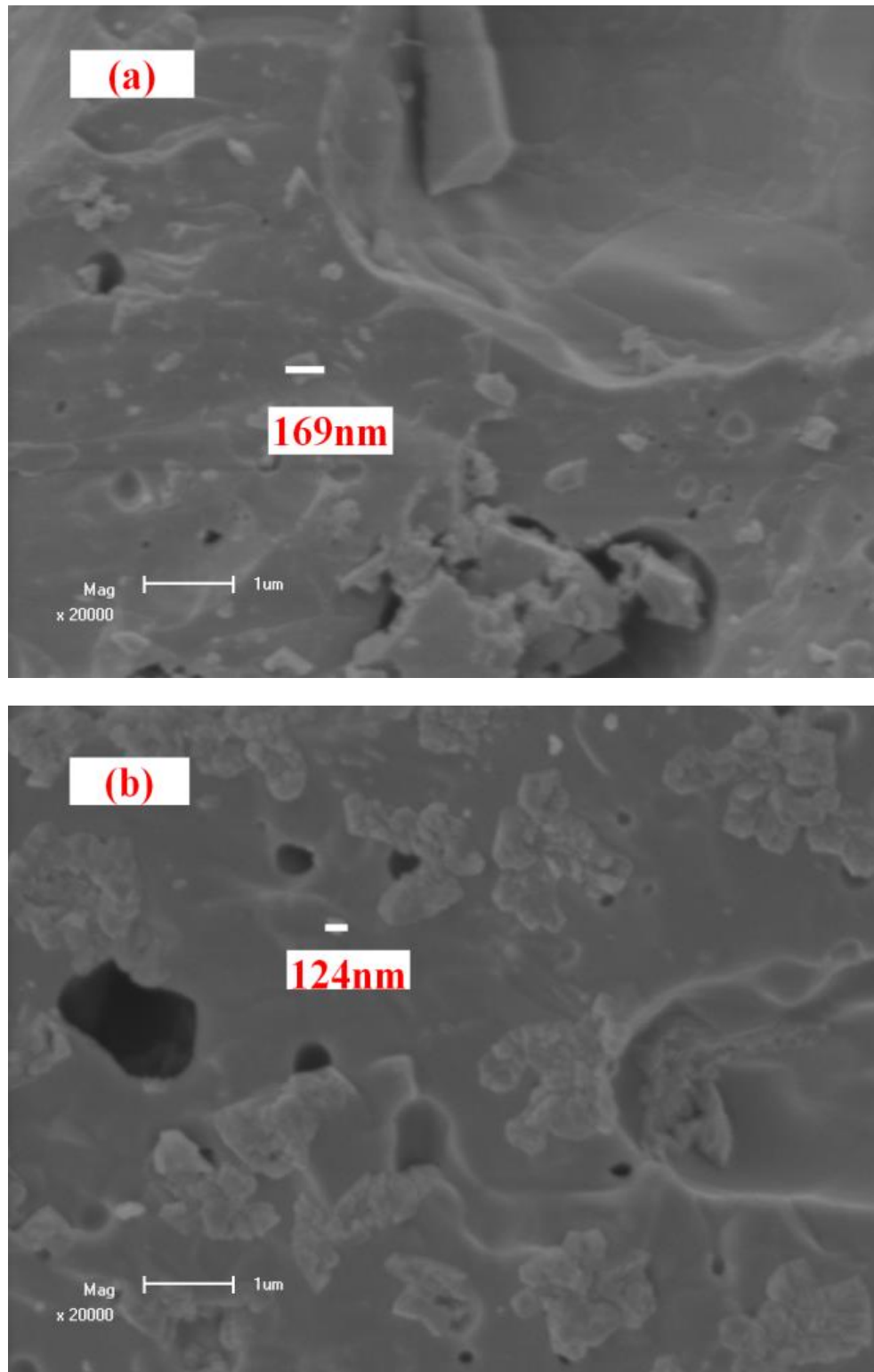


Figure 5.2: SEM micrographs for (a) 0.4% Ca sample and (b) 0.8% Ca sample respectively.

Scanning electron microscopy (SEM) study was carried out to investigate the surface morphology and crystalline sizes of the synthesized phosphor powder.

Figure 5.2 shows the representative SEM micrographs taken for the 0.4% Ca sample and 0.8% Ca sample respectively. As can be seen, the surfaces display many cracks and pores formed by the escaping gases during the combustion reaction. The material also presented agglomeration as can be observed in Figure 5.2 (b). This tends to reduce the luminescent properties when the sample is ground.

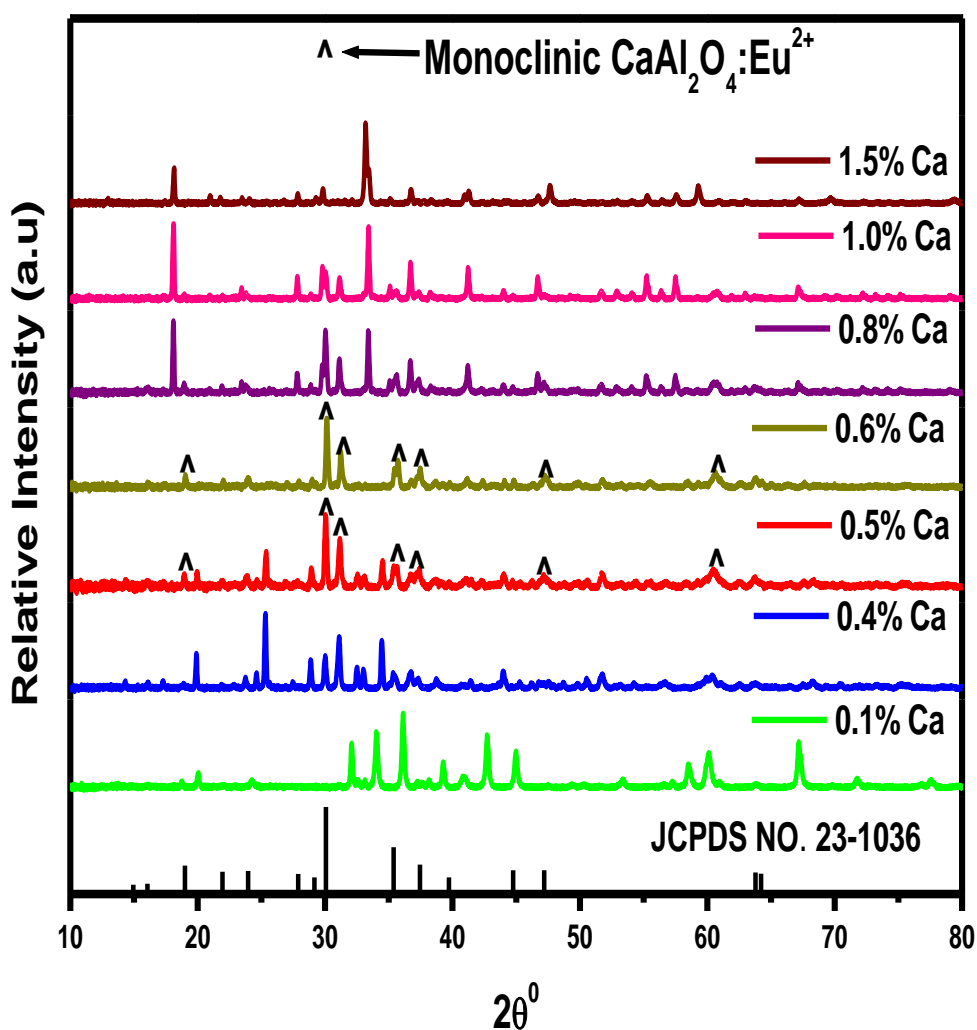
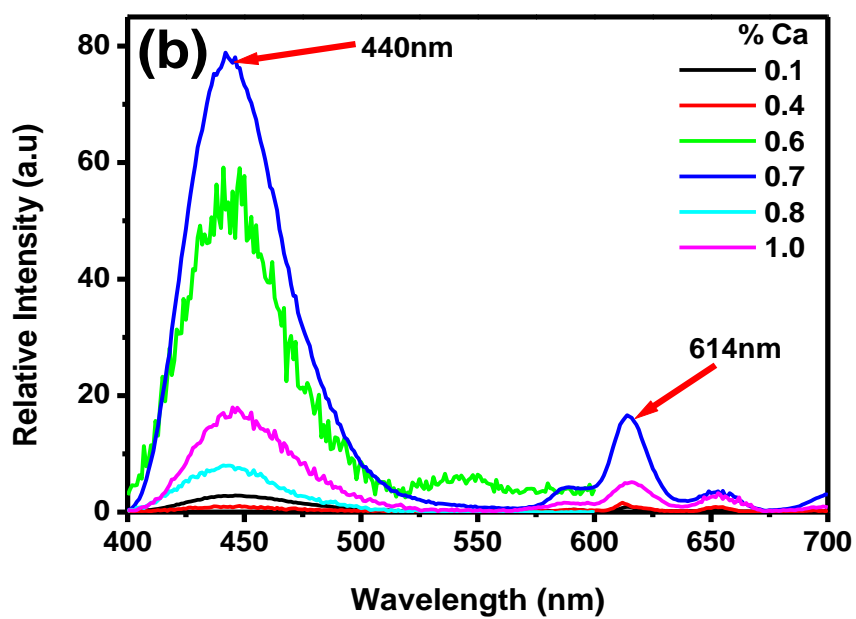
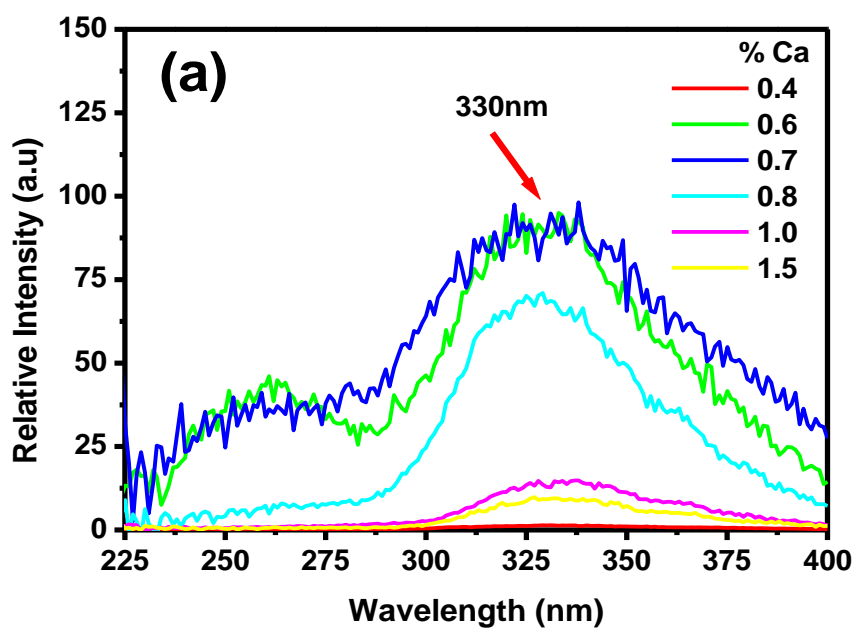


Figure 5.3: (a) Monoclinic phase of $\text{CaAl}_2\text{O}_4:\text{Eu}^{2+},\text{Nd}^{3+},\text{Dy}^{3+}$ phosphors.

Figure 5.3 shows the powder XRD pattern for the $\text{CaAl}_2\text{O}_4:\text{Eu}^{2+},\text{Nd}^{3+},\text{Dy}^{3+}$. Several phases are easily observable. Analysis of these diffractive peaks reveal that 0.5% Ca and 0.6% Ca favour pure monoclinic phase matching with the JCPDS data file (no. 23-1036) while higher concentrations of calcium; 0.8% Ca, 1.0% Ca and 1.5% Ca seem to favour the formation of cubic phase. Weak diffraction peaks of CaAl_4O_7 compound formed due to incomplete combustion were also observed. The calculated lattice parameters for the monoclinic crystal system were $a=8.6942\text{\AA}$, $b=8.0930\text{\AA}$, $c=15.2097\text{\AA}$ and $\beta=90.17^\circ$ while for the cubic system was $a=11.9868\text{\AA}$.

5.3.2. The effects of Ca : Al mass ratio on photoluminescence properties

Figure 5.4 (a) shows the excitation spectrum of the phosphor. There is an excitation peak at around 325 nm in the emission spectrum, $\lambda_{\text{em}}=440\text{ nm}$ which is in conformity with the absorption of the host CaAl_2O_4 . It's known that CaAl_2O_4 has a broad band excitation spectrum ranging from 250 to 340 nm. This means that in a broad range ($\lambda_{\text{ex}} \leq 360\text{ nm}$), $\text{CaAl}_2\text{O}_4:\text{Eu}^{2+},\text{Dy}^{3+},\text{Nd}^{3+}$ phosphor can be activated to produce long persistence. As can be seen in Figure 5.4(b), the emission spectrum at $\lambda_{\text{ex}} = 325\text{ nm}$ shows a broad band from the $4f^65d^1$ to the $4f^7$ configuration of the Eu^{2+} ions at about 440 nm, which is consistent with the literature [25]. Energy levels are located between excited state $4f^65d^1$ and ground state $4f^7$ of Eu^{2+} , and there is the energy gap (ET) between the energy levels and the excited state energy level. When the material is excited, some of the Eu^{2+} excitation electrons get stored in the trap energy level through the relaxation process. When the excitation stops, the electrons stored up in the trap energy level obtain energy through thermal agitation at room temperature, overcome the energy level gap between the trap energy level and the excited state energy level, return to the excited state, then transit back to the ground state and emit light energy. From the decay spectrum of Figure 5.4(c), It can be seen that the samples show quite long time especially when the powder was efficiently activated by using 0.7% Ca. In general all the PL results show 0.7% Ca as the optimal concentration for the excitation, emission and decay characteristics. Additional emission peaks observed between 525 nm and 675 nm are attributed to the unreduced Eu^{3+} ions in the host lattice.



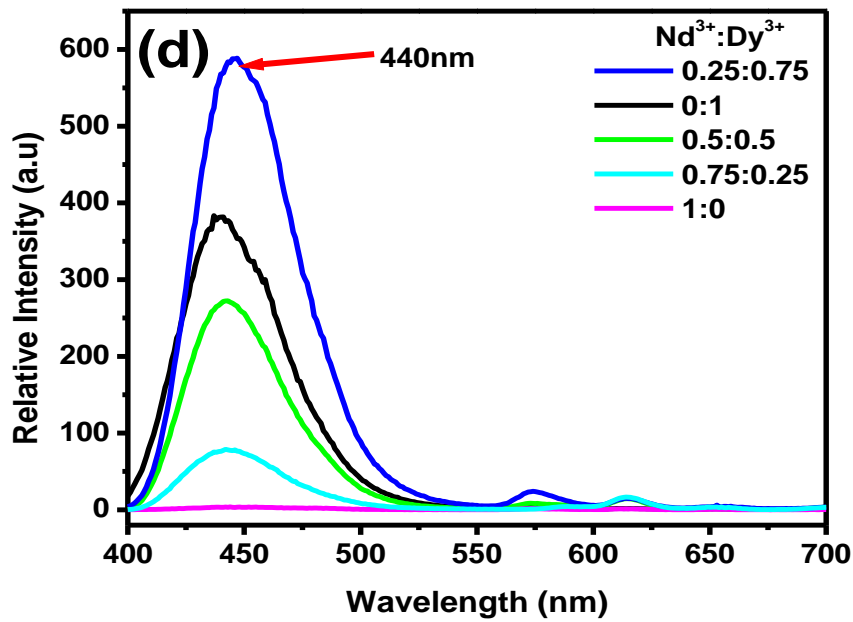
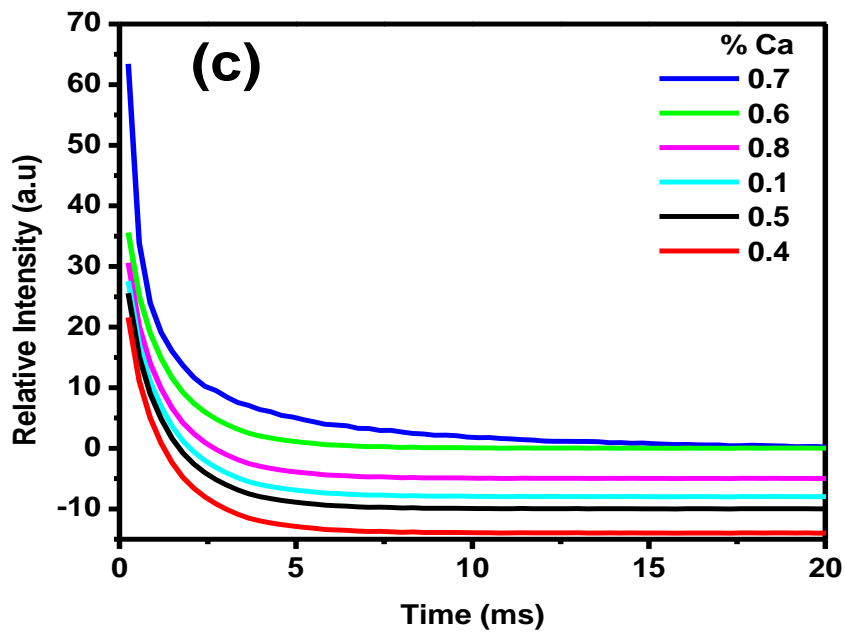


Figure 5.4: (a) Excitation, (b) emission (c) decay characteristics of the phosphors dependence on Ca: Al mass ratio and (d) emission intensities of the varying $\text{Nd}^{3+} : \text{Dy}^{3+}$ co-dopant ratio obtained at room temperature.

5.3.3. The effects of co-dopants mass ratio ($\text{Nd}^{3+}:\text{Dy}^{3+}$) on the photoluminescence properties

Figure 5.4(d) shows the emission intensities of the $\text{CaAl}_2\text{O}_4:\text{Eu}^{2+},\text{Nd}^{3+},\text{Dy}^{3+}$ phosphors while the phosphors are excited at a wavelength of 325 nm. Within the scope of content ratio 0.25:0.75, Nd^{3+} and Dy^{3+} ions seem to improve the luminescent properties of the phosphors $\text{CaAl}_2\text{O}_4:\text{Eu}^{2+},\text{Nd}^{3+},\text{Dy}^{3+}$. The peak wavelength of the phosphor does not vary with the doped $\text{Nd}^{3+}:\text{Dy}^{3+}$. This implies that the crystal field, which affects the 5d electron states of Eu^{2+} , is not significantly changed by the variations in the co-dopants. When the phosphor is doped with Nd^{3+} and Dy^{3+} , Ca^{2+} ions are replaced by Nd^{3+} and Dy^{3+} ions. But Ca^{2+} ions and $\text{Nd}^{3+}/\text{Dy}^{3+}$ ions are different resulting in unequal replacement. This causes more trap energy level and the depth of the energy level becomes deeper. Thus, Nd^{3+} seem to possess high affinity toward the electrons more than Dy^{3+} in the energy level.

When the concentration of Eu^{2+} ion is fixed, the number of electron-hole pairs is fixed. As the concentration of Nd^{3+} ion increases in a range, the number of the Nd^{3+} traps increases, and the traps capture more holes. However, if the doped amount of Nd^{3+} is too large, it may result in concentration quenching and may lower the luminescent effect, as can be observed from Figure 5.4(d), when the value of $\text{Nd}^{3+}:\text{Dy}^{3+}$ was 1:0, the emission intensity was relatively low for this phosphor.

Conclusion

The phosphor $\text{CaAl}_2\text{O}_4:\text{Eu}^{2+},\text{Nd}^{3+},\text{Dy}^{3+}$ can be prepared by solution-combustion method. The influences of the quantity of mixed Nd^{3+} , Dy^{3+} and varying concentrations of Ca: Al on the phosphor were studied. The analytical results indicate that the broad emitted band of the $\text{CaAl}_2\text{O}_4:\text{Eu}^{2+},\text{Nd}^{3+},\text{Dy}^{3+}$ is observed in the blue region ($\lambda_{\text{max}} = 440$ nm) due to transitions from the $4f^65d^1$ to the $4f^7$ configuration of the Eu^{2+} ion. It may serve as a promising material for use as a lamp phosphor in the blue region. Furthermore, the solution-combustion method is cost-effective, saves energy and time.

References

- [1] T. Justel, J. C Krupa and D. U. Wiechert *J. Lumin.* 2001 **93** 179.
- [2] L .Y Zhou, J. L Huang, L. H Yi, M .L Gong and J. X. Shi *J. Rare Earths* 2009 **27** 54.
- [3] J. Hölsä, H. Jungner, M. Lastusaari and J. Niittykoski *J. Alloys Compd.* 2001 **323** 326–30.
- [4] A. Nag and T.R.N Kutty *J. Alloys Compd.* 2003 **354** 221–31.
- [5] Y. Lu, Y. Li, Y. Xiong, D. Wang, Q. Yin *J. Microelectron.* 2004 **35** 379–82.
- [6] P. Dorenbos, *J. Electrochem. Soc.* 2005 **152** H107–H110.
- [7] J. Holsa, H. Jungner, M. Lastusaari and J. Niittykoski, *J Alloys Compd.* 2001 **323–324**, 326–330.
- [8] W. Hörkner and H .K Müller-Buschbaum *J. Inorg. Nucl. Chem.* 1976 **38** 983–984.
- [9] D. Ravichandran, S.T Johnson, S. Erdei, R. Roy and W. B White *Displays* 1999 **19** 197–203.
- [10] T. Aitasalo, P. Deren, J. Holsa, H. Jungner, M. Lastusaari, J. Niittykoski and W. Streck *Radiat. Meas.* 2004 **38** 515–518.
- [11] J. Hölsä, T. Laamanen, M. Lastusaari, M. Malkamäki, E. Welter and D. A Zajac *Spectrochimica Acta B* 2010 **65** 301–305.
- [12] Y. Lin, Z. Tang, Z. Zhang and C. Nan *J. Eur. Ceram. Soc.* 2003 **23** 175–178.

Chapter 6

Properties of blue emitting $\text{CaAl}_2\text{O}_4:\text{Eu}^{2+},\text{Nd}^{3+}$ phosphors by optimizing the amount of flux and fuel.

6.1. Introduction

Inorganic materials have practical luminescence applications as artificial light sources in many devices. Rare earth doped aluminates form a group of luminescence materials which exhibit high stability, brightness, and versatile industrial processing characteristics suitable for manufacture of lighting and display devices [1, 2]. Long persistent phosphors with many applications such as dark vision display devices [3], emergency route markings [4], warning sign boards [5], sensing of structural damage and fracture of materials [6], etc have been developed. Calcium aluminate (CaAl_2O_4) has been found to be an efficient host material with broad band emissions. Divalent Europium doped $\text{CaAl}_2\text{O}_4:\text{Eu}^{2+}$ phosphor is well-known for a bluish- green emission with a bright afterglow under UV irradiation [7]. As part of a large group of stuffed tridymite tetrahedral framework structures, CaAl_2O_4 consists of three Ca^{2+} sites. One Ca^{2+} site is coordinated with nine oxygen atoms, and the others with six oxygen atoms [8]. Many research works on phosphors with calcium aluminate as a host have been conducted based on their persistent luminescence and photoconductivity spectrum [9]. A few studies outline the synthesis of $\text{CaAl}_2\text{O}_4:\text{Eu}^{2+},\text{Nd}^{3+}$ phosphor which has a broad emission peak at 440 nm [10, 11]. At the same time, the effect of flux on synthesis techniques and on the structural and luminescent properties has become one of the hotspots in the luminescent aluminate materials activated by rare earth metal ions [12–15]. However, the action and mechanism of H_3BO_3 and $\text{CO}(\text{NH}_2)_2$ in the phosphor are not completely resolved. In this

paper, we present the active role of boric acid (H_3BO_3) as flux and urea ($\text{CO}(\text{NH}_2)_2$) as fuel in determining the blue phosphorescence of the $\text{CaAl}_2\text{O}_4:\text{Eu}^{2+},\text{Nd}^{3+}$ phosphor. H_3BO_3 was chosen in this study as it has very good solubility with the oxide materials employed while $\text{CO}(\text{NH}_2)_2$ is readily available, commercially cheap and generates the highest temperature. Metal nitrates are the preferred salts because they easily dissolve in water hence good homogenization can be achieved and low temperatures are enough to melt them. Hydrated salts are even more suitable although the water molecules do not have any effect on the total valencies of the nitrates and are, therefore, irrelevant for the chemistry of the combustion. To investigate how the oxidizer/fuel ratio affected the characteristics of the resultant powder, samples were prepared with below stoichiometric, stoichiometric and above the stoichiometric urea content. Finally, the solution-combustion technique has the merits of low temperature, low cost and time saving in addition to allowing uniform mixing and dissolving of the reactants.

6.2. Experimental

6.2.1 Synthesis

$\text{CaAl}_2\text{O}_4:\text{Eu}^{2+},\text{Nd}^{3+}$ phosphors were synthesized using the solution - combustion method. The starting raw materials used in the experiment include various proportions of analytical pure grade $\text{Ca}(\text{NO}_3)_2 \cdot 4\text{H}_2\text{O}$, $\text{Al}(\text{NO}_3)_3 \cdot 9\text{H}_2\text{O}$, $\text{Eu}(\text{NO}_3)_3 \cdot 5\text{H}_2\text{O}$, $\text{Nd}(\text{NO}_3)_3$, urea ($\text{CO}(\text{NH}_2)_2$) and/or boric acid (H_3BO_3). The raw materials were weighed according to the chemical composition of $\text{CaAl}_2\text{O}_4:\text{Eu}^{2+},\text{Nd}^{3+}$, dissolved in 10 ml of de-ionized water and thoroughly mixed using a magnetic stirrer for 15 minutes without heating to obtain a uniform saturated aqueous solution. To investigate the effect of flux, six samples were prepared with concentrations; 0, 1.9, 3.8, 5.8, 7.7 and 9.7 mol% of H_3BO_3 with a constant 4.25 mol of $\text{CO}(\text{NH}_2)_2$ as a fuel. The second set consists of seven samples used to study the influence of variation of urea on the structural and luminescent properties of the $\text{CaAl}_2\text{O}_4:\text{Eu}^{2+}$ phosphor. The samples were prepared without flux with varying concentrations; 0.3, 0.5, 0.6, 0.7, 0.9, 1.2, and 2.1 mol% of $\text{CO}(\text{NH}_2)_2$. The solutions were then poured into China crucibles and placed one at a time in a muffle furnace pre-heated at 500°C . The mixture ignites and a self-sustaining and rather fast combustion reaction takes off, resulting in a dry, usually crystalline, fine oxide powder. The combustion time was 5–6 min per sample. White voluminous foam was obtained by combusting the mixture at temperatures of $400\text{--}500^\circ\text{C}$. Initially, the solution boiled and underwent dehydration, followed by decomposition releasing large amounts of gases (oxides

of carbon, nitrogen and ammonia and steam (H_2O). Then, spontaneous ignition and smoldering occurred which gradually led to an explosion with enormous swelling. When taken out of the muffle furnace and cooled down, voluminous foam was obtained. The foam was milled to obtain fine white powders. The powders were stored in transparent glass sample bottles for characterization.

6.2.2 Characterization

The synthesized products were characterized by an X-ray diffraction (XRD) using a Bruker Advance D8 X-ray diffractometer (Bruker Corporation of Germany) operating at 40 kV and 4 mA using $\text{Cu K}\alpha = 0.15406$ nm. The morphologies were investigated using a Shimadzu model ZU SSX-550 Super scan Scanning Electron Microscope (SEM) and an Energy Dispersive X-ray Spectrometer (EDS). The decay curves, excitation and emission spectra were measured at room temperature using a Cary Eclipse fluorescence spectrophotometer (Model: LS- 55) with a built-in 150W xenon flash lamp as the excitation source and a grating to select a suitable excitation wavelength.

6.3. Results and Discussion

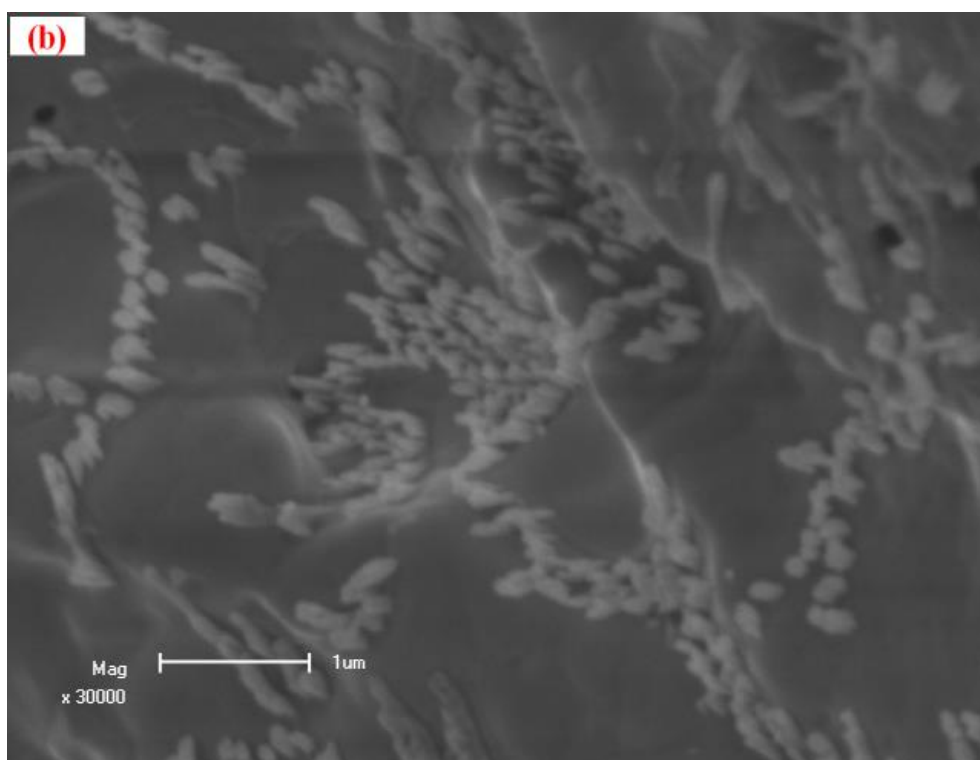
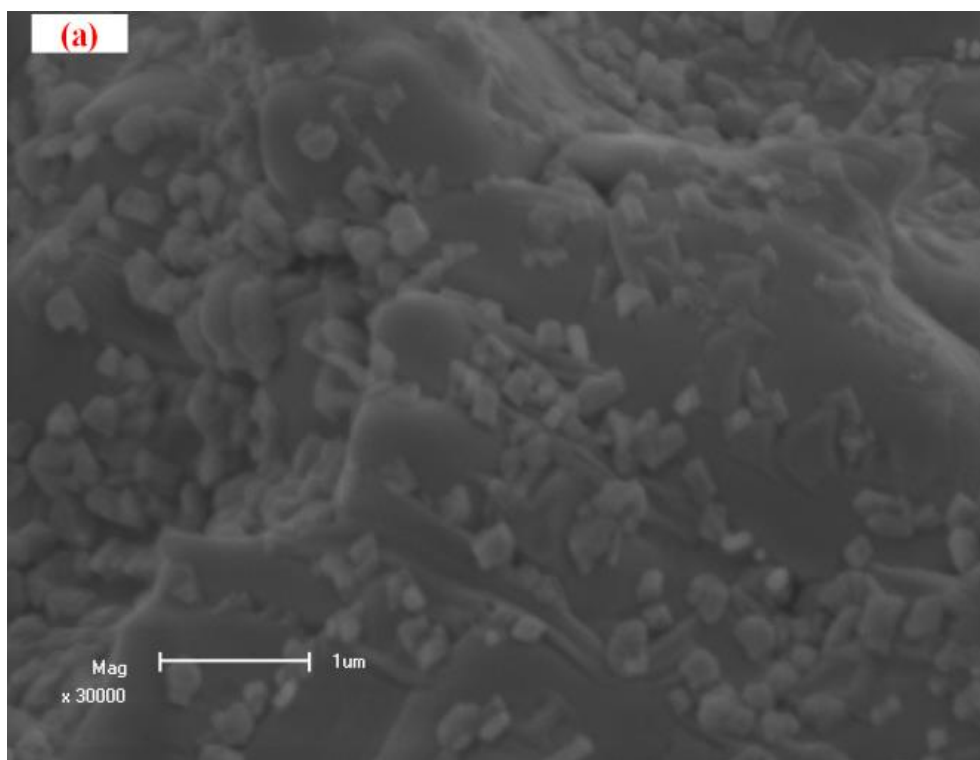
6.3.1 Influence on structure

6.3.1.1. SEM and EDS analysis

Fig. 1 shows the representative SEM micrograph taken for (a) 1.9 mol% H_3BO_3 , (b) 3.8 mol% H_3BO_3 , (c) 0.3 mol% $\text{CO}(\text{NH}_2)_2$ and (d) 0.5 mol% $\text{CO}(\text{NH}_2)_2$ samples respectively. It can be observed from Fig.1 (a) and (b) that the particle size of phosphor synthesized with 1.9 mol% H_3BO_3 is smaller than that of 3.8 mol% H_3BO_3 .

The presence of urea allows the growth of faceted crystals by forming liquid interfaces among crystal grains and causing the crystal grains to reunite resulting in bigger particles, Figure 6.1(c). The endothermic reactions during the solution-combustion process are characterized by decomposition and removal of nitric oxides and significantly vary depending on the precursor ingredients and the ratio of metal nitrate to urea [16, 17].

The nucleation process and subsequent growth of nanoparticles is greatly influenced by systematic release of constituent anions and/or cations and is achieved by the spontaneous release of anions from organic molecules. For instance, solutions containing urea, $\text{CO}(\text{NH}_2)_2$, when heated liberate hydroxide (OH) ions, which can cause precipitation of metal oxide or hydroxide [18-20].



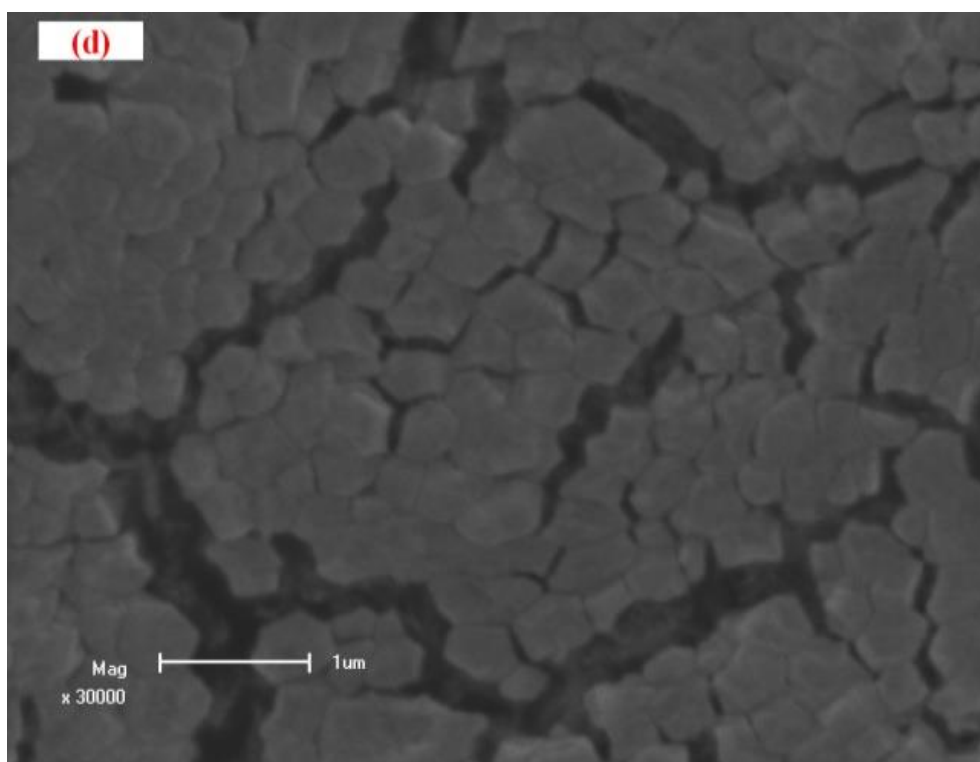
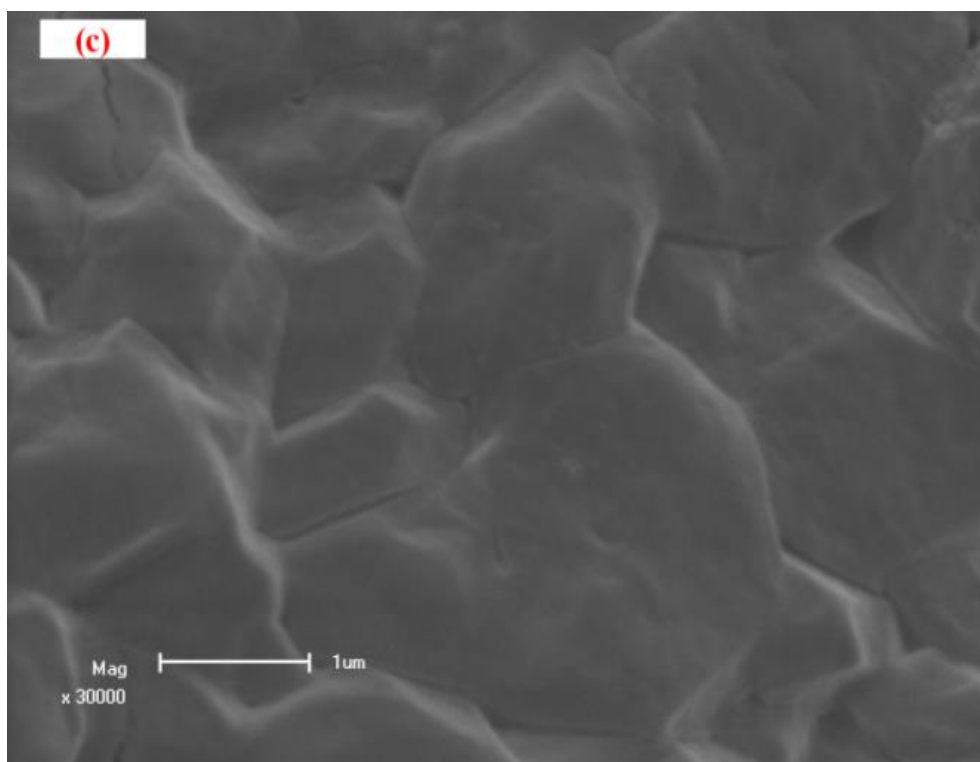


Figure 6.1: Sample SEM micrographs for (a) 1.9 mol% H_3BO_3 acid (b) 3.8 mol% H_3BO_3 acid (c) 0.3mol% $\text{CO}(\text{NH}_2)_2$ and (d) 0.5 mol% $\text{CO}(\text{NH}_2)_2$ all at $\times 30000$ magnification.

The decomposition of urea is therefore used to control the nucleation process in the synthesis of $\text{CaAl}_2\text{O}_4:\text{Eu}^{2+}$ nanoparticles [19]. The nanostructures also crystallize to form fine, regular hexagonal platelets exhibiting smooth surface and well-developed faces that showed size around 316 nm as shown in Figure 6.1 (d). Hence it can be deduced that addition of urea favors the formation of hexagonal crystalline structures in these phosphors. Moreover, it is well known that phosphors with regular morphology can improve the packing density, slurry properties and improve the luminescence of phosphor [21]. Two types of agglomerates can be observed. One is the needle-like particle, Figure 6.1(b) and another is the large size tetrahedral particle, Figure 6.1(c).

The (EDS) spectra of $\text{CaAl}_2\text{O}_4:\text{Eu}^{2+},\text{Nd}^{3+}$, (Figure 6.2) revealed the presence of the constituent elements in the materials prepared by the solution-combustion synthesis

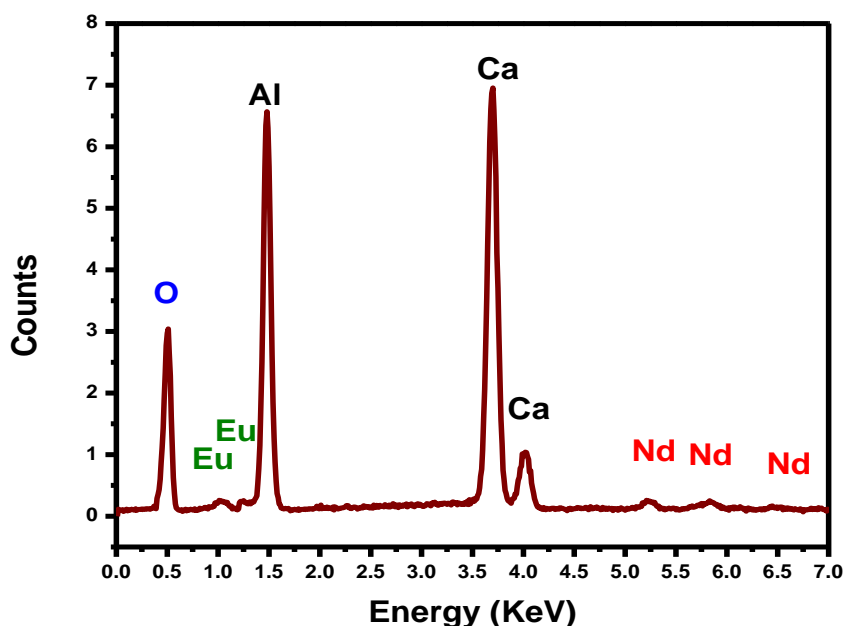


Figure 6.2. EDS micrograph revealing the composition of the $\text{CaAl}_2\text{O}_4:\text{Eu}^{2+},\text{Nd}^{3+}$.

6.3.1.2. XRD analysis

Figures 6.3(a) and 6.3(b) show the powder XRD pattern for the $\text{CaAl}_2\text{O}_4:\text{Eu}^{2+},\text{Nd}^{3+}$ synthesised with H_3BO_3 and $\text{CO}(\text{NH}_2)_2$ respectively. From Figure 6.3(a), it can be observed that boric acid strongly enhances phase stabilization (no phase change) because it melt at low temperature and act as flux for the synthesis of the phosphor and help to urge activator ions

enter crystal lattice and form luminescent and trap centers which makes it feasible to obtain single pure phase of CaAl_2O_4 [22]. In Figure 6.3(b), two phases are easily observable. The main diffraction peaks indexed well with the monoclinic structure of CaAl_2O_4 according to the card file (JCPDS: no: 70 - 0134). The additional impurity phases can be due to the presence of CaAl_4O_7 [24] or some of the unreacted precursors which may be attributed to the fact that the combustion was not uniform [23].

Peak	2 θ (Degree)	FWHM(Degree)	SIZE(nm)
[211]	27.043	0.15494	52.73
[220]	30.157	0.16291	50.5
[301]	31.219	0.19139	43.1
AV. SIZE(nm)			54.25

Table 6.1: Average crystal size of the monoclinic $\text{CaAl}_2\text{O}_4:\text{Eu}^{2+},\text{Nd}^{3+}$ phase.

Analysis of these diffractive peaks reveal that 1.2 mol% urea favour pure monoclinic CaAl_2O_4 phase, while with lower concentrations (<1.2 mol %), the reaction leads to formation of CaAl_4O_7 phases as a result of incomplete combustion as shown in Figure 6.3 (b) i.e the temperature was not enough to promote the crystallization of the desired phase and the reaction will have to be carried out only at higher temperatures. However, the as-prepared powders containing ≥ 1.2 mol% urea ignited easily, the high temperature was sustained longer and the combustion resulted in crystalline phase. Table 6.1 gives the average crystal size from the three major crystal peaks calculated using the Debye Scherrer equation.

The Debye-Scherrer method is used to obtain X-ray diffraction measurements in powders. It is well known that broadening occurs in the diffraction rings as the particle size of the powders decreases. The width at half height of the diffracted ray, as shown in Figure 6.4, is related to the particle diameter D of the crystallite by the Scherrer equation:

$$D = \frac{K\lambda}{\beta \cos \theta} \dots\dots\dots (1)$$

where $K=0.9$ a constant, λ is the wavelength of monochromatic X-ray, θ is the Bragg angle (the diffracted ray appears at angle 2θ), β is the peak width at half height for small and large (larger than $\sim 10 \mu\text{m}$) crystallites, respectively, as shown in the figure.

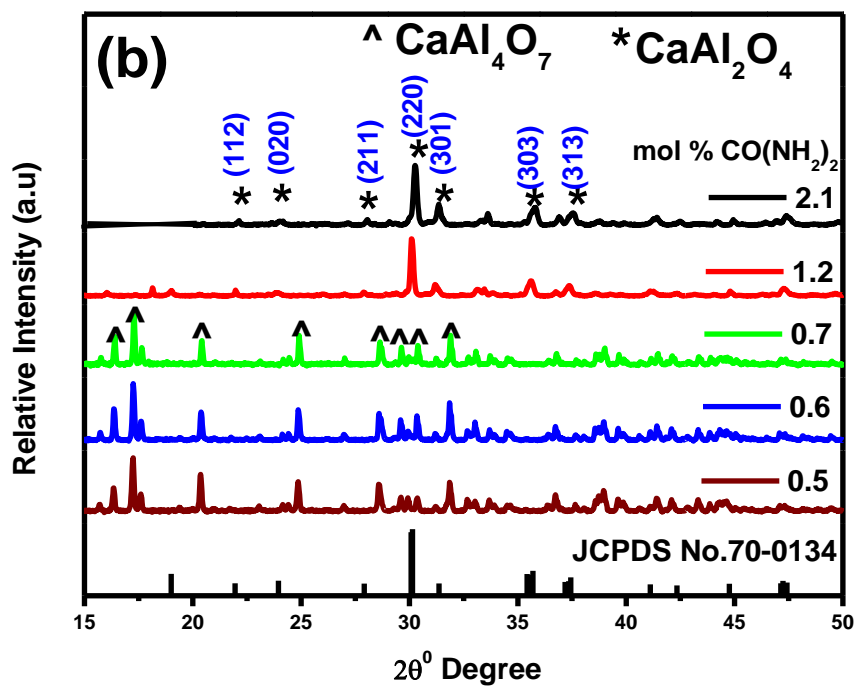
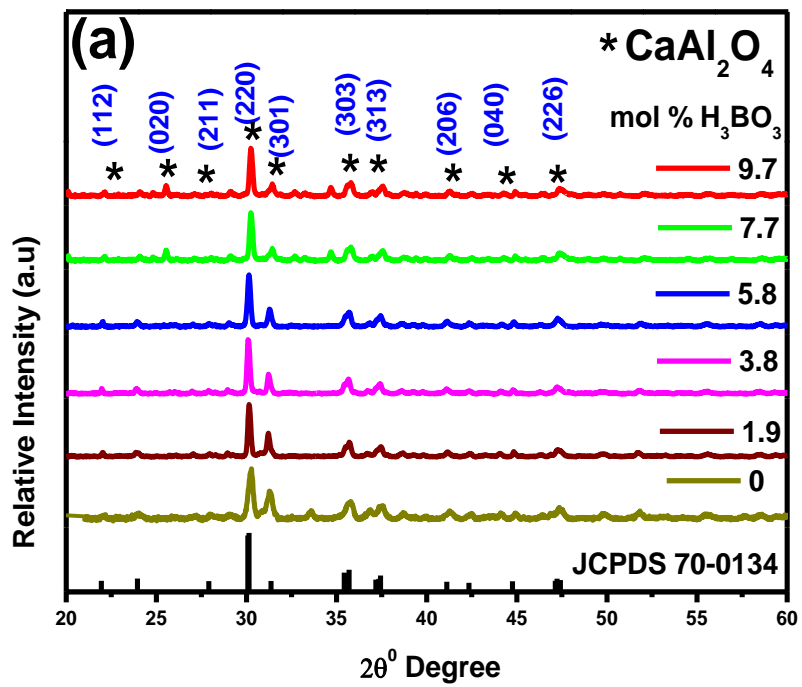


Figure 6.3. Effect of (a) amount of flux and (b) fuel (urea) on the structure of the $\text{CaAl}_2\text{O}_4:\text{Eu}^{2+},\text{Nd}^{3+}$ phosphor.

This method is applicable to crystallites ranging from 1.0 to 0.01 μm in diameter, but the grains must have good crystallinity.

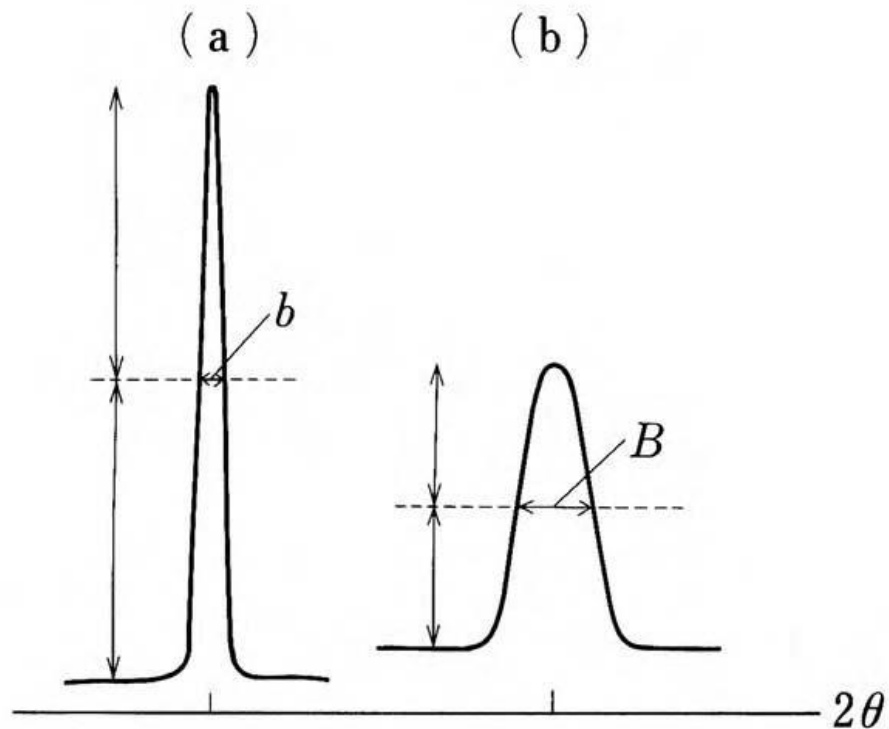


Figure 6.4. Intensity curves of X-ray diffraction profiles for (a) large and (b) small particles.

For crystals with particle size ranging from 1 to 200 nm, the method for measuring the angular distribution of the intensity of the scattered X-ray called the **small angle method** (because only small incident angles are involved) is applicable. According to this method, the intensity of the scattered radiation is given approximately by:

$$\log I(\theta) = \log I_0 - \frac{\pi^2 D^2 s^2}{3\lambda^2} \dots\dots\dots(2)$$

where by $s = \left(\frac{4\pi}{\lambda}\right) \sin\left(\frac{\theta}{2}\right) \sim \frac{2\pi\theta}{\lambda}$.

Table 6.2 gives the respective values;

θ	$I(\theta)$	$\log I(\theta)$	S	S^2
22.023	602	2.7796	8.017	64.27
27.043	383	2.5832	9.836	96.75
30.157	7917	3.8986	10.963	120.18
31.219	5703	3.7561	11.346	128.74

Table 6.2: Values of $\log I(\theta)$ and S^2

Inserting these values into equation (2) and plotting $\log I(\theta)$ versus s^2 a linear relation is obtained as shown in Figure 6.5 and its slope gives the particle diameter as 34.68 nm.

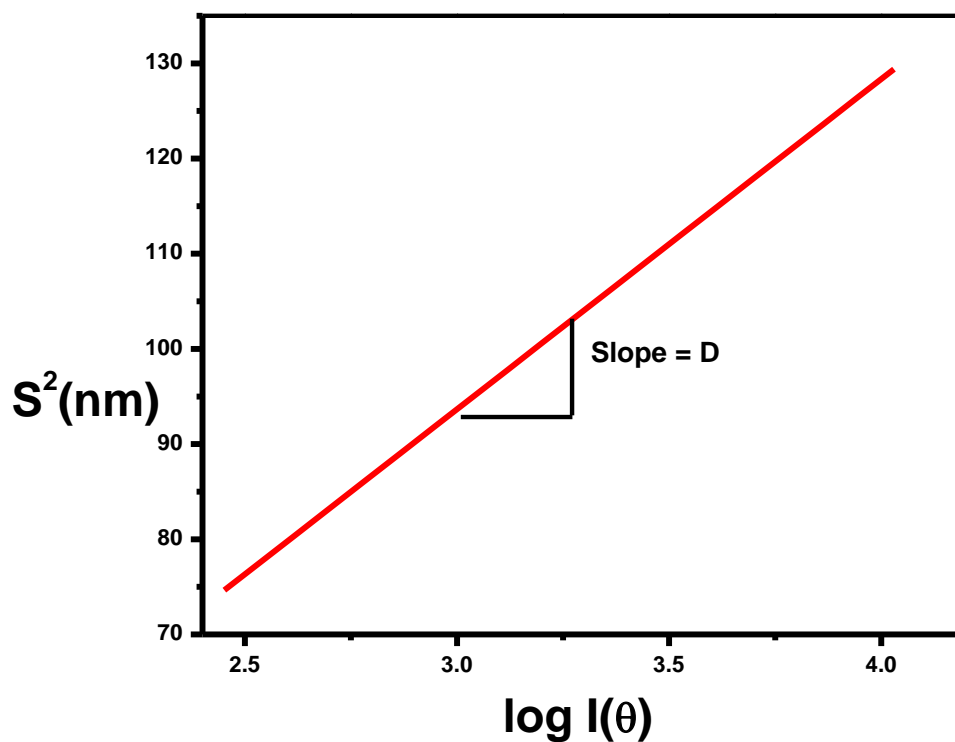


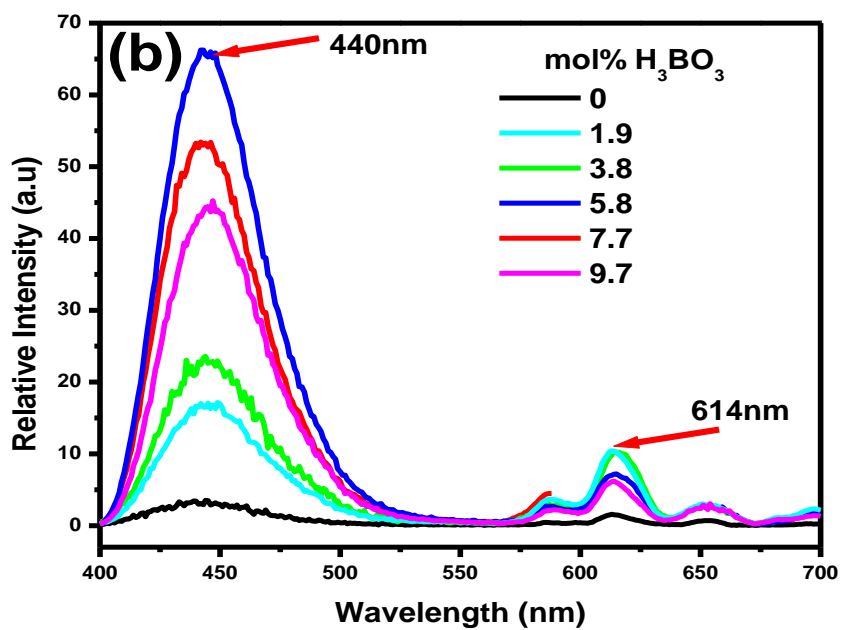
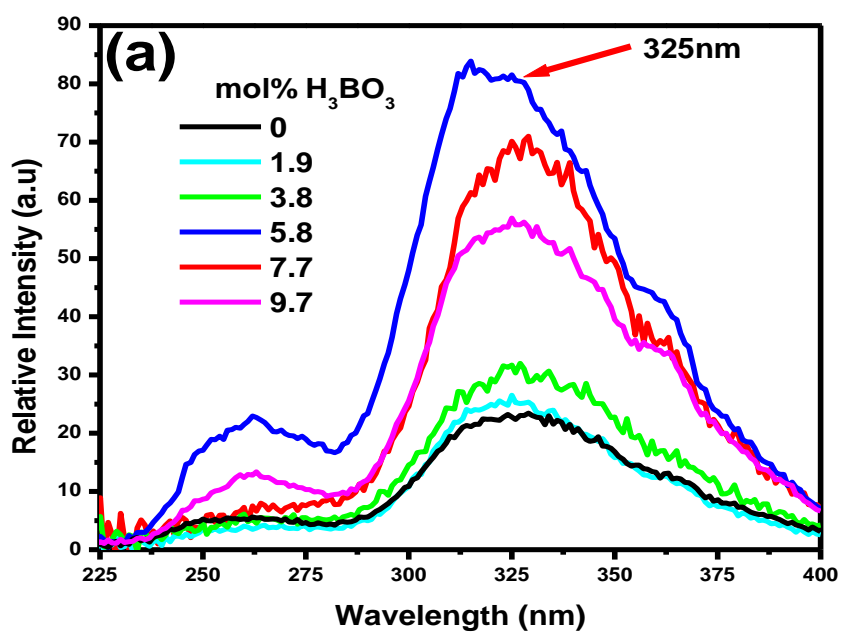
Figure 6.5. A plot of $\log I(\theta)$ versus s^2 .

6.3.2 Influence on photoluminescence properties

6.3.2.1 Effect of Boric Acid.

Figure 6.6 depicts the effect of H_3BO_3 on the PL spectra of the phosphor. From Figure 6.6(a) there is an excitation peak at around 325nm in the excitation spectrum ($\lambda_{\text{em}} = 440 \text{ nm}$) which is in conformity with the absorption of the host CaAl_2O_4 . Also the position of excitation peaks did not change evidently when the phosphor was synthesized with addition of H_3BO_3 . Figure 6.6(b) represents the emission spectra of Eu^{2+} ion in various calcium aluminate host lattices. It is clear from the figure that the samples gave emission at 440 nm but its intensity varied with the H_3BO_3 content. It also showed some narrow emission lines in red region that arise from the f-f transitions of the remnant unreduced Eu^{3+} ions. It is well known that if the crystallization is done properly, it is the flux that facilitates the entry of activator into the crystal lattice and aids in the formation of luminescent center [24]. The change in the PL intensity can be mainly attributed to the amount of H_3BO_3 and its influence on the crystalline phase (CaAl_2O_4) formation and enhanced luminescent properties. Figure 6.6(c) shows the effect of different content of H_3BO_3 on decay properties of $\text{CaAl}_2\text{O}_4:\text{Eu}^{2+},\text{Nd}^{3+}$. Obviously, at 5.8 mol% H_3BO_3 content the initial brightness of the phosphor is the best and the afterglow time is the longest. However, the luminescent properties become bad when the content of H_3BO_3 continues to increase (7.7 and 9.7 mol %).

From Figure 6.6 it is evident that the PL intensity is maximum for 5.8 mol% H_3BO_3 while in $< 5.8 \text{ mol\%}$ H_3BO_3 samples the intensity is low due to the presence of CaAl_2O_4 phase in small proportion owing to the formation of other non-luminescent phases formed due to incomplete combustion. The maximum PL in CaAl_2O_4 can be explained to be due to the $4f \leftrightarrow 5d$ electronic transition of Eu^{2+} ion associated with the change in electric dipole i.e. ${}^8\text{S}_{7/2} \leftrightarrow {}^2\text{D}_{5/2}$, which is a Laporte allowed transition. Because of strong crystal field effect of stuffed tridymite CaAl_2O_4 structure, the $4f^65d^1$ level of Eu^{2+} ion completely overlaps the $4f^7$ level, except for the ground state [25]. Therefore, the Eu^{2+} emission occurring from the lowest excited $4f^65d^1$ level lies in the visible region (440 nm) of the electromagnetic spectrum. Furthermore, it supports our argument that the other phases must be contributing to non-radiative transitions [26]. This may be the reason why the 0, 1.9, and 3.8 mol% H_3BO_3 showed less PL intensity.



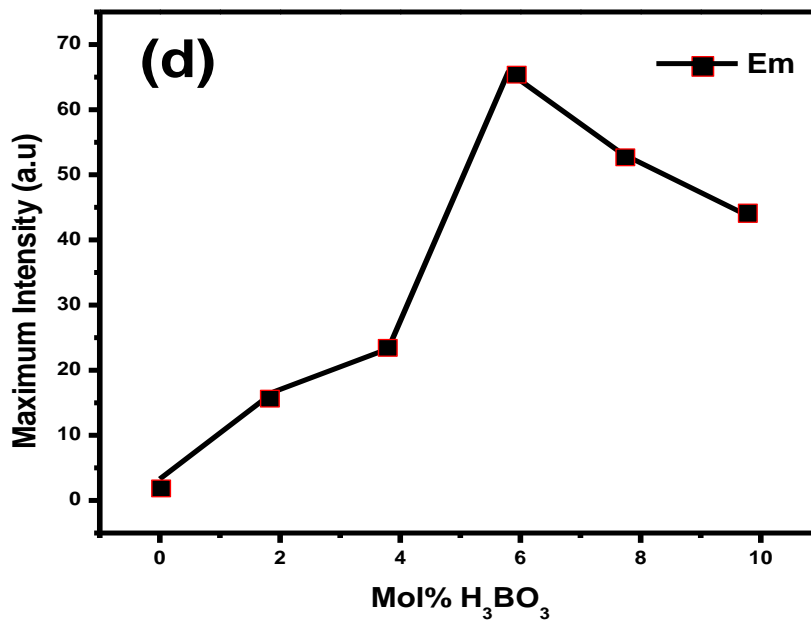
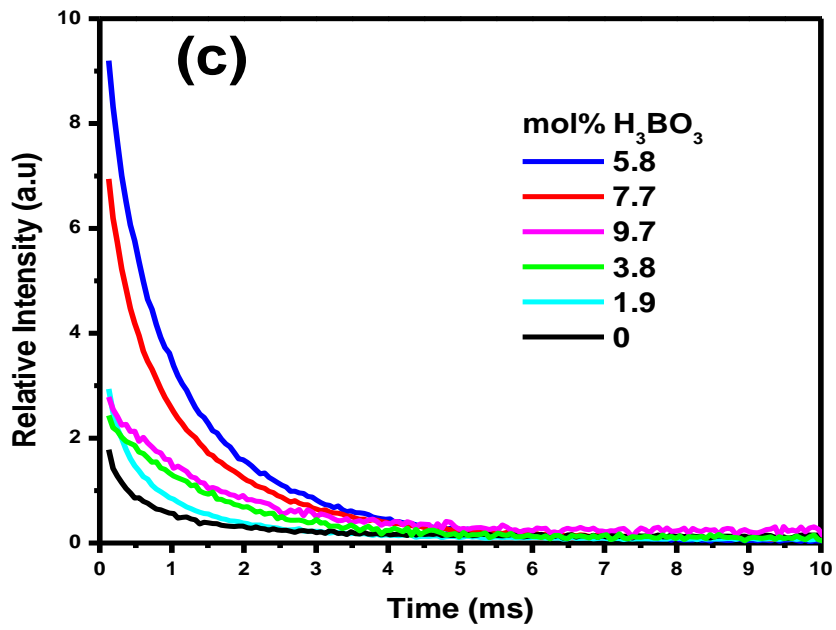
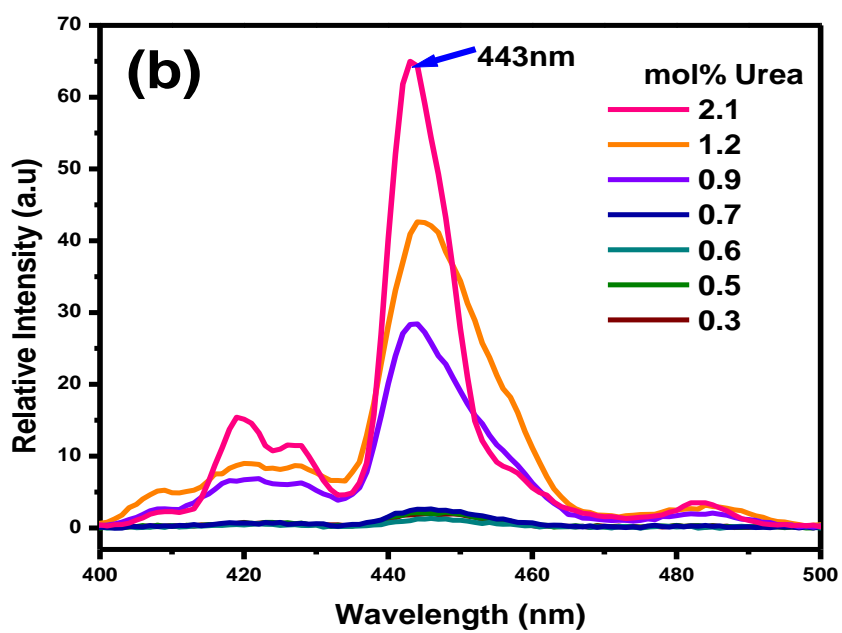
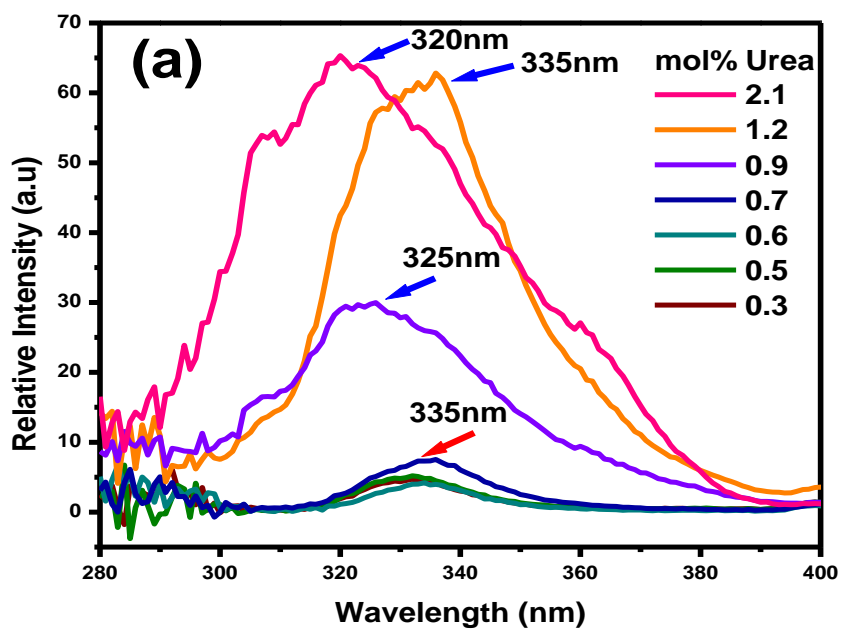


Figure 6.6. Effect of amount of flux on the luminescent characteristics.

6.3.2.2. Effect of Urea



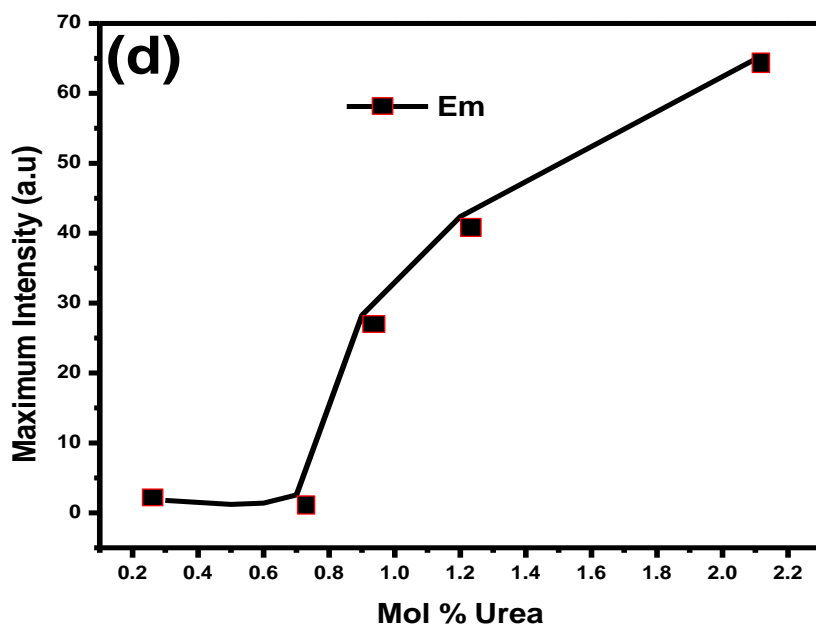
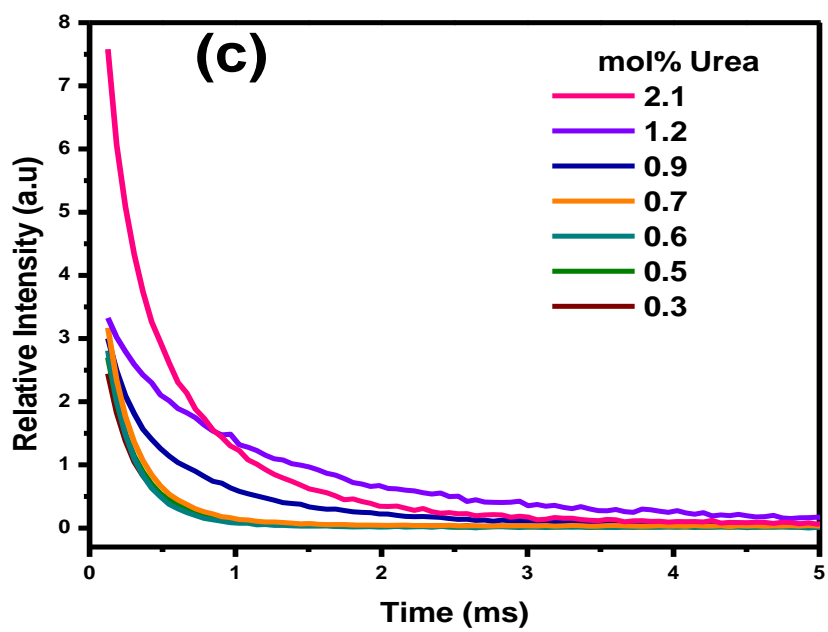


Figure 6.7. Effect of amount of urea on the luminescent characteristics.

As displayed by the spectral characteristics of Figure 6.7, it is evident that urea concentration significantly affects PL intensities of the $\text{CaAl}_2\text{O}_4:\text{Eu}^{2+}$ Phosphor. As can be seen, a concentration of 2.1 mol% urea enhances luminescence properties of the phosphor.

Conclusion

The phosphor $\text{CaAl}_2\text{O}_4:\text{Eu}^{2+},\text{Nd}^{3+}$ can be prepared by solution-combustion method which is cost-effective, saves energy and time. The influences of the varying quantity of H_3BO_3 and $\text{CH}_4\text{N}_2\text{O}$ on the structural and luminescent properties of the phosphor were studied. The analytical results indicate that the broad emitted band of the $\text{CaAl}_2\text{O}_4:\text{Eu}^{2+},\text{Nd}^{3+}$ is observed in the blue region ($\lambda_{\text{max}} = 440 \text{ nm}$) due to transitions from the $4f^65d^1$ to the $4f^7$ configuration of the Eu^{2+} ion. It is observed that by changing the fuel concentration, one can control particulate and hence the luminescence properties of the phosphor. Reaction in the presence of urea allows the growth of faceted crystals since urea acts as a reduction reagent. Liquid interfaces are produced among crystal grains, and then the crystal grains reunite and result in bigger particles. $\text{CaAl}_2\text{O}_4:\text{Eu}^{2+},\text{Nd}^{3+}$ may serve as a promising material for use as a lamp phosphor in the blue region.

References

- [1] J.T Krupa, J.C Wiechert, J. Lumin., 2001, **93**(3) 179.
- [2] L.Y Zhou, J.L Huang, L.H Yi, M.L Gong, J.Shi J. Rare Earths, 2009, **27**(1) 54.
- [3] T. Matsuzawa, Y. Aoki, N .Takeuchi and Y. Murayama J. Electrochem. Soc. 1996, **43** 2670.
- [4] E. Nakazawa and T. Mochida J. Lumin. 1997, **236** 72.
- [5] M. Kowatari, D. Koyama, Y. Satoh, K. Linuma and S. Uchida Nucl. Instrum.Methods Phys. Res. A 2000, **480** 431.
- [6] C.N. Xu, T. Watanabe, M. Akiyama and X. Zheng, Appl. Phys. Lett. G 1999, **74** 241.
- [7] Y. Murayama, S. Shionoya, W.M. Yen (Eds.), Phosphor Handbook, CRC Press, Boca Raton, FL, USA, 1999, 651.
- [8] Y.J Park, Y. J Kim, Ceram. Int., 2008, **34**(4) 1109.
- [9] T. Aitasalo, J. Hölsä, H. Jungner, M. Lastusaari, J. Niittykoski, J. Phys. Chem. B, 2006, **110**(10) 4589.
- [10] F.C Palilla, A.K Levine and M.R Tomkus J. Electrochem. Soc. 1968, **115** 642.
- [11] T. Aitasalo, J. Holsa, H. Jungner, M . Lastusaari and J. Nittykoshi J. Lumin. 2001, **59** 94–95.
- [12] J. Niittykoski, T. Aitasalo, J. H'ols'a, H. Jungner, M. Lastusaari, M. Parkkinen, M. Tuka, J. Alloys. Compd. 2004, **374** 108–111.
- [13] Y. Li, Rare earth 1998, **19** (3) 68–72.
- [14] N. Wang, D. Wang, Mater. Sci. Eng. 1998, **16** (4) 40–43.
- [15] T. Abanti, R.N. Kutty, J. Alloys. Compd. 2003, **354** 221–231.
- [16] P. D Sarkisov, N. V Popovich, A. G Zhelnin, Glass and Ceramics, 2003, **60**(9-10) 309.
- [17] S. Ekambaram and K.C. Patil, Journal of Alloys and Compounds, 1997 **248** 7.
- [18] E. MatijeviC and W.P. Hsu, 1 Colloid Interf Sci. 1987, **118** 506.

- [19] D. Sordélet and M. Akinc, *J. Colloid. Sci.* 1988, **122** 47.
- [20] G. Wakefield, E. Holland, P.J. Dobson and J.L Hutchison , *Adv. Mater.* 2001, **13**1557.
- [21] T. Xiaoming, Z. Weidong, H. Yunsheng, Z. Chunlei, H. Huaqiang and H. Xiaowei, *J. Alloys Compd.* 2008, **458** 446 – 449.
- [22] M. Ohring, Academic Press, San Diego, CA.
- [23] C. Zhao and D. Chen *Mater. Lett.* 2007, **61** 3673–3675.
- [24] D. Haiyen, L. Gengshen and S. Jaiyue, *J.Rare Earths* 2007, **25** 19-22.
- [25] G.F.J Garlick, Oxford University Press, UK, 1949, 73.
- [26] G. Blasse and A. Brill *Philips Tech. Rev.* 1970, **31** 303.

Chapter 7

Effect of Eu^{2+} and Nd^{3+} on the properties of blue $\text{CaAl}_2\text{O}_4:\text{Eu}^{2+}, \text{Nd}^{3+}$ long afterglow phosphor.

7.1. Introduction

The phenomenon of persistent luminescence refers to the ability of a material to absorb and store artificial energy from lighting, including visible and ultraviolet (UV) radiation, around it and to gradually release it as light in the dark at room temperature [1]. Persistent luminescent materials, which demonstrate an afterglow measured in hours, are of interest for various applications such as light emitting devices, fluorescent lamps, plasma display panels, lamps for medical applications, dark vision applications involving signage, intentional blackouts, emergency guidance systems and luminous watches among others. Although persistent luminescence has been known since the early 1600s after the discovery of the Bologna stone [2], the details behind the storage and slow release of energy are still not completely resolved. Rare earth co-doped calcium aluminate $\text{CaAl}_2\text{O}_4:\text{Eu}^{2+}, \text{Nd}^{3+}$ forms a large group of alkaline earth aluminates $\text{MAl}_2\text{O}_4:\text{Eu}^{2+}, \text{R}^{3+}$ (M=Ca, Sr, Ba) which are replacing the traditional $\text{ZnS}:\text{Cu}, \text{Co}$ due to their persistent luminescence properties and also because they are chemically stable, can be easily grown in crystalline form, and have a wide band gap of around 6 eV. Studies on the mechanism of persistent luminescence have focused on the interchange of the rare earth ions with the host band structure and the lattice defects.

Although it is known that the Eu^{2+} ion acts as the luminescence center, the effect of Eu^{2+} and Nd^{3+} concentration in the enhancement (or decrease) of the luminescence properties of $\text{CaAl}_2\text{O}_4:\text{Eu}^{2+}, \text{Nd}^{3+}$ co-doping has not been established. For long persistence materials, the depth and number of traps are critical factors in determining their performance. To achieve long persistence, rare earth ions are usually doped into hosts with complicated structures, because it is easier to form defect-related traps in such hosts. The ability of the rare earth species to trap electrons or holes can be determined from the location of the 4f and 5d levels of the Eu^{2+} and the Nd^{3+} ions in the band structure of the host [4], but the positions of these

levels alone cannot offer enough explanation of the energy storage and luminescent mechanism [1] hence the role of lattice defects.

This work focuses on the luminescence properties of blue emitting $\text{CaAl}_2\text{O}_4:\text{Eu}^{2+},\text{Nd}^{3+}$ phosphor. The effect of Eu^{2+} doping and Nd^{3+} co-doping concentration in the enhancement (or decrease) of the luminescence properties of $\text{CaAl}_2\text{O}_4:\text{Eu}^{2+},\text{Nd}^{3+}$ were investigated. Samples of $\text{CaAl}_2\text{O}_4:\text{Eu}^{2+},\text{Nd}^{3+}$ were synthesized by solution-combustion method in liquid phases so that the amount of each component can be accurately controlled and uniformly mixed. Compared with other conventional methods, the combustion process is very facile, safe, energy saving and only takes a few minutes.

7.2. Experimental

7.2.1. Synthesis

The starting materials consisting of analytical pure grade $\text{Ca}(\text{NO}_3)_2 \cdot 4\text{H}_2\text{O}$, $\text{Al}(\text{NO}_3)_3 \cdot 9\text{H}_2\text{O}$, $\text{Eu}(\text{NO}_3)_2$, and $\text{Nd}(\text{NO}_3)_3$ together with a certain amount of $\text{CO}(\text{NH}_2)_2$ were dissolved in 10 ml of de-ionized water in a 100 ml beaker according to the stoichiometric chemical composition of $\text{CaAl}_2\text{O}_4:\text{Eu}^{2+},\text{Nd}^{3+}$. Then, a flux, H_3BO_3 , was added into the solution and stirred for 15 minutes at room temperature.

To study the effect of dopant Eu^{2+} six samples were prepared with concentrations; 0.18, 0.36, 0.72, 0.93, 1.08 and 1.45 mol% of $\text{Eu}(\text{NO}_3)_2$ without Nd^{3+} . The second set consists of five samples used to study the influence of variation of amount of co-dopant Nd^{3+} on the structural and luminescent properties of the $\text{CaAl}_2\text{O}_4:\text{Eu}^{2+},\text{Nd}^{3+}$ phosphor. The samples were prepared with varying concentrations; 0.09, 0.18, 0.36, 0.72, and 1.44 mol% of $\text{Nd}(\text{NO}_3)_3$ with a constant concentration of $\text{Eu}(\text{NO}_3)_2$. These percentages of $\text{Eu}(\text{NO}_3)_2$ and $\text{Nd}(\text{NO}_3)_3$ are in relation to the sum total moles of all the nitrates that went into the solution.

The solutions were then poured into China crucibles and placed one at a time in a muffle furnace pre-heated at 500 °C. Initially, the solution boiled and underwent dehydration, followed by decomposition with the evolution of large amounts of gases (oxides of carbon, nitrogen and ammonia). Then, spontaneous ignition occurred and underwent smoldering combustion with enormous swelling, producing white foamy and voluminous ash. The voluminous and foamy combustion ash was then milled to obtain the phosphor powders which were stored in glass sample bottles for characterization.

7.2.2. Characterization

The synthesized products were characterized by X-ray diffraction (XRD) using a Bruker D8 (Bruker Co., Germany) X-ray diffractometer with graphite monochromatized Cu K α irradiation ($\lambda=1.5406$ Å). The morphologies were investigated using a Shimadzu model ZU SSX-550 Super scan Scanning Electron Microscope (SEM) and an Energy Dispersive X-ray Spectrometer (EDS). FTIR measurements were done using Bruker Tensor 27 spectrometer. The Excitation and emission spectra were measured at room temperature using a Cary Eclipse fluorescence spectrophotometer (Model: LS - 55) with a built-in 150W xenon flash lamp as the excitation source and a grating to select a suitable excitation wavelength.

7.3. Results and Discussion

7.3.1. Influence on structure

7.3.1.1 SEM and EDS analysis

Figure 7.1 shows the SEM results of CaAl₂O₄:Eu²⁺,Nd³⁺. The non-uniform and irregular shapes of particles shown in Figure 7.1(a) may be due to the non-uniform distribution of temperature and mass flow in the combustion flame. The morphology of a porous product of Figure 7.1(b) showed irregular network like structures with lots of voids, pores and networks. The pores and voids were produced during the escaping of gaseous products during the combustion of nitrates and fuel.

The EDX analysis was carried out to confirm the presence of Eu²⁺ and Nd³⁺ ions in the phosphor and the results of Figure 7.2(a) confirmed their presence.

Figure 7.2(b) and (c) show the FTIR spectra of the samples. The bands at 3450 cm⁻¹ represent the vibration of a calcium nitrate. The absorption band at 2990–3000 cm⁻¹ is characteristic of highly hydrated carbo-aluminates. The bands at 420 cm⁻¹ confirmed the presence of a hydrate of the hexagonal type [5]. The bands at 1430 cm⁻¹ confirmed the presence of calcium carbonate which can be attributed to have resulted from the presence of excess CO(NH₂)₂. From Figure 7.2(c) we observe an increase in the absorbance intensity indicating that Nd³⁺ enhances absorption as compared to Eu²⁺ as shown in Figure 7.2(b). The same is also reflected in the PL spectra of Figure 7.4 and Figure 7.5 respectively.

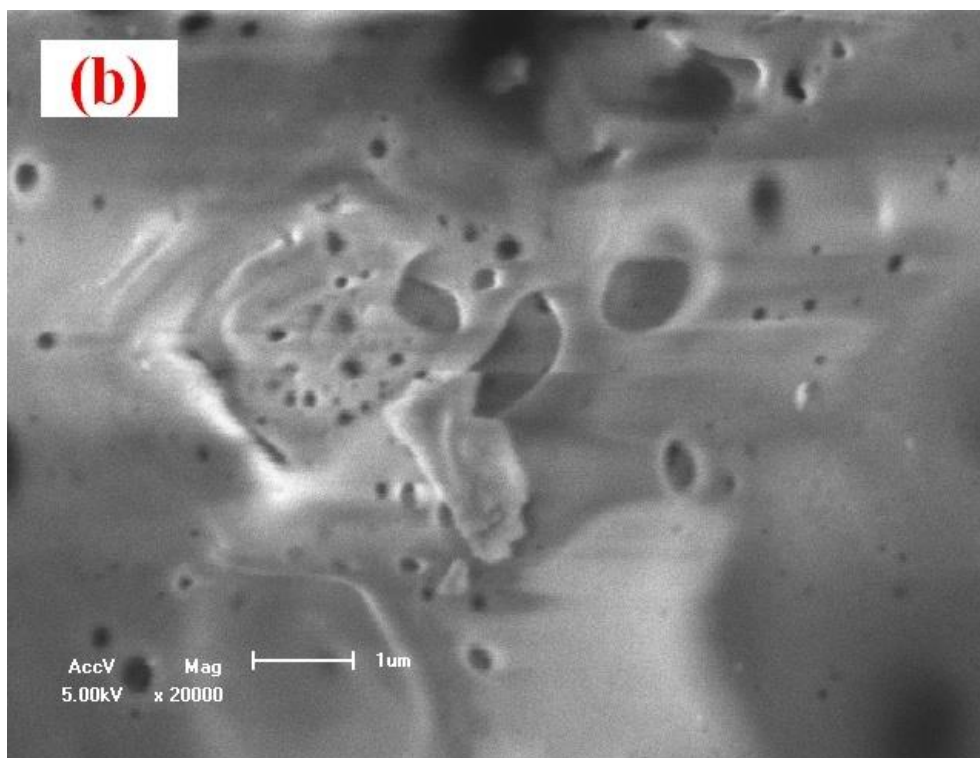
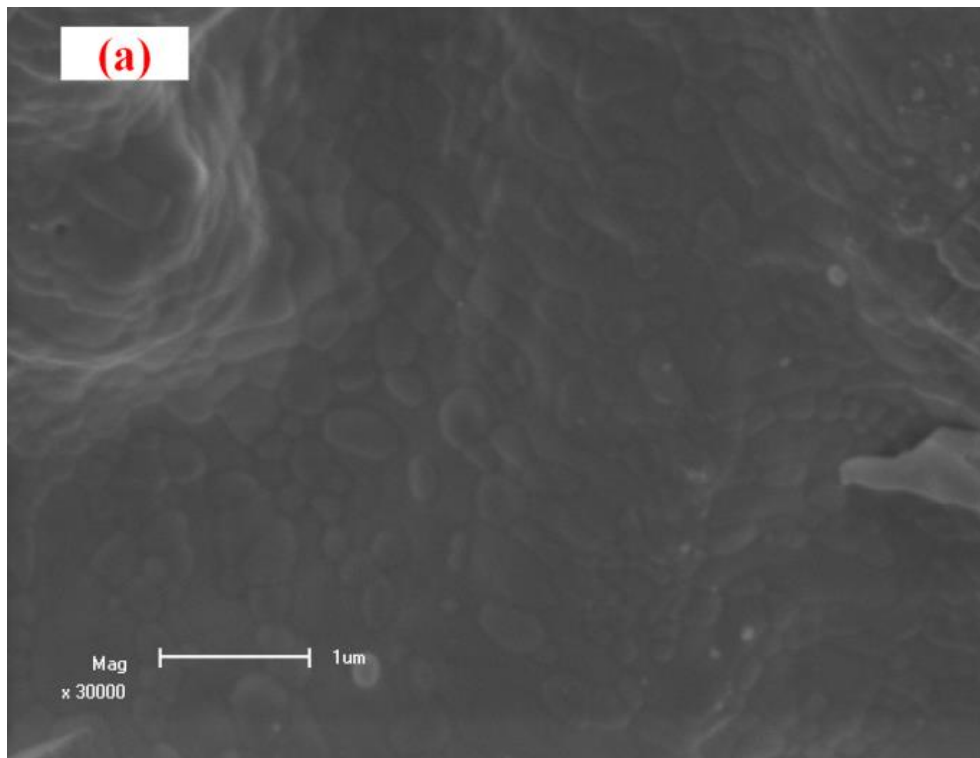
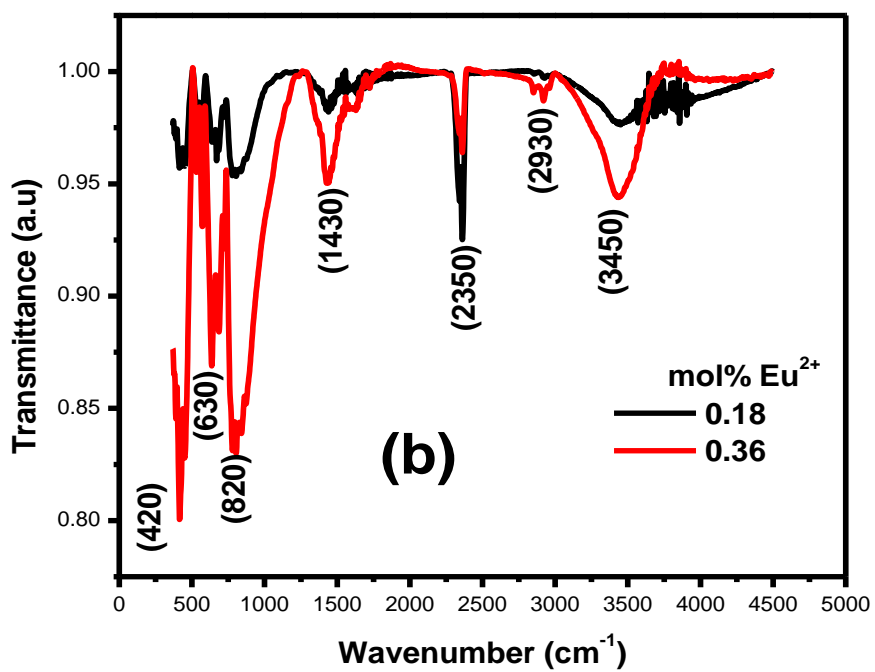
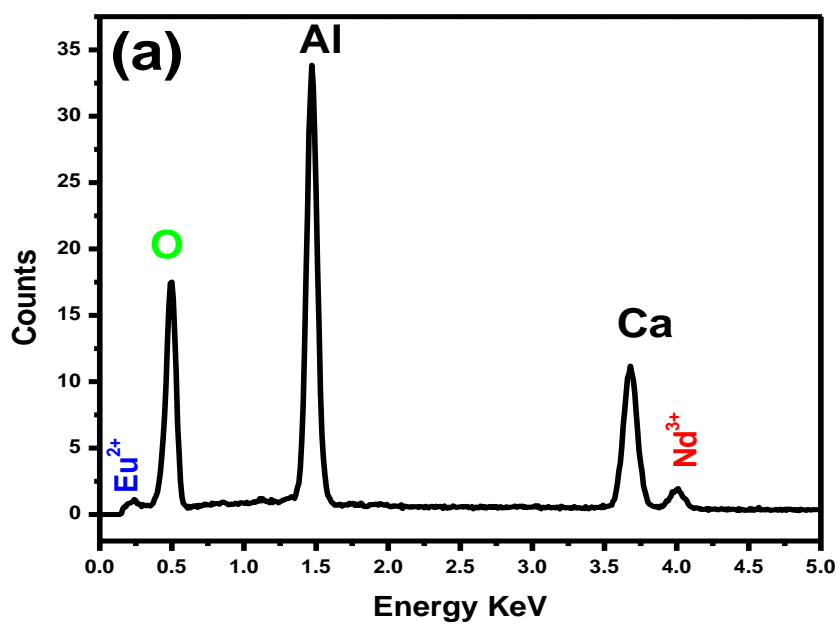


Figure 7.1: Sample SEM microstructures for (a) 0.18 mol% Eu^{2+} (b) 0.09 mol% Nd^{3+} .



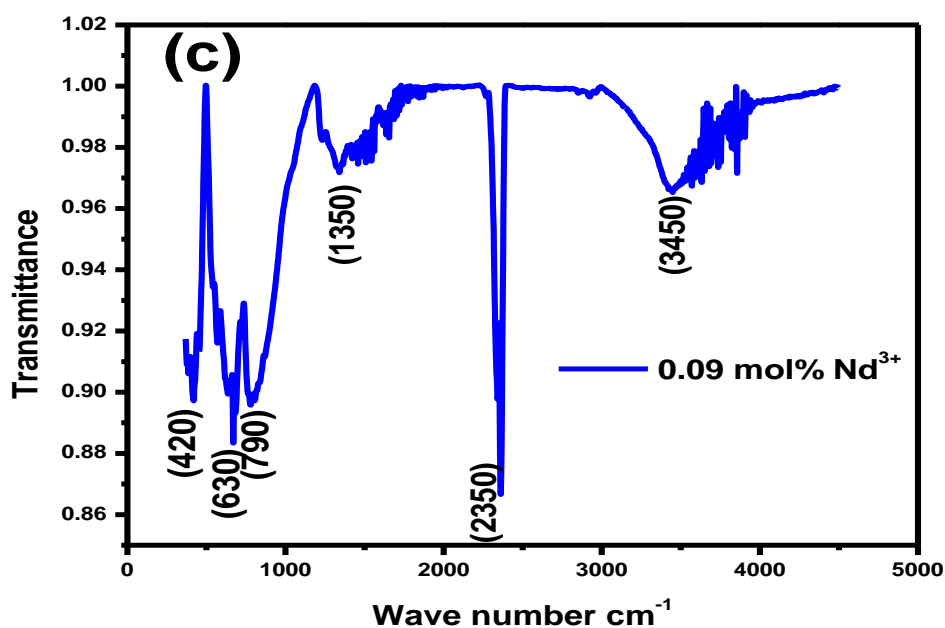
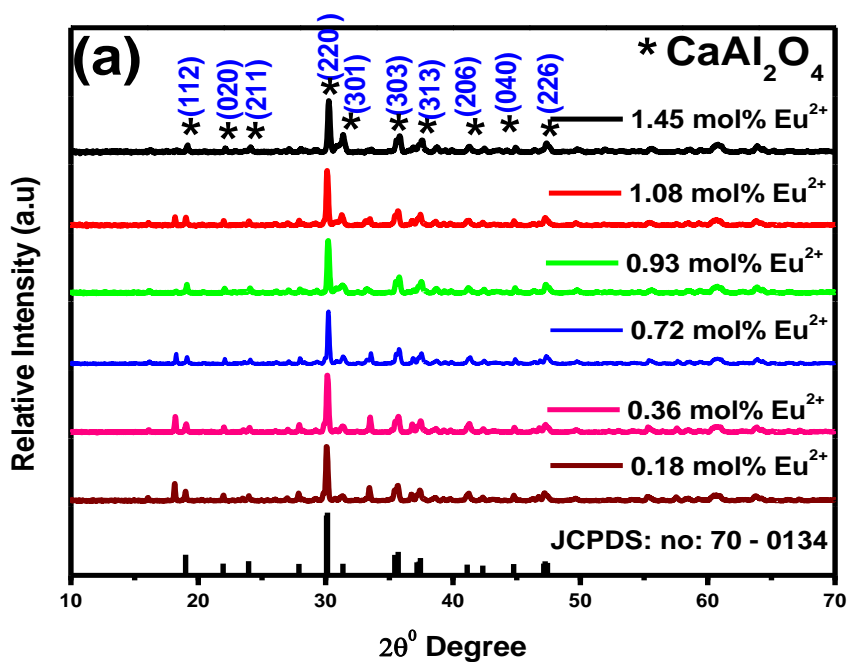


Figure 7.2: (a) EDS micrograph revealing the composition of the $\text{CaAl}_2\text{O}_4:\text{Eu}^{2+},\text{Nd}^{3+}$, FTIR spectrum for (b) 0.18,0.36 mol% Eu^{2+} and (c) 0.09 mol% Nd^{3+} .

7.3.1.2 XRD analysis

Figure 7.3 (a) and (b) shows the XRD patterns of the $\text{CaAl}_2\text{O}_4:\text{Eu}^{2+}, \text{Nd}^{3+}$ powder samples.



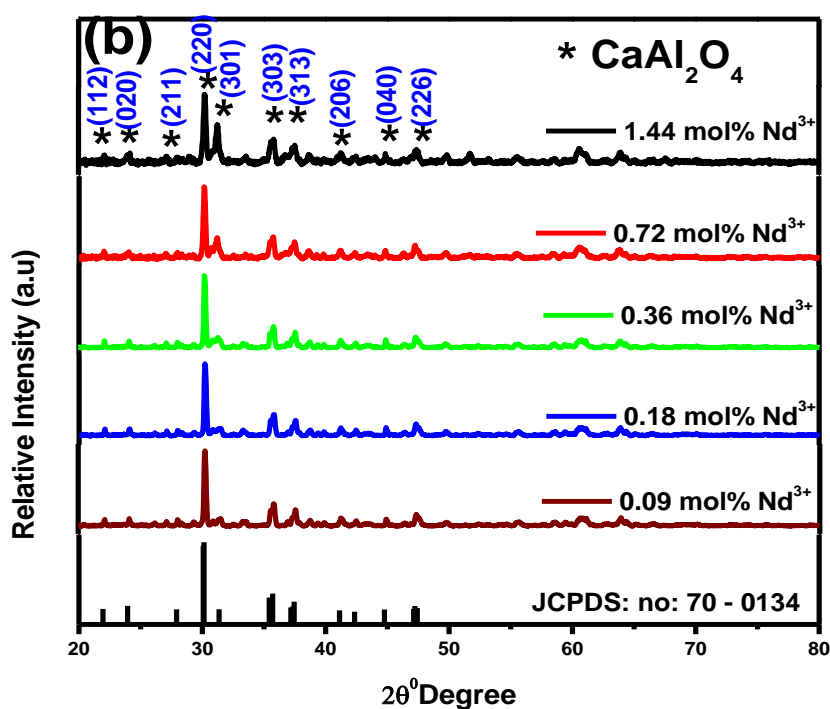


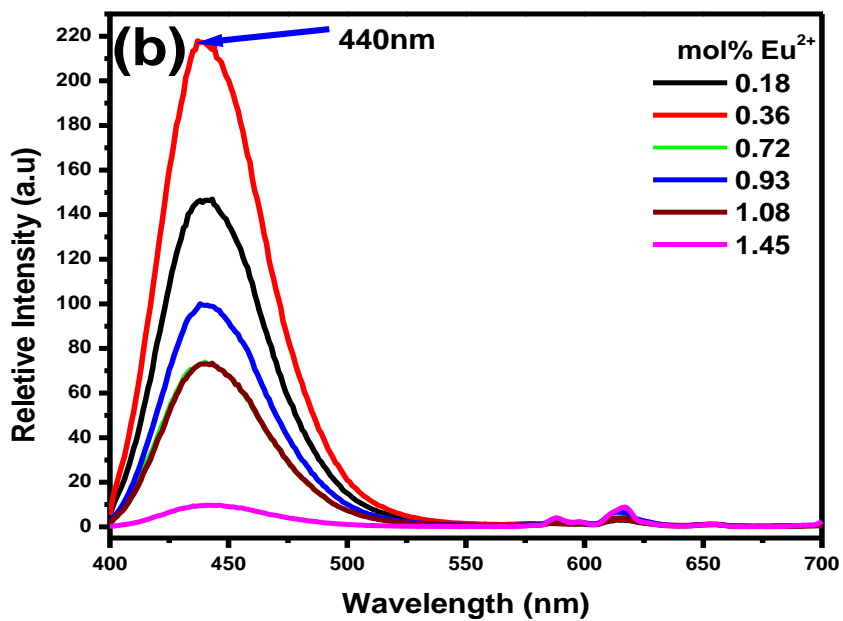
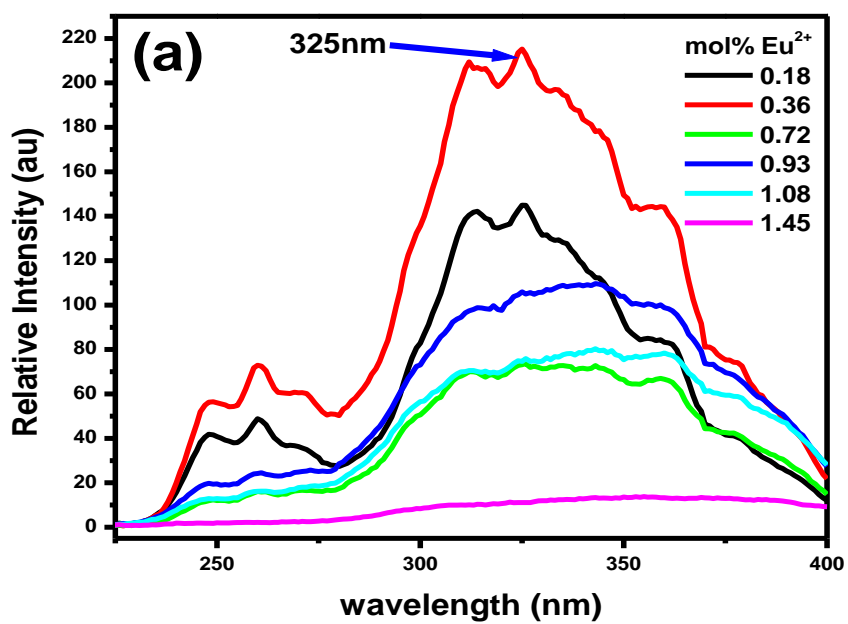
Figure 7.3: Effect of (a) amount of Eu^{2+} and (b) Nd^{3+} on the structure of the $\text{CaAl}_2\text{O}_4:\text{Eu}^{2+},\text{Nd}^{3+}$ phosphor.

As can be seen, the monoclinic phase diffraction peaks of CaAl_2O_4 (Contrast JCPDS date file No. 70-0134) are predominant in the XRD patterns of the powders. No impurities were observed. This is in good accordance with the reports [6]. Furthermore, a little amount of doped rare earth ions has almost no effect on the CaAl_2O_4 phase composition.

7.3.2 Influence on photoluminescence properties

The excitation and emission spectra of $\text{CaAl}_2\text{O}_4:\text{Eu}^{2+},\text{Nd}^{3+}$ phosphor with various contents of Eu^{2+} are shown in Figure 7.4. The excitation spectra of Figure 7.4(a) show a broad band from 280 to 400 nm, and its emission Figure 7.4(b) is a symmetrical band at 440 nm which is attributed to the typical $4f^65d^1-4f^7$ transition of Eu^{2+} .

High concentrations of Eu^{2+} generally reduce both intensity and lifetime of the phosphor powders. The PL intensity increased with concentration from 0.18 - 0.36 mol% of Eu^{2+} and drops from 0.72 - 1.45 mol% of Eu^{2+} .



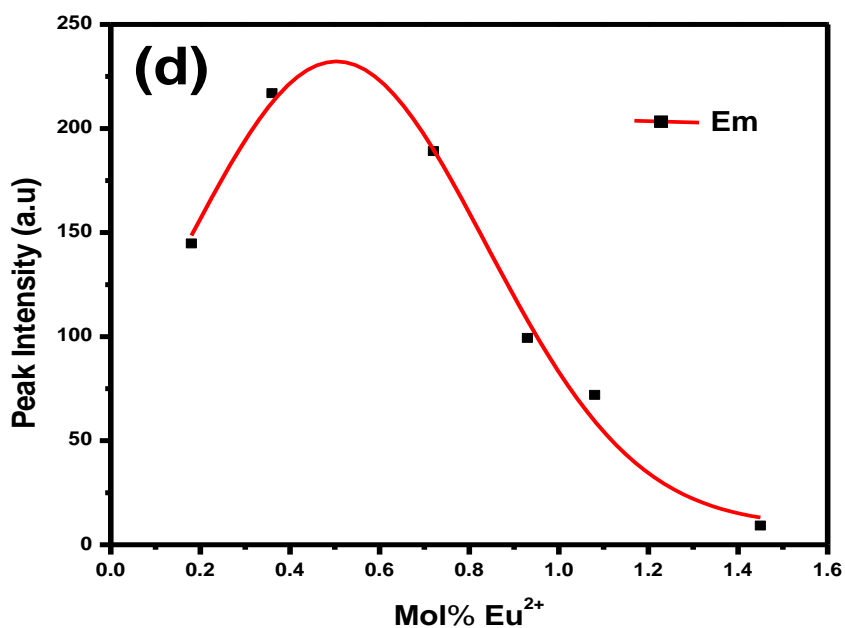
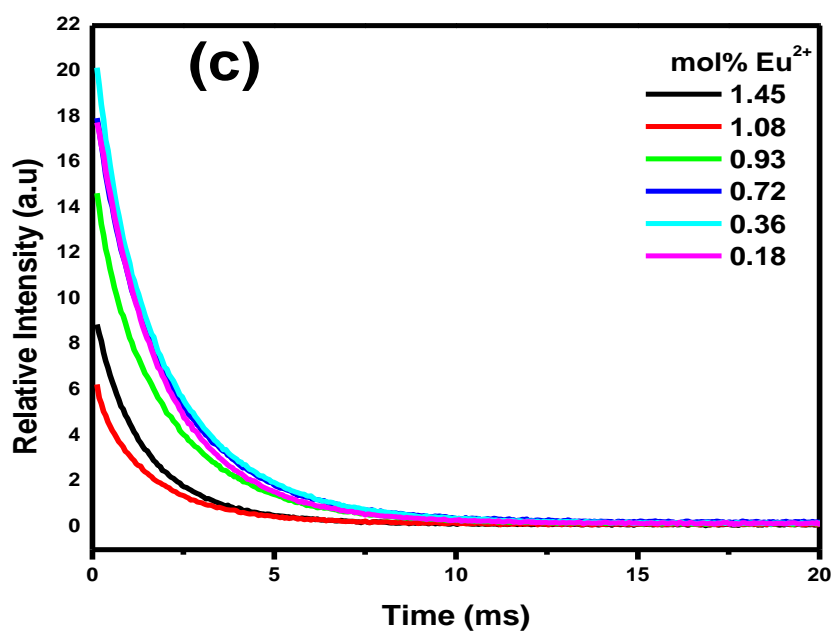
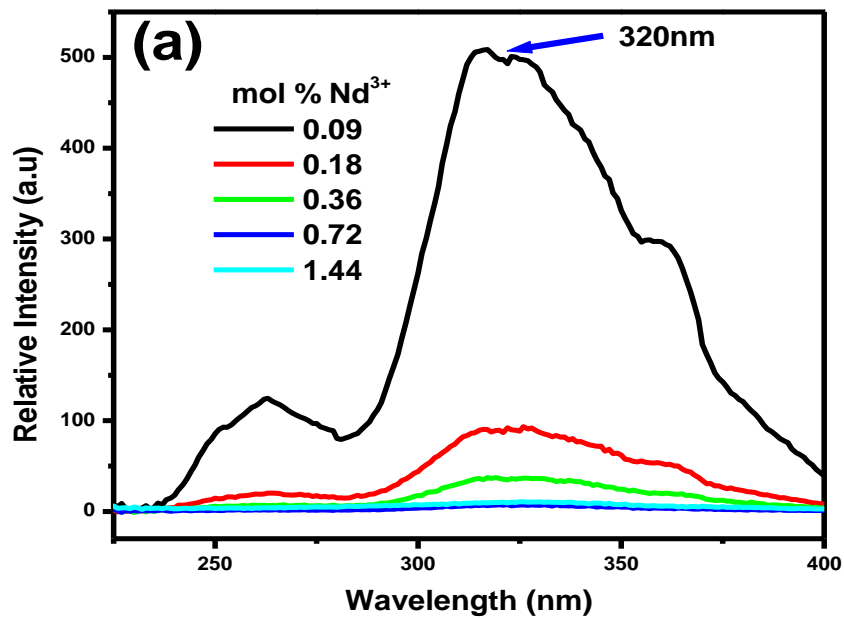


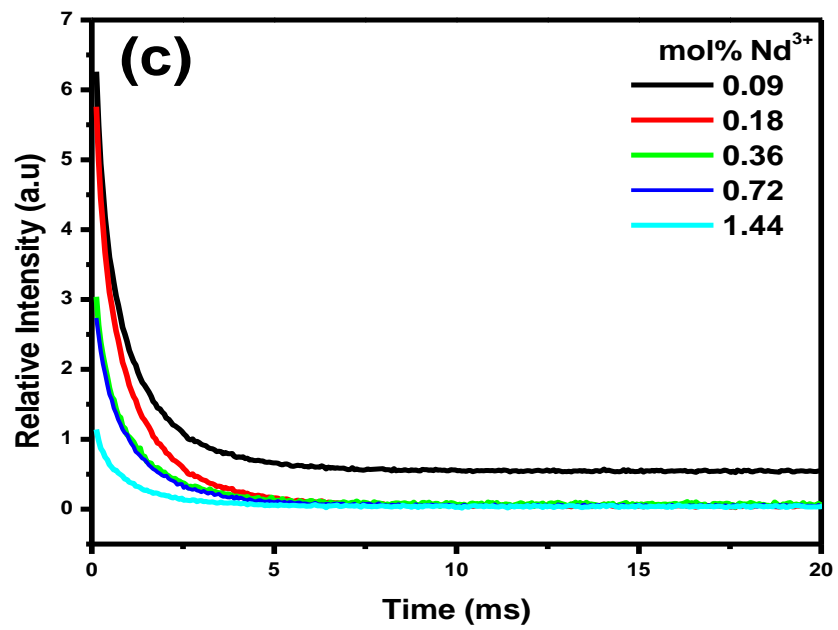
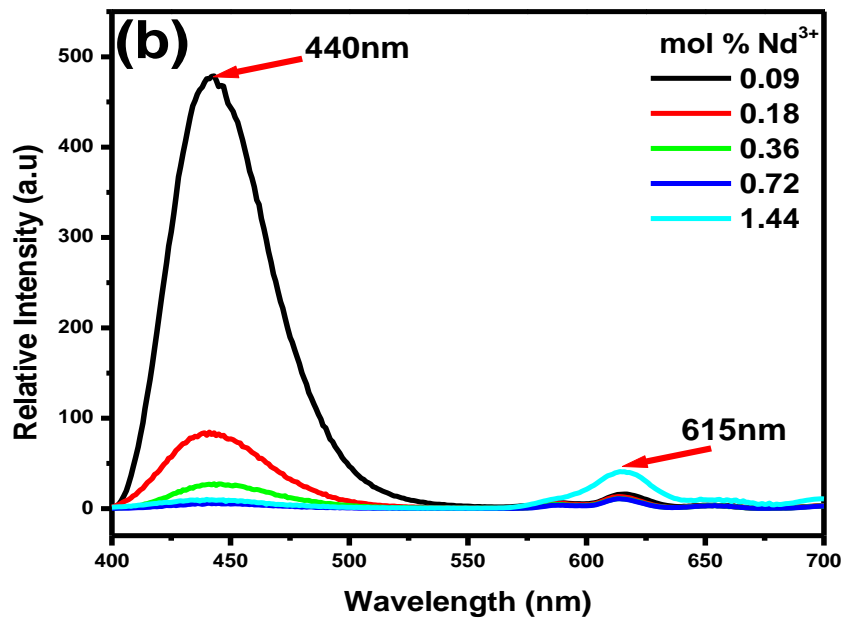
Figure 7.4: (a) Excitation (b) Emission and (c) decay spectra of CaAl_2O_4 as a function of $\text{mol}\% \text{Eu}^{2+}$ (d) Peak emission intensities as a function of $\text{mol}\% \text{Eu}^{2+}$.

Similarly Figure 7.5 shows the emission spectra of the $\text{CaAl}_2\text{O}_4:\text{Eu}^{2+},\text{Nd}^{3+}$ phosphor with various contents of Nd^{3+} . The optimum PL intensity was observed with the 0.09 mol% of

Nd^{3+} but drops as concentration of Nd^{3+} increases from 0.18 – 1.44 mol%. This behavior can be attributed to concentration quenching effects [7].

The mechanism of the long persistence is due to the holes trapped–transported– de-trapped process [8]. Nd^{3+} ion works as traps of holes, and the trap levels lie in-between the excited state and the ground state of Eu^{2+} ion. After excitation by the irradiation lights, electron and hole pairs are produced in Eu^{2+} ions, and the Nd^{3+} traps capture some free holes moving in the valence band.





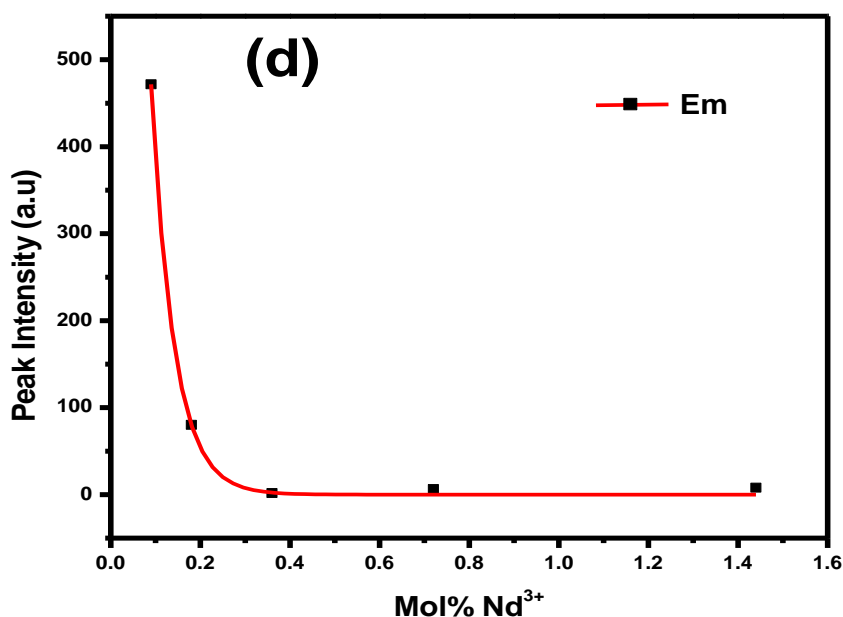


Fig. 7.5: (a) Excitation (b) Emission and (c) decay spectra of CaAl_2O_4 as a function of mol% Nd^{3+} (d) Peak emission intensities as a function of mol% Nd^{3+}

When the excitation source is cut off, some holes captured by the Nd^{3+} traps are thermally released slowly and relaxed to the excited state of Eu^{2+} , finally, returning to the ground state of Eu^{2+} accompanied with emission of light. This is the reason why phosphor maintains a long persistent period after the excitation is cut off.

Conclusion

The phosphor $\text{CaAl}_2\text{O}_4:\text{Eu}^{2+},\text{Nd}^{3+}$ can be prepared by solution-combustion method which is cost-effective, saves energy and time. Scanning electron microscopy (SEM) observations showed that regular morphology and fine particles were achieved by solution combustion method. The influences of the varying quantity of Eu^{2+} and Nd^{3+} on the structural and luminescent properties of the phosphor were studied. The analytical results indicate that the broad emitted band of the $\text{CaAl}_2\text{O}_4:\text{Eu}^{2+},\text{Nd}^{3+}$ is observed in the blue region ($\lambda_{\text{max}} = 440 \text{ nm}$) due to transitions from the $4f^65d^1$ to the $4f^7$ configuration of the Eu^{2+} ion.

References

- [1] T. Aitasalo, J. Hölsä, H. Jungner, M. Lastusaari, J. Niittykoski, *J. Phys. Chem. B* 2006, **110** 4589.
- [2] E. Newton Harvey, *A History of Luminescence: From the Earliest Times until 1900*.
- [3] T. Matsuzawa, Y. Aoki, N. Takeuchi, Y. Murayama, *J. Electrochem. Soc.* 1996, **143** 2670.
- [4] P. Dorenbos, *J. Electrochem. Soc.* 2005, **152** H107.
- [5] A. Foil, Miller and C.H. Wilkins, Department of Research in Chemical Physics, Mellon Institute, Pittsburgh 13, Pa.
- [6] D.A. Fumo, M.R. Morelli, A.M. Segadães, *Mater. Res. Bull.* 1996, **31** 1243.
- [7] C. R. Ronda, Willy-VCH, Germany, 2008, 3.
- [8] J.Y. Zhang, Z.T. Zhang, T.M. Wang, W.C. Hao, *Mater. Lett.* 2003, **57** 315.

Chapter 8

Thermoluminescence Study of Long Persistent $\text{CaAl}_2\text{O}_4:\text{Eu}^{2+}, \text{Nd}^{3+}, \text{Dy}^{3+}$.

8.1. Introduction

An increased after-glow called Thermally Stimulated Luminescence (TSL) is observed when a phosphor with deep traps is excited with UV for a while at rather low temperatures and then heated, due to the recombination of electrons thermally reactivated from the deep traps. Such an emission is also referred to as thermoluminescence (TL). Irradiation with α -rays, β -rays, UV-rays, χ -rays, or γ -rays transfers electrons and holes to their respective traps. Thermoluminescence (TL) measurements provide information concerning the trap levels. In order to obtain information about luminescence process of phosphors and to apply them in various fields, the knowledge of defects or traps and their location in the band gap of materials is very important. The temperature dependence of the emission intensity is called the glow curve [1]. Since in most cases the TL glow curve consists of several overlapping peaks, the isolation of one of the glow peaks from the others in the experimental glow curve structure enables the calculation of trap levels and activation energy among other parameters. The excitation energy partly does the work of moving electrons to traps. Some of these electrons are trapped and locate themselves at a depth E below the conduction band. The trap levels or centers play a significant role in energy storage for persistent photoluminescent and thermoluminescent phosphors. This radiation energy stored in the form of trapped electrons is released by raising the temperature of the material and the released energy is converted to luminescence. This trapping process followed by the release of the stored energy in thermoluminescent materials is widely applied in radiology such as in ionizing radiation dosimeters. Materials that exhibit TSL include glasses, ceramics, plastics and some organic solids.

TL measurements are obtained after turning off the irradiating source and monitoring the thermally stimulated luminescence under a condition of gradually increasing temperature.

The shape and position of the resultant thermoluminescence (TL) glow curve can be analyzed to obtain information on the various parameters of the trapping process such as activation energy, amount of trap depth, trapping rates, etc [2]. The term peak shape method is reserved in the TL literature for such methods, although there are other methods for finding activation energy, E which are also based on the glow-peak shape (i.e. curve fitting methods) [3, 4]. The work by Chen [5] is a reference point in the derivation of the peak shape methods. CaAl_2O_4 has been studied by many researchers on its use as luminescent material. Nevertheless, there are very few reports dealing with the use of CaAl_2O_4 as a TL material. In this paper, the thermoluminescent properties of calcium aluminate doped with divalent rare earth ions Eu^{2+} and co-doped with mixed trivalent rare earth ions $\text{Nd}^{3+}/\text{Dy}^{3+}$ are studied to find out its suitability in various TL applications.

8.2. Experimental

8.2.1. Synthesis

$\text{CaAl}_2\text{O}_4:\text{Eu}^{2+},\text{Nd}^{3+},\text{Dy}^{3+}$ phosphors were synthesized using the solution - combustion method. The starting raw materials used in the experiment include various proportions of analytical pure grade $\text{Ca}(\text{NO}_3)_2 \cdot 4\text{H}_2\text{O}$, $\text{Al}(\text{NO}_3)_3 \cdot 9\text{H}_2\text{O}$, $\text{Eu}(\text{NO}_3)_3 \cdot 5\text{H}_2\text{O}$, $\text{Nd}(\text{NO}_3)_3$, $\text{Dy}(\text{NO}_3)_3$, urea ($\text{CH}_4\text{N}_2\text{O}$) and boric acid (H_3BO_3). The raw materials were weighed according to the chemical composition of $\text{CaAl}_2\text{O}_4:\text{Eu}^{2+},\text{Nd}^{3+}$ dissolved in 10 ml of de-ionized water and thoroughly mixed using a magnetic stirrer for 15 minutes without heating to obtain a uniform solution. To study the influence of variation of co-dopants, Nd^{3+} and Dy^{3+} molar ratio on the TL properties of the $\text{CaAl}_2\text{O}_4:\text{Eu}^{2+}$ phosphor five samples were prepared with concentrations; 0:1, 0.25:0.75, 0.5: 0.5, 0.75:0.25 and 1:0 of $\text{Nd}^{3+}:\text{Dy}^{3+}$. The solutions were then poured into China crucibles and placed one at a time in a muffle furnace pre-heated at 500°C . Combustion reaction time was 5–6 min per sample. White voluminous foam was obtained by firing the mixture at temperatures of $400\text{--}500^\circ\text{C}$. Initially, the solution boiled and underwent dehydration, followed by decomposition releasing large amounts of gases (oxides of carbon, nitrogen and ammonia). Then, spontaneous ignition and smoldering occurred which gradually led to an explosion with enormous swelling. When taken out of the muffle furnace and cooled down, voluminous foam was obtained, which was easily milled to obtain the synthesized fine, white powders of $\text{CaAl}_2\text{O}_4:\text{Eu}^{2+},\text{Nd}^{3+},\text{Dy}^{3+}$. A mixture of the

incomplete combustion compound CaAl_4O_7 and the complete combustion compound CaAl_2O_4 , which appear light- purple in colour when exposed to sunlight, was formed. The powders were stored in transparent sample glass bottles for characterization.

8.2.2. Characterization

The TSL glow curves were obtained by using a Nucleonix 1009I TL reader with PMT type 9924 supplied by M/s Nucleonix Systems Pvt. Ltd., India interfaced to a PC where the TL signals were analyzed. Prior to the TL measurements, the materials were exposed to a 254 nm UV radiation from a Lohuis FT (South Africa) standard lamp model T8 BLB1006 with a power of 18 W, kept above the sample, as an excitation source for 10 minutes before recording the TL spectrum so as to enable the traps to be filled as a result of this exposure. Glow curves were recorded in the temperature range from room temperature 25 to 400 °C operating with linear heating rates of 2, 4, 5, 6, 8, and 10 °C s⁻¹. The TL emission was monitored. During all the TL experiments in this study, in order to guarantee the comparison of glow curve relative intensities, TL measurements were carried out under the same conditions of excitation intensity, the amount of each phosphor kept constant (10 mg), the condition of preparation, and so on. Other factors such as sample packing and position, which are very difficult to control, may however, induce error for the TL intensity. On the other hand, we repeated our synthesis experiment and measurements three times in order to decrease errors.

8.3. Results and Discussion

8.3.1. Analysis of the TL glow curves

The depth of trap levels could be estimated by general order kinetics formula [7] which is expressed as;

$$I(T) = n_0 S \exp\left(-\frac{E}{kT}\right) \left[(b-1) \left(\frac{S}{\beta}\right) \times \int_{T_0}^T \exp\left(-\frac{E}{kT}\right) dT + 1 \right]^{\frac{-b}{(b-1)}}, \quad (1)$$

where n_0 is the number of trapped charges at $T=0$, E the activation energy (or trap depth), k the Boltzmann's constant, β the heating rate, S the frequency factor and b the order of

kinetics. E and n_0 are characteristic of the physical properties of the traps formed by the co-dopants whereby the trap level depth E is proportional to one corresponding glow peak temperature and the trap density n_0 correlates with the afterglow time of the phosphor and the intensity of glow peaks respectively. The shape of a TL glow-peak plays an important role in basic research and in TL applications. In the case of basic TL research it is the basis of important and convenient methods for calculating the trapping parameters of distinct energy levels within the crystal [8]. The TL glow curve usually consists of several overlapping peaks, (Figure 8.1(a) and (b)). Various TL analysis methods that have been described by many researchers include initial rise and peak shape method among others. The peak shape method is particularly useful for determining the trapping parameters of distinct energy levels within the crystal and the activation energy E . This method is based on determination of a few relevant parameters on a single glow-peak as shown in Figure 8.2. The parameters necessary for use with the various expressions developed using the peak shape method include the peak maximum temperature T_{max} , the temperatures at half maximum TL intensity $T_1 (\frac{1}{2}max)$ and $T_2 (\frac{1}{2}max)$ at the low and high temperature side of the glow-peak respectively and half width parameters; $\omega = T_2 (\frac{1}{2}max) - T_1 (\frac{1}{2}max)$, $\delta = T_2 (\frac{1}{2}max) - T_{max}$ and $\tau = T_{max} - T_1 (\frac{1}{2}max)$ (2).

According to this method, the kinetic order of a single peak is easily obtained by means of the geometric/symmetry factor of the glow-peak ;

$$\mu_g = \frac{T_2 (\frac{1}{2}max) - T_{max}}{T_2 (\frac{1}{2}max) - T_1 (\frac{1}{2}max)} = \frac{\delta}{\omega} \quad (3)$$

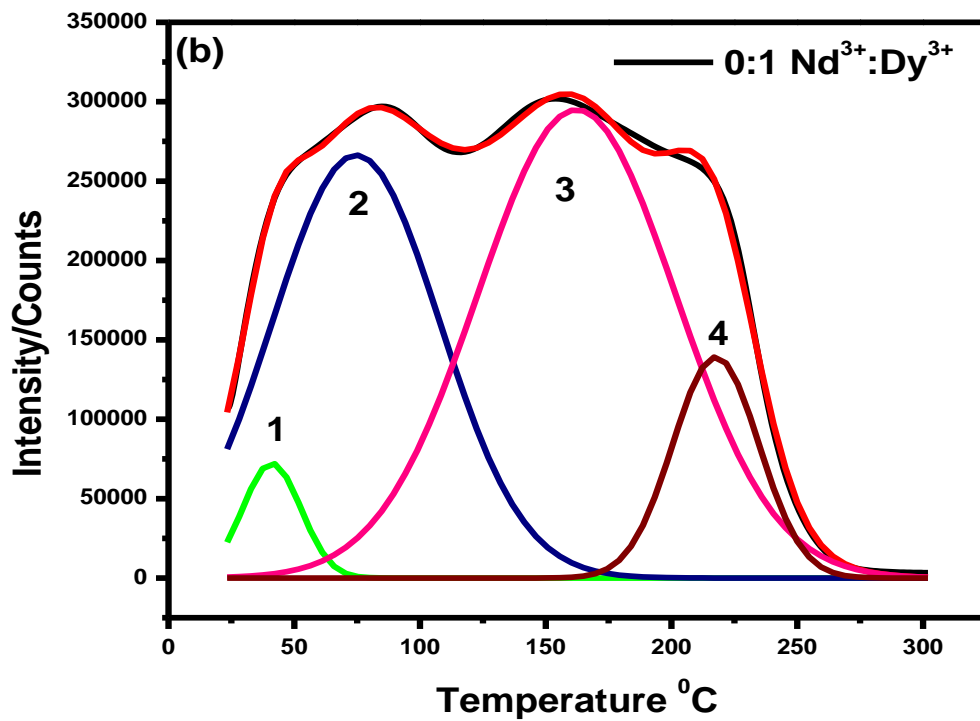
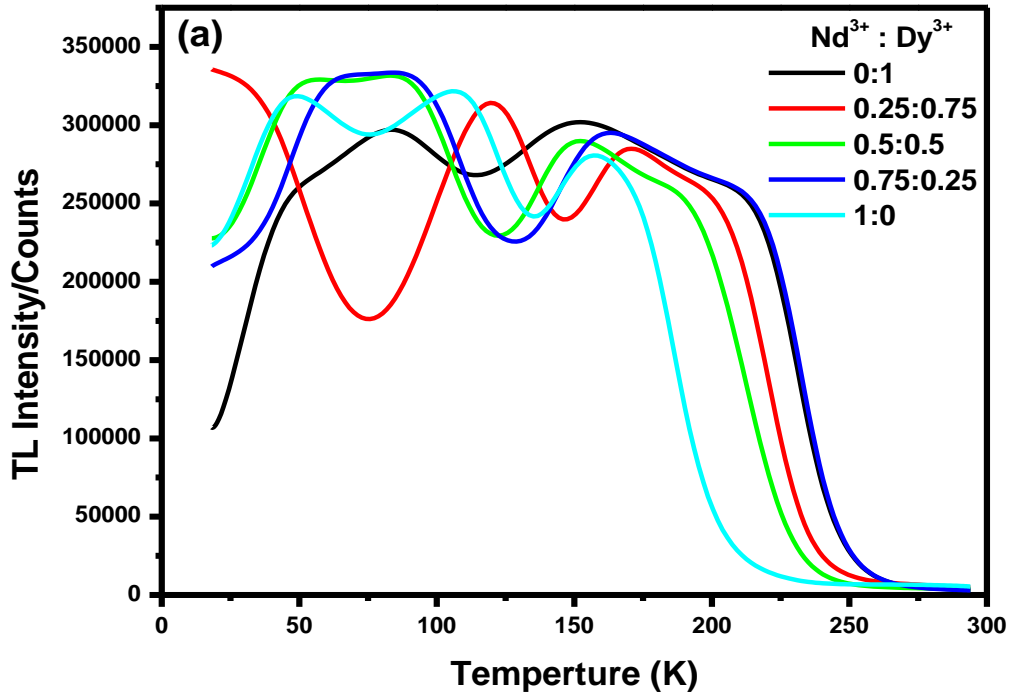


Figure 8.1:(a) Variation of TL intensity with concentration of Nd^{3+} and Dy^{3+} (b) TL glow curve for $\text{Nd}^{3+}:\text{Dy}^{3+} = 0:1$ sample.

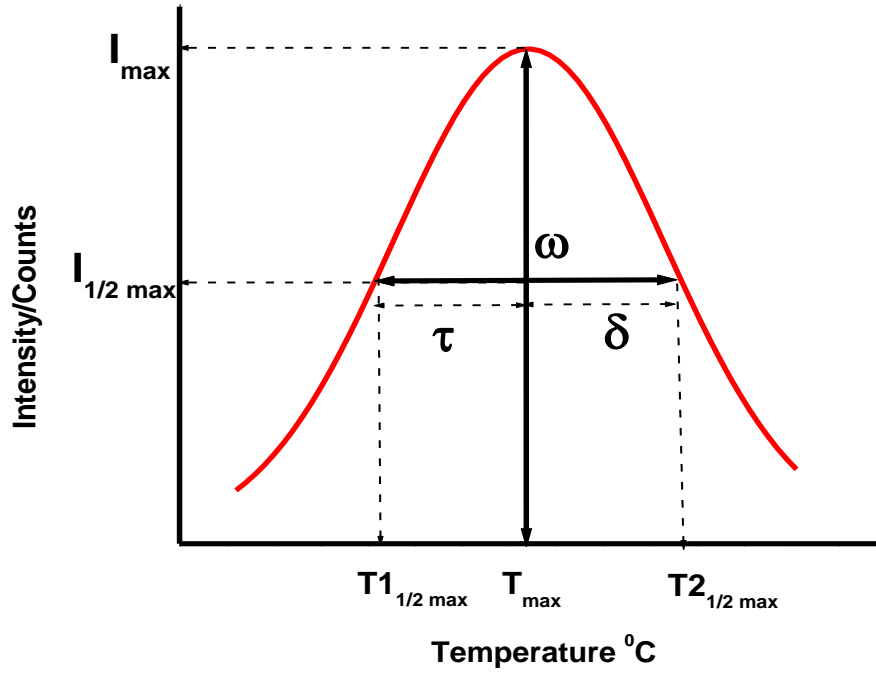


Figure 8.2: Schematic diagram of a TSL peak showing the different relevant parameters.

Chen (1969) deduced the following expression to determine E using the peak shape method:

$$E = c_{\alpha} \left(\frac{kT_m^2}{\alpha} \right) - b_{\alpha} (2kT_m) \quad (4)$$

Where stands for τ , δ or ω [9]. The values of c_{α} and b_{α} depend on which of these three observed parameters of the peak is used. In the form given by Chen [4, 5] these are;

$$c_{\omega} = \frac{\omega I_m}{\beta n_0} \quad (5)$$

$$c_{\delta} = \frac{\delta I_m}{\beta n_m} \quad (6)$$

$$c_{\tau} = \frac{\tau I_m}{\beta (n_0 - n_m)} \quad (7)$$

$$\text{with } n_m = \int_{t_m}^{\infty} I dt \quad (8)$$

where I_m is the peak maximum intensity, n_m the high temperature half integral of the glow peak, τ_m the time at peak maximum intensity and c_{ω} , c_{δ} and c_{τ} are quantities which describe the kinetic order. Chen [5, 6] evaluated the coefficients c_{α} and b_{α} for first and second order kinetics and used an interpolation – extrapolation method to evaluate the values for intermediate order kinetics. From equation 3, his final expressions are as deduced as follows;

When τ is used,

$$c_\tau = 1.15 + 3.0(\mu_g - 0.42), \quad b_\tau = 1.58 + 4.2(\mu_g - 0.42), \quad (9)$$

When δ is used,

$$c_\delta = 0.976 + 7.3(\mu_g - 0.42), \quad b_\delta = 0 \quad (10)$$

When ω is used,

$$c_\omega = 2.52 + 10.2(\mu_g - 0.42), \quad b_\omega = 1 \quad (11)$$

In these expressions $\mu_g = \frac{\delta}{\omega}$. Analysis of (TL) glow curves require the selection of one of the glow peaks from the others in the TL glow curve structure so as to determine the number of traps, depth of each trap (activation energy), trapping rates, etc. Figure 8.3 shows the relevant parameters for analysis of peak 1 in Figure 8.1 above.

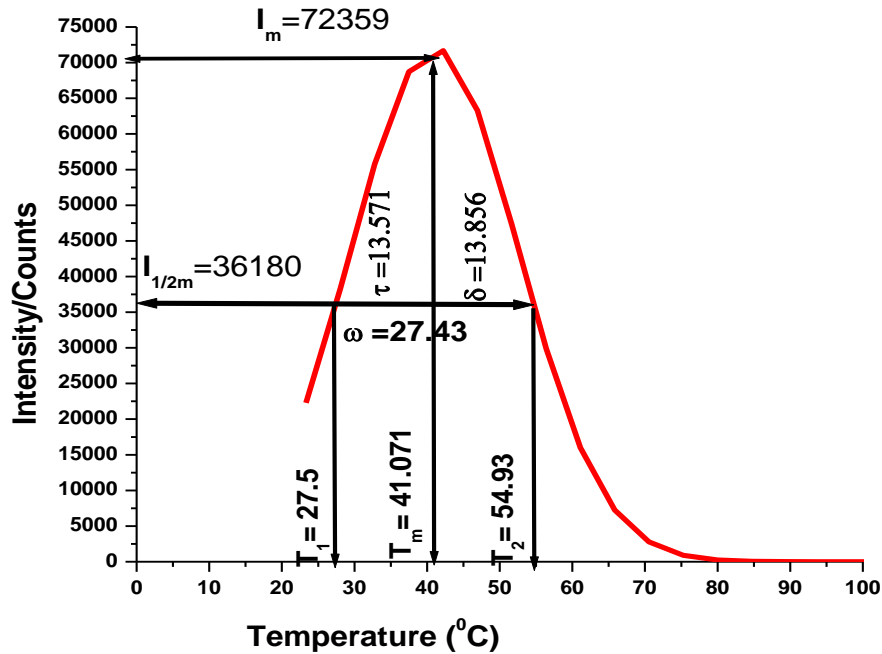


Figure 8.3: Parameters for glow peak 1.

For peak 1 using $\mu_g = \frac{\delta}{\omega} = \frac{13.856}{27.43} = 0.51$ in Eq.9, 10 and 11 we determine the relevant coefficients as follows;

$$c_\tau = 1.15 + 3.0(0.51 - 0.42) = 1.42$$

$$b_\tau = 1.58 + 4.2(0.51 - 0.42) = 1.958$$

$$c_\delta = 0.976 + 7.3(0.51 - 0.42) = 1.633$$

$$b_\delta = 0$$

$$c_{\omega} = 2.52 + 10.2(0.51 - 0.42) = 3.438$$

$$b_{\omega} = 1$$

From Eq.4 the values of E for the coefficients are calculated as follows;

$$\begin{aligned} E_{\tau} &= c_{\tau} \left(\frac{kT_m^2}{\tau} \right) - b_{\tau}(2kT_m) \\ &= 1.42 \left(\frac{1.381 \times 10^{-23} \times (314.071)}{13.571} \right) \\ &\quad - 1.958(2 \times 1.381 \times 10^{-23} \times 314.071) = 1.26 \times 10^{-19} = 0.784\text{eV} \end{aligned}$$

$$\begin{aligned} E_{\delta} &= c_{\delta} \left(\frac{kT_m^2}{\delta} \right) - b_{\delta}(2kT_m) = 1.633 \left(\frac{1.381 \times 10^{-23} \times (314.071)^2}{13.856} \right) - 0 \\ &= 1.605 \times 10^{-19} \\ &= 1.002\text{eV} \end{aligned}$$

$$\begin{aligned} E_{\omega} &= c_{\omega} \left(\frac{kT_m^2}{\omega} \right) - b_{\omega}(2kT_m) \\ &= 3.438 \left(\frac{1.381 \times 10^{-23} \times (314.071)^2}{27.43} \right) - 1(2 \times 1.381 \times 10^{-23} \times 314.071) \\ &= 1.62 \times 10^{-19} \\ &= 1.011\text{eV} \end{aligned}$$

The same calculations were done for peaks 2, 3 and 4 and the results are as shown in table 8.1

Table 8.1. Parameters for glow curve 1 Nd:Dy=0:1

PEAK	T_m	τ	δ	ω	μ_g	E_{τ} (eV)	E_{δ} (eV)	E_{ω} (eV)	E_{av} (eV)
1	314.071	13.571	13.856	27.43	0.505	0.784	1.002	1.011	0.932
2	347.563	39.763	39.067	78.83	0.496	0.247	0.408	0.375	0.343
3	435.28	45.98	45.99	91.97	0.500	0.350	0.554	0.517	0.474
4	490	19.7	20.65	40.35	0.512	1.33	1.65	1.69	1.56

Calculated activation energies for the other glow curves are as shown in tables 8.2, 8.3, 8.4 and 8.5 respectively.

Table 8.2. Parameters for glow curve 2 Nd:Dy=0.25:0.75

PEAK	T_m	τ	δ	ω	μ_g	E_τ (eV)	E_δ (eV)	E_ω (eV)	E_{av} (eV)
1	295.869	30.221	41.137	71.358	0.576	0.289	0.388	0.384	0.354
2	393.10	28.383	29.373	57.756	0.509	0.533	0.737	0.723	0.664
3	441.07	17.618	17.623	35.241	0.5	1.177	1.485	1.511	1.391
4	473.90	20.55	21.54	36.909	0.584	1.36	1.95	2.118	1.809

Table 8.3. Parameters for glow curve 3 Nd:Dy=0.5:0.5

PEAK	T_m	τ	δ	ω	μ_g	E_τ (eV)	E_δ (eV)	E_ω (eV)	E_{av} (eV)
1	328.723	48.946	50.903	99.849	0.51	0.159	0.299	0.264	0.241
2	371.268	20.557	20.557	41.114	0.5	0.681	0.902	0.900	0.828
3	422.77	22.511	23.498	46.009	0.512	0.833	1.080	1.085	0.999
4	465.24	23.49	23.5	46.99	0.5	0.950	1.239	1.244	1.144

Table 8.4. Parameters for glow curve 4 Nd:Dy=0.75:0.25

PEAK	T_m	τ	δ	ω	μ_g	E_τ (eV)	E_δ (eV)	E_ω (eV)	E_{av} (eV)
1	348.38	64.609	62.65	127.3	0.49	0.108	0.248	0.206	0.187
2	441.75	23.494	23.494	46.988	0.50	0.849	1.117	1.118	1.028
3	485.8	22.51	22.52	45.03	0.50	1.173	1.409	1.423	1.33

Table 8.5. Parameters for glow curve 5 Nd:Dy=1:0

PEAK	T_m	τ	δ	ω	μ_g	E_τ (eV)	E_δ (eV)	E_ω (eV)	E_{av} (eV)
1	323.904	44.052	45.03	89.082	0.51	0.182	0.328	0.293	0.268
2	383.46	21.529	22.522	44.051	0.51	0.707	0.919	0.923	0.849
3	435.65	25.451	25.452	50.903	0.50	0.749	1.002	0.997	0.916

Table 8.6. Correlation between co-dopant ratio (Nd³⁺:Dy³⁺) and E_{av} .

Nd ³⁺ :Dy ³⁺	0:1	0.25:0.75	0.5:0.5	0.75:0.25	1:0
E_{av} (eV)	0.8273	1.0545	0.803	0.85	0.678

When the results of table 8.6 are plotted we obtain a graph shown in figure 8.4. From the graph it can be observed that the ratio 0.25:0.75 of Nd³⁺:Dy³⁺ respectively offers the best optimal result which is in conformity with the reports [10]. This means that at these concentrations the samples have the highest number of traps and these correspond to deep traps and hence high luminescence intensity respectively.

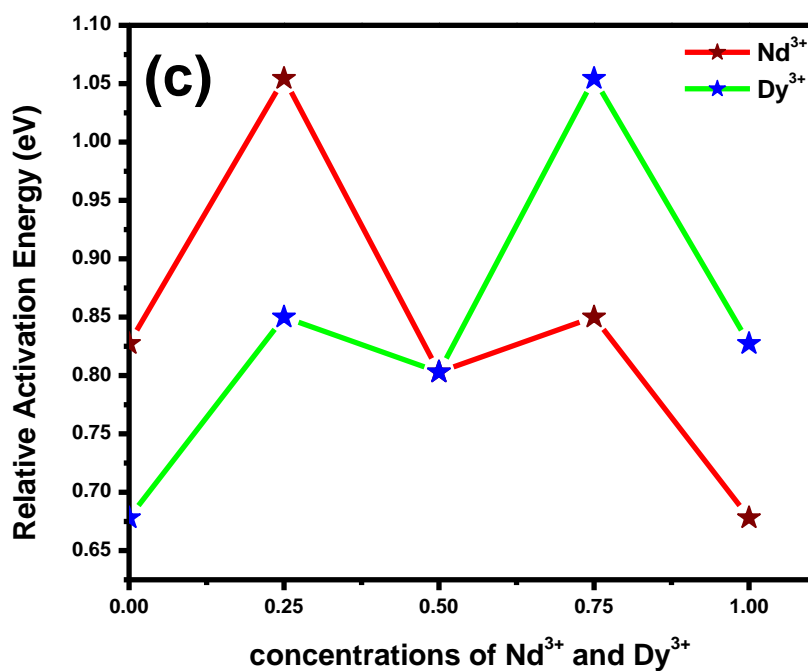


Figure 8.4: Correlation between dopant or co-dopant concentration and Activation Energy (eV).

Conclusion

The phosphor $\text{CaAl}_2\text{O}_4:\text{Eu}^{2+},\text{Nd}^{3+},\text{Dy}^{3+}$ was prepared by solution-combustion method. The solution-combustion method was employed since it is cost-effective, saves energy and time. The influences of the quantity of mixed Nd^{3+} and Dy^{3+} rare earth ions on thermoluminescence properties of the CaAl_2O_4 phosphor were studied. The analytical TL results indicate that the ratio 0.25:0.75 of $\text{Nd}^{3+}:\text{Dy}^{3+}$ respectively offers the best optimal results. Hence this phosphor may serve as a promising material for radiological applications such as in ionizing radiation dosimetry.

References

- [1] E. Nakazawa, Handbook of phosphors 90.
- [2] S. Basuna, G.F. Imbusch, D.D. Jiac, W.M. Yenc, J. Lumin. 2003, **104** 283.
- [3] R. Chen, Y. Kirsh, Pergamon Press, 1981 167.
- [4] R. Chen, S.W.S. McKeever, World Scientific, 1997.
- [5] R. Chen, J. Appl. Phys. 1969, **40** 570.
- [6] R. Chen, J. Electrochem. Soc. 1970, **116** 1254.
- [7] T. Katsumata, S. Toyomane, A. Tonegawa, Y. Kanai, U. Kaneyama, J. Cryst. Growth 2002, **237** 239.
- [8] G. Kitis, R. Chen, and V. Pagonis, phys. stat. sol. A 2008, **205** (5), 1181–1189 / DOI 10.1002/pssa.200723470
- [9] C.M. Sunta, Ayta W.E. Feria, T.M. Pifers, S. Watanabea, 1999, **30** 197.
- [10] A.H. Wako, F.B Dejene, and H.C. Swart, University of the Free State, SAIP proceedings 2011.

Chapter 9

Future work

1. Other different synthesis techniques should be explored. With the current synthesis technique multiple phases of CaAl_xO_z like CaAl_3O_6 , CaAl_2O_4 and CaAl_4O_7 are also formed in the process. This is affecting the PL intensity as well as the crystal structure and morphology. A technique should be found that is both fast, cheap and that is producing high quality, pure CaAl_2O_4 .
2. Investigation should be done using other techniques other than those applied in this study. This will help get more detailed information on the various properties of the phosphors which will consequently improve performance for the many applications.
3. Investigation on other different dopants and co-dopants should be emphasized so as to obtain a wide spectrum of colors and also to improve the lifetime of the phosphors. In addition, it would be exciting to investigate the effect of the different host materials.
4. In this study only two temperatures were investigated namely room temperature (un-annealed samples) and 500°C (annealed samples). Further work can include annealing the samples from 50°C up to 1000°C . This may have some good effect in obtaining pure CaAl_2O_4 . Also different ambient gasses can be introduced during synthesis process to prevent the formation of multi-phased CaAl_xO_z . Studies can also include an investigation to see what effect the annealing temperatures have on the structural and luminescent properties of the phosphor.
5. Research could also be done on growing $\text{CaAl}_x\text{O}_z:\text{Eu}$ in thin film form and investigating the effect of growth conditions.
6. It is also important to investigate the effect of the size and size distribution (narrow and broad), and the shape of the particles on the luminescence properties of the $\text{CaAl}_x\text{O}_z:\text{Eu}$ phosphors.

7. Studies on phase transformation of CaAl_xO_z : Eu from the low temperature structure (monoclinic) to the higher temperature structure (hexagonal) should be carried out to investigate its influence on the optical properties of the phosphors.

List of Figures

1. Figure 1.1: Surface area-to-volume ratio.....	11
2. Figure 1.2: Images of (a) $\text{CaAl}_2\text{O}_4:\text{Eu}^{2+},\text{Dy}^{3+}$ (b) $\text{BaAl}_2\text{O}_4:\text{Eu}^{2+},\text{Dy}^{3+}$ and (c) $\text{SrAl}_2\text{O}_4:\text{Eu}^{2+},\text{Dy}^{3+}$ long afterglow phosphors after UV excitation.....	12
3. Figure 1.3: Energy level scheme of the Eu^{2+} ions involved in the UV-excited and persistent luminescence processes in $\text{CaAl}_2\text{O}_4:\text{Eu}^{2+}$ [20].....	13
4. Figure 1.4: Model showing Persistent Luminescence Mechanism.....	15
5. Figure 2.1: Cross section of a low-pressure luminescent lamp; 1-glass tube; 2-luminescent powder; 3-Cathode; 4-lamp cap[1].....	30
6. Figure 2.2: Schematic diagram of a standard cathode ray tube (CRT); Electrons (e) leaving the electron gun (G) are reflected by systems L1,L2 and excite the luminescent material (P)	31
7. Figure 2.3: (a) Luminescent signs [43] and (b) a neon sign [44].....	33
8. Figure 2.4: Luminescent Paints [43].....	33
9. Figure 2.5: Luminescent (a) t-shirt and (b) shoes [46, 47].....	34
10. Figure 3.1: White body colour of phosphors.....	39
11. Figure 3.2: Phosphorescence mechanism proposed by Matsuzawa et al. [3] (Eu^{2+*} -excited state of Eu^{2+}).....	40
12. Figure 3.3: Phosphorescence mechanism proposed by Aitasalo et al [10].....	41
13. Figure 3.4: Phosphorescence mechanism proposed by F. Clabau et al [5, 8].....	42
14. Figure 4.1: (a) Schematic Diagram of a SEM [14] (b) SEM Centre for Microscopy at UFS.....	47
15. Figure 4.2: Electrons produced in SEM [19].....	48
16. Figure 4.3: (a) and (b) Characteristic x-ray radiation [22].....	49
17. Figure 4.4: Example of an EDS spectrum of $\text{CaAl}_2\text{O}_4:\text{Eu}^{2+},\text{Nd}^{3+},\text{Dy}^{3+}$	50
18. Figure 4.5: An x-ray powder diffractometer [27].....	51
19. Figure 4.6: Schematic diagram of an X-ray tube [27].....	52
20. Figure 4.7: (a) Characteristic X-ray Radiation [27].....	53

21. Figure 4.8: The continuous X-ray spectra [27].....	54
22. Figure 4.9: Intensity of characteristic $K\alpha$ X-rays and $K\beta$ X-rays [27].....	55
23. Figure 4.10: (a). Constructive interference (b) destructive interference [27].....	57
24. Figure 4.11: (a) [28] and (b) [27] Monochromatic X-rays entering a crystal.....	58
25. Figure 4.12: Excitation and Emission processes.....	60
26. Figure 4.13: (a) Schematic diagram of the PL system (b) PL system used to investigate the luminescent properties of phosphors and (c) Cary Eclipse fluorescence spectrophotometer.....	62
27. Figure 4.14: Simplified optical layout of a typical FTIR spectrometer. (Reprinted by permission of Nicolet Instrument Corporation.....	63
28. Figure 4.15: FTIR system at UFS Chemistry Department.....	64
29. Figure 4.16: Thermoluminescence Reader type TL1009I(35).....	66
30. Figure 5.1: (a). Persistent luminescence mechanism for $\text{CaAl}_2\text{O}_4:\text{Eu}^{2+},\text{R}^{3+}$ materials. (b) Parking diagram of monoclinic CaAl_2O_4	72
31. Figure 5.2: SEM micrographs for (a) 0.4% Ca sample and (b) 0.8% Ca sample respectively.....	75
32. Figure 5.3: (a) Monoclinic phase of $\text{CaAl}_2\text{O}_4:\text{Eu}^{2+},\text{Nd}^{3+},\text{Dy}^{3+}$ phosphors.....	76
33. Figure 5.4: (a) Excitation, (b) emission (c) decay characteristics of the phosphors dependence on Ca: Al mass ratio and (d) emission intensities of the varying $\text{Nd}^{3+}:\text{Dy}^{3+}$ co-dopant ratio obtained at room temperature.....	79
34. Figure 6.1: Sample SEM micrographs for (a) 1.9 mol% H_3BO_3 acid (b) 3.8 mol% H_3BO_3 acid (c) 0.3mol% $\text{CO}(\text{NH}_2)_2$ and (d) 0.5 mol% $\text{CO}(\text{NH}_2)_2$ all at $\times 30000$ magnification.....	86
35. Figure 6.2. EDS micrograph revealing the composition of the $\text{CaAl}_2\text{O}_4:\text{Eu}^{2+}, \text{Nd}^{3+}$..	87
36. Figure 6.3. Effect of (a) amount of flux and (b) fuel (urea) on the structure of the $\text{CaAl}_2\text{O}_4:\text{Eu}^{2+},\text{Nd}^{3+}$ phosphor.....	89
37. Figure 6.4. Intensity curves of X-ray diffraction profiles for (a) large and (b) small particles.....	90
38. Figure 6.5. A plot of $\log I(\theta)$ versus s^2	91
39. Figure 6.6. Effect of amount of flux on the luminescent characteristics.....	94
40. Figure 6.7. Effect of amount of urea on the luminescent characteristics.....	96
41. Figure 7.1: Sample SEM microstructures for (a) 0.18 mol% Eu^{2+} (b) 0.09 mol% Nd^{3+}	103

42. Figure 7.2: (a) EDS micrograph revealing the composition of the $\text{CaAl}_2\text{O}_4:\text{Eu}^{2+},\text{Nd}^{3+}$, FTIR spectrum for (b) 0.18,0.36 mol% Eu^{2+} and (c) 0.09 mol% Nd^{3+}	105
43. Figure 7.3: Effect of (a) amount of Eu^{2+} and (b) Nd^{3+} on the structure of the $\text{CaAl}_2\text{O}_4:\text{Eu}^{2+},\text{Nd}^{3+}$ phosphor.....	106
44. Figure 7.4: (a) Excitation (b) Emission and (c) decay spectra of CaAl_2O_4 as a function of mol% Eu^{2+} (d) Peak emission intensities as a function of mol% Eu^{2+}	108
45. Fig. 7.5: (a) Excitation (b) Emission and (c) decay spectra of CaAl_2O_4 as a function of mol% Nd^{3+} (d) Peak emission intensities as a function of mol% Nd^{3+}	111
46. Figure 8.1: (a) variation of TL intensity with concentration of Nd^{3+} and Dy^{3+} (b)TL glow curve for $\text{Nd}^{3+}:\text{Dy}^{3+}=0:1$ sample.....	117
47. Figure 8.2: Schematic diagram of a TSL peak showing the different relevant parameters.....	118
48. Figure 8.3: Parameters for glow peak 1.....	119
49. Figure 8.4: Correlation between dopant or co-dopant concentration and Activation Energy (eV).....	122

List of Tables

1. Table 4.1: Characteristic wavelengths of target materials.....	53
2. Table 6.1: Average crystal size of the monoclinic $\text{CaAl}_2\text{O}_4:\text{Eu}^{2+},\text{Nd}^{3+}$ phase.....	88
3. Table 6.2: Values of $\log I(\theta)$ and S^2	91
4. Table 8.1. Parameters for glow curve 1 $\text{Nd}:\text{Dy}=0:1$	120
5. Table 8.2. Parameters for glow curve 2 $\text{Nd}:\text{Dy}=0.25:0.75$	121
6. Table 8.3. Parameters for glow curve 3 $\text{Nd}:\text{Dy}=0.5:0.5$	121
7. Table 8.4. Parameters for glow curve 4 $\text{Nd}:\text{Dy}=0.75:0.25$	121
8. Table 8.5. Parameters for glow curve 5 $\text{Nd}:\text{Dy}=1:0$	121
9. Table 8.6. correlation between co-dopant ratio ($\text{Nd}^{3+}:\text{Dy}^{3+}$) and E_{av}	121

Publications

The following papers have been submitted for publication by the authors;

Wako A.H., Dejene B.F. and Swart H.C.

1. Synthesis and Characterization of Structural and Luminescent properties of long afterglow $\text{CaAl}_2\text{O}_4:\text{Eu}^{2+},\text{Nd}^{3+},\text{Dy}^{3+}$ nano-scaled phosphors by solution – combustion technique. Proceedings of the 56th Annual Conference of the SAIP (Pretoria), page 354-358.
2. Properties of blue emitting $\text{CaAl}_2\text{O}_4:\text{Eu}^{2+},\text{Nd}^{3+},\text{Dy}^{3+}$ phosphors by optimizing the amount of flux and fuel, Phosphoros 2011, Ghent, Belgium
3. Effect of Eu^{2+} and Nd^{3+} on the properties of blue $\text{CaAl}_2\text{O}_4:\text{Eu}^{2+},\text{Nd}^{3+},\text{Dy}^{3+}$ long afterglow phosphor, Phosphoros 2011, Ghent, Belgium
4. Thermoluminescence Study of Long Persistent $\text{CaAl}_2\text{O}_4:\text{Eu}^{2+},\text{Nd}^{3+},\text{Dy}^{3+}$, MRS-Africa 2011, Zimbabwe

Conferences

- **56th Conference of South African Institute of Physics Pretoria (RSA)** 12th - 15th July 2011, Synthesis and Characterization of Structural and Luminescent properties of long afterglow $\text{CaAl}_2\text{O}_4:\text{Eu}^{2+},\text{Nd}^{3+},\text{Dy}^{3+}$ nano-scaled phosphors by solution – combustion technique, Wako A.H., Dejene B.F. and Swart H.C.
- **1st international workshop on persistent phosphors ‘phosphoros 2011’** Ghent, Belgium 19th - 20th September 2011, Properties of blue emitting $\text{CaAl}_2\text{O}_4:\text{Eu}^{2+},\text{Nd}^{3+}$ phosphors by optimizing the amount of flux and fuel, Wako A.H., Dejene B.F. and Swart H.C.
- **1st international workshop on persistent phosphors ‘phosphoros 2011’** Ghent, Belgium 19th - 20th September 2011, Effect of Eu^{2+} and Nd^{3+} on the properties of blue $\text{CaAl}_2\text{O}_4:\text{Eu}^{2+},\text{Nd}^{3+}$ long afterglow phosphor, Wako A.H., Dejene B.F. and Swart H.C.
- **6th Africa MRS conference Zimbabwe**, 11th - 16th December 2011, Thermoluminescence Study of Long Persistent $\text{CaAl}_2\text{O}_4:\text{Eu}^{2+},\text{Nd}^{3+}$, Wako A.H., Dejene B.F. and Swart H.C.